

**A NUMERICAL STUDY OF ELASTICA
USING CONSTRAINED OPTIMIZATION METHOD**

WANG TONGYUN

NATIONAL UNIVERSITY OF SINGAPORE

2004



**A NUMERICAL STUDY OF ELASTICA
USING CONSTRAINED OPTIMIZATION METHODS**

WANG TONGYUN
(B. ENG)

A THESIS SUBMITTED FOR THE DEGREE
OF MASTER OF ENGINEERING
DEPARTMENT OF CIVIL ENGINEERING
NATIONAL UNIVERSITY OF SINGAPORE

2004

ACKNOWLEDGEMENTS

First, I would like to express my sincere gratitude to my supervisors, Prof. Koh Chan Ghee and Assoc. Prof. Liaw Chih Young, for their guidance and constructive suggestions pertaining to my research and thesis writing. I have learnt much valuable knowledge as well as serious research attitude from them in the past two years. What I have learnt from them benefit not only this work but also my future road.

I would also like to thank all my research fellows, especially Mr. Zhao Shuliang, Mr. Cui Zhe, Mr. Sithu Htun, for their helpful discussions with me and their friendship.

The financial support by means of research scholarship provided by the National University of Singapore is also greatly appreciated.

Finally, I would like to thank my family. My parents' and sister's love and supports have always been with me throughout my postgraduate study. My wife has been my soul mate, encouraging me when I was frustrated; taking care of my daily life. Her love and devotion made my study much smoother. My grandmother who brought me up passed away when I was writing this thesis. Even at the last stage of her life, she expressed her love on me and cares toward my study. Without them, this thesis would not be possible. I dedicate this thesis with best wishes to my beloved family.

TABLE OF CONTENTS

ACKNOWLEDGEMENTS.....	I
TABLE OF CONTENTS.....	II
SUMMARY.....	V
NOTATIONS.....	VII
LIST OF FIGURES.....	IX
LIST OF TABLES.....	XIII

CHAPTER 1 Introduction

1.1	Historical background.....	1
1.2	Analytical solution of elastica.....	3
1.3	Literature review, significance and applications of elastica.....	6
1.3.1	Kirchhoff analogy.....	6
1.3.2	Cosserat rod theory.....	7
1.3.3	Other study tools and discussion.....	8
1.3.4	Significance and applications.....	10
1.4	Scope and objective.....	14
1.5	Organization of thesis.....	14

CHAPTER 2 Modelling: Continuum and Discrete Models

2.1	Continuum model.....	16
2.1.1	Formulation based on equilibrium.....	16
2.1.2	Formulation based on energy method.....	17

2.2	Discrete model.....	19
2.2.1	Discrete system based on energy principle.....	19
2.2.2	Mechanical analogue of the discrete system based on equilibrium.....	22
2.3	Castigliano's first theorem and Lagrange multipliers.....	23
2.4	Alternative model.....	25
2.5	Boundary conditions.....	26
2.6	Extra constraints by sidewalls.....	28

CHAPTER 3 Numerical Techniques

3.1	Sequential quadratic programming (SQP).....	31
3.1.1	Necessary and sufficient conditions.....	31
3.1.2	Karush-Kuhn-Tucker conditions.....	33
3.1.3	Quasi-Newton approximation.....	34
3.1.4	Framework of SQP.....	35
3.2	Genetic algorithm.....	38
3.2.1	Selection.....	40
3.2.2	Genetic operators.....	41
3.2.3	Initialization and termination.....	42
3.2.4	Constraints handling.....	43
3.3	Framework of energy based search strategy.....	45
3.4	Shooting method.....	47
3.5	Pathfollowing strategy.....	49

CHAPTER 4 Numerical Examples and Applications

4.1	Elastica with two ends simply supported.....	51
4.1.1	Comparison study with analytical results.....	51
4.1.2	Path following study of the pin-pin elastica.....	53
4.1.3	Stability of post-buckling region.....	58
4.1.4	Shooting method.....	61
4.2	Elastica with one end clamped, one end pinned.....	64
4.3	Elastica with both ends clamped.....	70
4.4	Spatial elastica with both ends clamped.....	74
4.5	Spatial elastica with two ends clamped but not locate on x-axis.....	84
4.6	Pin-pin elastica with sidewall constraints.....	89
4.7	Other applications concereng elastic curve.....	98

CHAPTER 5 Conclusion and Recommendations

5.1	Conclusions.....	101
5.2	Recommendations for further study.....	101

REFERENCES.....	107
------------------------	------------

SUMMARY

Many of structural mechanics problems, such as post-buckling of elastica, elasticity of nanotubes and DNA molecules, require the study of elastic curves. The first step to understand the behaviour of such elastic curve is to determine the configurations. In order to achieve this goal, two methods can be employed. One is to search for one or multiple local energy minima of this geometric nonlinear problem based on Bernoulli's Principle. The other is to turn this boundary value problem into an initial value problem based on Kirchhoff's analogue. The former one is straightforward and can be easily implemented, hence our major numerical tool in this work. The behaviour of a perfect elastica under various boundary conditions and constraints will be the main subject to be studied.

Instead of utilizing elliptical integration to obtain the closed form solution of elastica, two discrete models are developed so that we can employ the numerical optimization techniques to solve this geometric nonlinear problem. The key difference between two models is the physical meaning of variables. Both models have their own advantages. One gives simple form of constrained optimization problem, while the other is more sensitive and is thus suitable for the study of instability in post-buckling region. Adopting either model, the problem to determine the post-buckling configuration of elastica can be expressed in a standard constrained optimization form. In addition, a penalty term can be added to address extra constraints imposed by the existence of sidewalls.

In order to minimize the energy of the discretized elastica, sequential quadratic programming (SQP) and genetic algorithm (GA) are employed. SQP is powerful to solve such minimization problem subject to nonlinear constraints. However, it requires

a good initial guess to guarantee convergence. GA, on the other hand, is robust and has no rigid requirement on initial guess. But GA alone is not computationally efficient to generate fine solutions especially when the optimization involves a large number of variables. To improve performance, two numerical tools are combined: using GA to generate a rough configuration, and then passing the result to SQP to produce the final result. The path-following strategy employing the same algorithm will enable us to further understand global behaviour of elastica. Extensive numerical examples are carried out to cover elastica under most end conditions. The problem of elastica under sidewalls constraints can also be easily solved using the same algorithm. Bifurcation is observed in such problem of constrained Euler buckling, and it is discussed from the viewpoint of energy.

This work develops discrete model for elastica, or elastic curve, and devises an algorithm to minimize the energy of such system. The algorithm combines the robustness of GA and computational efficiency of SQP. It is also straightforward and can be readily adjusted to apply to problems under different constraints.

Keywords: Elastica; Constrained Optimization; Sequential Quadratic Programming; Genetic Algorithm; Constrained Euler Buckling; Instability; Out-of-Plane Buckling.

NOTATIONS

a	Distance between two ends of elastica
$\mathcal{A}(x)$	Active constraint set
B_k	Approximation of Hessian
b	Parameter defining the characteristic of sidewall
C	A user-defined penalty weight
c	Displacement of the moving end in z direction
cp_i	The i th individual's cumulative probability
cr	Crossover rate
D	Displacement of the moving end in x direction
\mathbf{d}	Difference of $\mathbf{x} - \mathbf{x}^*$
E	Young's modulus
\mathcal{E}	Equality constraints set
F_i	The i th individual's fitness value
h_1, h_2	Distance from either sidewall to x axis
$h_i(x)$	The i th active constraint function
$h_{ie}(x), h_{il}(x)$	The i th equality / inequality constraint function
I	Moment of inertia of the cross section
\mathcal{I}	Inequality constraints set
$J(x)$	Jacobian matrix
K_i	Spring constant of elastic rotational spring connecting
L	Total length of elastica, usually normalized to 1 in this work
\mathcal{L}	Lagrangian function

\mathcal{N}	Neighborhood of set \mathcal{R}
P	Load applied at the ends of elastica
P_{cr}	Critical Euler buckling load
r	Random number
\mathcal{R}	Long term memory containing all existing solutions (updating continually)
s	Arc length
s_i	The i th segment length
U	Objective function
$W(x, \lambda)$	Hessian of Lagrangian function
w	Maximum deflection
X, Y	The parent in genetic algorithm mating pool
X', Y'	The offspring in genetic algorithm mating pool
\mathbf{x}^*	Local minimum
$\alpha(s)$	Slope of the tangent to the deformed elastica relative to the x axis
ϵ	A user defined small number
κ	Curvature
λ_1	Lagrange multiplier, reaction force in x direction
λ_2	Lagrange multiplier, reaction force in y direction
ψ_i	The i th variable, slope at the i th node with respect to x axis; Relative angle of adjacent two segments s_i and s_{i-1} in the alternative model
Π	Functional, total potential energy

LIST OF FIGURES

Figure 1.1	The Augusti column.....	3
Figure 1.2	Geometry of a classical elastica.....	4
Figure.2.5	Geometry of alternative discrete model.....	25
Figure 2.6	Elastica with sidewall constraints.....	28
Figure 2.7	Characteristics of the added penalty term.....	29
Figure 3.1	Flowchart of SQP.....	37
Figure 3.2	Flowchart of Genetic Algorithm.....	40
Figure 3.3	Framework of direct search using energy principle.....	47
Figure 3.4	Framework of path following strategy using energy principle.....	50
Figure.4.1	Basic Configurations with $a=0.3879$ (1,3,4) and $a=0$ (2).....	52
Figure 4.2	Configurations of elastica with $a=0.5$, both ends simply supported	53
Figure 4.3	Diagram of $D - \lambda_1 / P_{cr}$ (pin-pin elastica).....	54
Figure 4.4	Diagram of $D - M$ (pin-pin elastica).....	55
Figure 4.5	Diagram of $D - w / L$ (pin-pin elastica).....	55
Figure 4.6	Diagram of $D - PE$ (pin-pin elastica).....	56
Figure 4.7	Several typical configurations of pin-pin elastica.....	56
Figure 4.8	Superimposition of configurations of pin-pin elastica.....	58
Figure 4.9	Several configurations of pin-pin elastica when two ends meet.....	59
Figure 4.10	Diagram of $D - P / P_{cr}$ (pin-pin elastica, snap through happens when $D=1$).....	60
Figure 4.11	Superimposition of configurations of pin-pin elastica $D \in [0.5, 1.5]$ (Snap-through when $D = 1$).....	60
Figure 4.12	Configurations at first mode.....	62

Figure 4.13	Configurations at second mode.....	62
Figure 4.14	Configurations at third mode.....	63
Figure 4.15	Configurations at fourth mode.....	63
Figure 4.16	Diagram of $\psi_0 - P / P_{cr}$ (shooting method).....	64
Figure 4.17	Geometry of Clamp-pin elastica.....	64
Figure 4.18	Diagram of $D - P / P_{cr}$ (clamp-pin elastica).....	65
Figure 4.19	Diagram of $D - \lambda_2 / P_{cr}$ (clamp-pin elastica).....	66
Figure 4.20	Diagram of $D - M$ (clamp-pin elastica).....	66
Figure 4.21	Diagram of $D - PE$ (clamp-pin elastica).....	67
Figure 4.22	Several critical configurations of clamped-pinned elastica.....	67
Figure 4.23	Superimposition of all configurations of clamp-pin elastica.....	69
Figure 4.24	Geometry of planar clamp-clamp elastica.....	70
Figure 4.25	Diagram of $D - P / P_{cr}$ (clamp-clamp elastica).....	70
Figure 4.26	Diagram of $D - \lambda_2 / P_{cr}$ (clamp-clamp elastica).....	71
Figure 4.27	Diagram of $D - w / L$ (clamp-clamp elastica).....	71
Figure 4.28	Diagram of $D - M$ (clamp-clamp elastica).....	72
Figure 4.29	Diagram of $D - PE$ (clamp-clamp elastica).....	72
Figure.4.30	Several typical configurations of clamp-clamp elastica.....	73
Figure.4.31	Superimposition of all the configurations of clamp-clamp elastica ($D \in [0, 1.8]$).....	74
Figure 4.32	Geometry of spatial elastica with both ends clamped.....	74
Figure 4.33	Three kinds of deformation of spatial elastica.....	75
Figure 4.34	Geometry of a spatial rigid segment.....	76
Figure 4.35	Geometry of a spatial rigid segment with circular section.....	79
Figure 4.36	Several critical configurations of clamp-clamp elastica ($T = \pi$).....	81

Figure 4.37	Diagram of $D - \lambda_1 / P_{cr}$ (spatial clamp-clamp elastica).....	82
Figure 4.38	Diagram of $D - \lambda_3 / P_{cr}$ (spatial clamp-clamp elastica).....	82
Figure 4.39	Diagram of $D - \text{Strain energy}$ (spatial clamp-clamp elastica).....	83
Figure 4.40	Geometry of clamp-clamp spatial elastica (two ends paralell).....	84
Figure 4.41	Diagram of $c - \lambda_1 / P_{cr}$ (spatial clamp-clamp elastica, $D=0.7$).....	85
Figure 4.42	Diagram of $c - \lambda_3 / P_{cr}$ (spatial clamp-clamp elastica, $D=0.7$).....	85
Figure 4.43	Configurations when $D=0.7$ and $c=0$ (i), 0.18 (ii), 0.36 (iii).....	86
Figure 4.44	Diagram of $c - \lambda_1 / P_{cr}$ (spatial clamp-clamp elastica, $D=1$).....	87
Figure 4.45	Diagram of $c - \lambda_3 / P_{cr}$ (spatial clamp-clamp elastica, $D=1$).....	87
Figure 4.46	Configurations when $D=1$, $c=0, 0.1, 0.2$, and 0.3	88
Figure 4.47	Geometry of pin-pin elastica with side-wall constraints.....	89
Figure 4.48	Several configurations of pin-pin elastica with side-wall constraints ($h=0.25/L$).....	90
Figure 4.49	Diagram of $D - \lambda_1 / P_{cr}$ (pin-pin elastica, $h=0.25/L$).....	90
Figure 4.50	Diagram of $D - \lambda_2 / P_{cr}$ (pin-pin elastica, $h=0.25/L$).....	91
Figure 4.51	Diagram of $D - \lambda_2 / P_{cr}$ (the elastica jumps to asymmetric configuration that is opposite to the one shown in Fiugre 4.50).....	93
Figure 4.52	Critical configurations of pin-pin elastica with side-wall constraints ($h=0.15/L$).....	94
Figure 4.53	Configuration of second mode when two pin ends coincide.....	94
Figure 4.54	Diagram of $D - \lambda_1 / P_{cr}$ (constrained pin-pin elastica, $h=0.15/L$).....	95
Figure 4.55	Diagram of $D - \lambda_2 / P_{cr}$ (constrained pin-pin elastica, $h=0.15/L$).....	95
Figure 4.56	Diagram of $D - \text{Strain energy}$ (constrained pin-pin elastica, $h=0.15/L$).....	96
Figure 4.57	Demonstration of how asymmetric configuration evolves to symmetric Configuration.....	98

Figure 4.58	Using clamp-clamp elastica to represent half the revolution curve of Lipsome.....	99
Figure 4.59	Configurations of revolution curve of Lipsome.....	99
Figure 5.1	A tentative algorithm for constrained Euler buckling.....	106

LIST OF TABLES

Table 4.1	Comparison with analytical solutions.....	52
Table 4.2	Numerical results at configurations shown in Figure 4.7 (pin-pin).....	57
Table 4.3	Numerical results at configurations shown in Figure 4.22 (clamp-pin).....	68
Table 4.4	Numerical results at configurations shown in Figure 4.30 (clamp-clamp).....	73

CHAPTER 1 Introduction

This work is devoted to the post-buckling behavior of discrete elastica, or elastic chain. There are basically two ways to solve this problem. One is the energy based method, which solves this two point boundary value problem (BVP) based on Bernoulli's principle with the aid of broadly recognized and available optimization algorithm. Another way is to transform the two point BVP into an initial value problem (IVP); shooting technique is the main numerical tool for the latter way. These two methods are complementary to each other. But the energy method is the main subject developed and discussed in this thesis.

In this chapter, historical background, literature review, significance of this topic, and potential applications are discussed.

1.1 Historical background

Elastica problem has been connected to *Leonhard Euler* (1707-1783) since his investigation in 1744. He found 9 classes of solutions of elastic curve. The first one, which is a small excursion from the linear form and known as "*Euler* buckling load", is of practical importance in the past years. Since then, the variational method has been widely accepted in the field of mechanics. Preceding the work of *Euler*, *James Bernoulli* made a start in 1691 on the determination of the shape of any bent elastic structural member. He stated that the curvature of any point of a uniform beam, whose initial state is straight, is proportional to the bending moment at that point. After *Euler's* work in 1744, *Daniel Bernoulli* demonstrated that the resulting elastic curve of a bending beam gives minimum strain energy in terms of bending. It was also his suggestion to *Euler* that the calculus of variations should be applied to the inverse problem of finding the shape of the curve with given length, satisfying given end-

conditions of position and direction, so that the strain energy being minimized. *Lagrange* (1770) obtained the exact analytical solution in terms of elliptic integrals. *Navier* collected all these in his work in 1826, and gave a recognizably modern account of the small elastic deflections of beams. *Kirchhoff* found that the equation describing the equilibrium state of an elastic rod was mathematically identical to those describing the dynamics of heavy top. In twentieth century, *Love* and *Antman* also continually contributed to the problem of elastica.

What is elastica? In engineering applications, when a structure member is slender with the longitudinal dimension being much larger than the transverse dimensions, we call it a rod. Elastica belongs to this category. Besides its slenderness, it is assumed isotropic and hyperelastic, which ensures that nonlinearity arises only from the geometry configuration but not from the material characteristics. Therefore, only the centerline of the elastica is crucial to be studied. This centerline can be non-dimensionalized as a spatial curve.

In the field of structural engineering, our concern of buckling arises from the wide use of steel structure. The study of column and beam-column problems is mostly based on the linearized theory; buckling under critical load marks the collapse of a structural member. When a column is studied in a plane, linearized critical buckling is well known. Linearization may account for most problems of elastic columns with sufficient accuracy for practical applications. However, in studying of elastica, which may undergo large deformation, linearized approximation is not acceptable.

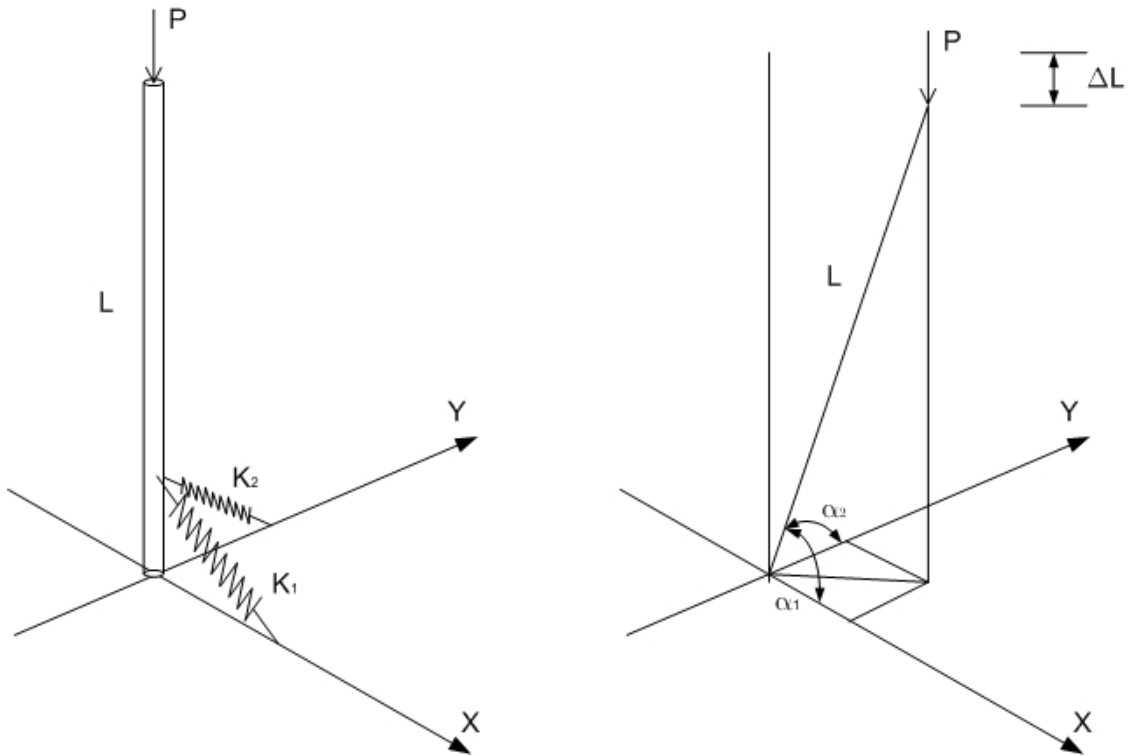


Figure 1.1 The Augusti column

If the critical buckling of a column with two degrees of freedom, Fig 1.1, is studied based on the linearization theory, as presented by Italian civil engineer *Augusti* in 1964, the column is under the interaction between two modes caused by K_1 and K_2 . The strain energy stored in the two elastic rotational springs is given by $\frac{1}{2}(K_1(\frac{\pi}{2}-\alpha_1)^2 + K_2(\frac{\pi}{2}-\alpha_2)^2)$ [Godoy, 2000]. This problem can be approximated using linear theory. However, when large deformation happens, the linear approximation is no longer valid. In the following section, we revisit first the analytical solution to the planar elastica problem.

1.2 Analytical solution of elastica

In linearized buckling analysis, the curvature of a column is approximated by $\frac{d^2y}{dx^2}$. When the critical buckling load is reached, indeterminate value, in terms of

lateral deflection, arises. However, the actual behaviour of elastica is not indeterminate. So, as a geometrically nonlinear elastic structure system, elastica requires us to use exact expression for curvature.

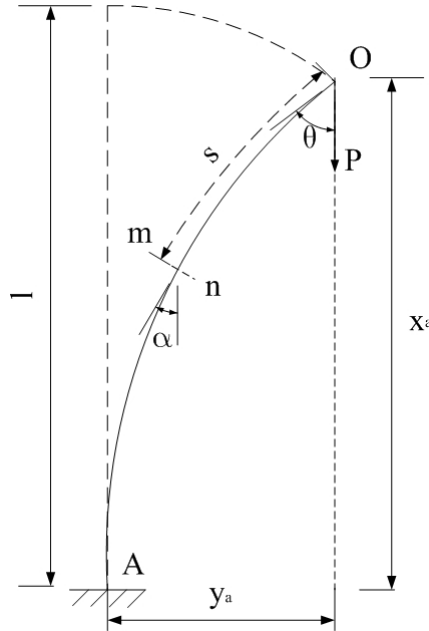


Figure 1.2 Geometry of a classical elastica

Considering the slender rod illustrated in Figure.1.2, we summarize briefly the classical solutions of a simple elastica [Timoshenko 1961]. The elastica considered is one end fixed and the other end free. Suppose the vertical load P applied at the free end is larger than the well known critical value $P_{cr} = \frac{\pi^2 EI}{4l^2}$. As shown in Fig. 1.2, the

arch length is denoted as s , measuring from the upper end, O . The exact expression for the curvature is $\frac{d\alpha}{ds}$, as indicated by *J. Bernoulli*, $M = EI\kappa$, where κ is the curvature.

The length change in longitudinal dimension is negligible for most structural materials.

The equilibrium of the moments gives:

$$EI \frac{d\alpha}{ds} = -Py \quad (1.1)$$

Differentiating (1.1) with respect to s and noticing the relationship $\frac{dy}{ds} = \sin \alpha$:

$$EI \frac{d^2\alpha}{ds^2} = -P \sin \alpha \quad (1.2)$$

Kirchhoff commented that the differential equation (1.2) is of the same form of the differential equation governing oscillations of pendulum. This analogy is well known as *Kirchhoff's dynamical analogy*. First, we can multiply both sides of (1.2) with $\frac{1}{EI}$

and integrate to obtain

$$\frac{1}{2} \left(\frac{d\alpha}{ds} \right)^2 = \left(\frac{P}{EI} \right) \cos \alpha + C \quad (1.3)$$

Now, taking the boundary condition into account:

$$\frac{d\alpha}{ds} = 0 \quad \text{at } s = 0; \quad \alpha = 0 \quad \text{at } s = l. \quad (1.4)$$

At $s = 0$, let $\theta = \alpha$ as illustrated in Figure.1.2, and substitute (1.4) into (1.3):

$$C = - \left(\frac{P}{EI} \right) \cos \theta \quad (1.5)$$

Finally, substitute (1.5) back into (1.3), after rearranging:

$$\frac{d\alpha}{ds} = \pm \left(\sqrt{\frac{2P}{EI}} \right) \sqrt{\cos \alpha - \cos \theta} \quad (1.6)$$

In the system shown in Figure.1.2, the curvature is always negative, thus the positive sign can be dropped. Integrate to the total length using (1.6) about ds :

$$l = \int ds = \int_0^\alpha \left(\sqrt{\frac{EI}{2P}} \frac{d\alpha}{\sqrt{\cos \alpha - \cos \theta}} \right) = \frac{1}{2} \sqrt{\frac{EI}{P}} \int_0^\theta \frac{d\alpha}{\sqrt{\sin^2 \frac{\theta}{2} - \sin^2 \frac{\alpha}{2}}} \quad (1.7)$$

After introducing new notation $p = \sin \frac{\theta}{2}$ and ϕ that satisfies $\sin \frac{\alpha}{2} = \sin \frac{\theta}{2} \sin \phi$, we

can simplify (1.7) into:

$$l = \sqrt{\frac{EI}{P}} \int_0^{\pi/2} \frac{d\phi}{\sqrt{1 - p^2 \sin^2 \phi}} = \sqrt{\frac{EI}{P}} K(p) \quad (1.8)$$

The value of $K(p)$ can be obtained by the *complete elliptic integration of the first kind*. To calculate the maximum deflection y_a and distance x_a , we can use the previous relationships and equations, and obtain:

$$y_a = 2p\sqrt{\frac{EI}{P}} \quad (1.9)$$

$$x_a = 2\sqrt{\frac{EI}{P}} \int_0^{\pi/2} \sqrt{1 - p^2 \sin^2 \phi} d\phi - l \quad (1.10)$$

The integral term in (1.10) is known as the *complete elliptic integral of the second kind*. The results derived above can be used to obtain other classes of elastic curves.

This can be done by joining the clamped-free elastic curve of $\frac{1}{2n}$ to obtain a new class,

where n is a positive integer. The shortcomings are, however, obvious. When the elastica is subjected to different boundary conditions or other constraints, or the elastica itself is non-uniform, it will be difficult and tedious, if not impossible, to obtain the closed-form analytical solutions.

1.3 Literature review, significance and applications of elastica

Although it is an old problem, the behavior of elastica has continuously aroused interests of researchers since it was first studied. The post-buckling behavior concerns the researchers not only in structural engineering, but also in various other fields.

1.3.1 Kirchhoff analogy

In the preceding section, *Kirchhoff's analogy* demonstrates that the static system governed by (1.2) can be solved using *Euler* equations describing the motion of a rigid body with a fixed point under external force field. This analogy is not limited to planar system, but spatial system as well. Based on this analogy, rich literature is

available, which studied particular configurations of the system. Love treated the helices [Love 1944]. Zajac analysed the elastica with two loops [Zajac 1962]. Goriely and Tabor's work was on the instability of helical rods [Goriely 1997a]. Goriely *et.al* also contributed to the loop and local buckling of nonlinear elastic filament [Goriely 1997b] [Goriely 1998]. Wang analyzed an elastica bent between two horizontal surfaces, with each end of the elastica tangential to one of the surfaces [Wang 1981]. Iseki *et.al* considered a curved strip compressed by a flat plate [Iseki 1989a] [Iseki 1989b].

1.3.2 Cosserat rod theory

Another important tool, which has been widely used, is the Cosserat rod theory. Duhem first introduced the concept of a directed media in 1893. Later, Cosserat brothers presented a systematic development of the theories for directed continua in 1909. The motion of a directed medium is characterized by the position vector as well as additional quantities, known as director. For a geometric nonlinear rod, the direction associated with the axis along the centerline is defined as the director. Two components constitute a Cosserat rod: directors along axis and material curves together with the collection of directors assigned to each particle that is able to deform independently. Basically, the rod is studied as an oriented body. As summarized in [Antman 1995], [Rubin 2000], and [Villaggio 1997], equilibrium gives a system of equations:

$$\frac{d}{ds} \vec{F} = 0 \quad (1.11)$$

$$\frac{d}{ds} \vec{M} = \vec{F} \times \vec{d}_3 \quad (1.12)$$

$$\frac{d}{ds} \vec{R} = \vec{d}_3 \quad (1.13)$$

$$\frac{d}{ds} \vec{d}_i = \vec{u} \times \vec{d}_i \quad (1.14)$$

$$\vec{M} = \begin{pmatrix} EI_1 & 0 & 0 \\ 0 & EI_2 & 0 \\ 0 & 0 & GJ \end{pmatrix} \vec{u} \quad (1.15)$$

In the above 7 equations, there are 7 unknowns to be solved. They are $\vec{F}(s)$, $\vec{M}(s)$, $\vec{R}(s)$, $\vec{d}_1(s)$, $\vec{d}_2(s)$, $\vec{d}_3(s)$, and $\vec{u}(s)$; $\vec{d}_1(s)$, $\vec{d}_2(s)$ and $\vec{d}_3(s)$ are generally defined as the right-handed rod-centered orthonormal co-ordinate frame. The vector $\vec{d}_3(s)$ is the local tangent to the rod center. While $\vec{d}_1(s)$ and $\vec{d}_2(s)$ are two vectors in the normal cross-section that chosen to enable us to follow the twist along the longitudinal dimension. As commented by *Neukirch et.al* [Neukirch 2001], this system is only integrable when $EI_1 = EI_2$. When the rod is described as an oriented body, the Euler angles are indispensable in the framework of Cosserat rod theory. Manning also utilizes Euler parameters to investigate the conjugate points of elastic rod buckling into a soft wall [Manning 1998]. M. B. Rubin has provided an in-depth summerization

In recent years, *Maddocks* [Maddocks 1999] [Maddocks 2000], *Thompsons* [Thompson 2000], and *Heijden* [Neukirch 2003] and their co-workers have investigated extensively spatial rods using cosserat rod theory. They also extended this elastic rod model into the modeling of supercoiled DNA, where the backbone of macromolecule was simplified using the elastic rod model. One of the typical implementation is introduced in section 1.3.4.

1.3.3 Other study tools and discussion

Kehrbaum and Maddocks also gave a Hamiltonia formulation in [Kehrbaum 1997]. G. Domokos and Philippe Holmes studied the chaotic behavior of discrete planar elastica. They applied the tool of symbolic dynamics and standard map to this problem.

Domokos also applied a group theory approach to the elastic ring. Shi and Hearst have obtained a closed form of the general solution of the static Kirchhoff equations for circular cross-section elastic rod using Schrödinger equation [Shi 1994].

The Kirchhoff's analogy only solves the initial value problem of a thin symmetric rod in equilibrium. It does not address the boundary value problem with the boundary points specified in a Cartesian coordinate, and the direction of force in the member is not known. Bifurcation phenomena may arise while following the path of equilibrium as the loading condition changes gradually. *Kirchhoff's* analogy also does not account for this problem.

To the author's knowledge, it was not until Kuznetsov's work [Kuznetsov 2002], has the stability of the equilibrium configurations of the column in the region of postcritical bending been investigated. In his work, pin-pin planar elastica is studied as Sturm-Liouville boundary value problem. Later, Heijden and Neukirch studied the instability spatial elastic rod [Heijden 2003].

Most of the methods used in the previous works studying the spatial elastica employ Euler angles to describe the system equilibrium: balance of momenta and director momenta. It results highly nonlinear forms of equations, and the closed form solution is elusive to obtain. Cosserat rod theory is also applicable to planar configurations of elastica. However, most of literature assumes readers' familiarity with tensor analysis in general curvilinear coordinates. They are not intelligible to many practicing structural engineers. Often, the constitutive equations are not in forms for nonlinear deformations, which are of interests in practical applications. In addition, although some closed-form solutions to certain continuum elasticity problem are available, the using of elliptical integration is not helpful when numerical results are

desired, especially when these numerical results are controlled rigidly by displacement or loading.

1.3.4 Significance and applications

Buckling and post-buckling behavior of the elastica has various applications and potential applications. On the one hand, these works are closely related to the engineering problems such as in ocean engineering. The formation of loop of under sea cable may cause the cable fail to function. Therefore, the study of configurations of elastica is important to the understanding of formation and elimination of the loops. The related literature can be found in [Coyne 1990] and [Tan 1992].

In fields other than civil engineering, post-buckling behaviours may be more widely observed. First of all, the behaviours of structures in micro and nano scales, for example, nano-tubes demonstrate geometrically nonlinearity. DNA as a kind of polymer is of great significance and focus of recent research. The elastic property of DNA is vital to our understanding toward how this macromolecule functions *in vivo*. Apart from the modelling of supercoiled DNA, post-buckling of elastica is also used to address the problems of fiber preparation of nonwoven fabrics such as polypropylene fibers [Domokos 1997]. In image processing of CAD, both the true nonlinear spline and image in painting process are closely related to elastica as well [Tony 2002], [Bruckstein 1996].

As the experimental techniques developing, manipulation in micro scale even nano scale becomes feasible. Structures under such scales usually demonstrate geometrical nonlinearity, whereas materially is still linearly elastic. Single walled nanotubes have been observed under high-resolution transmission electron microscopes to exhibit that they are capable of resisting compression, while fracture

are less likely to happen like normal carbon fibre. Under compression, buckling modes are observed and shown in Figure 1.3 and Figure 1.4 [Wagner 1999].

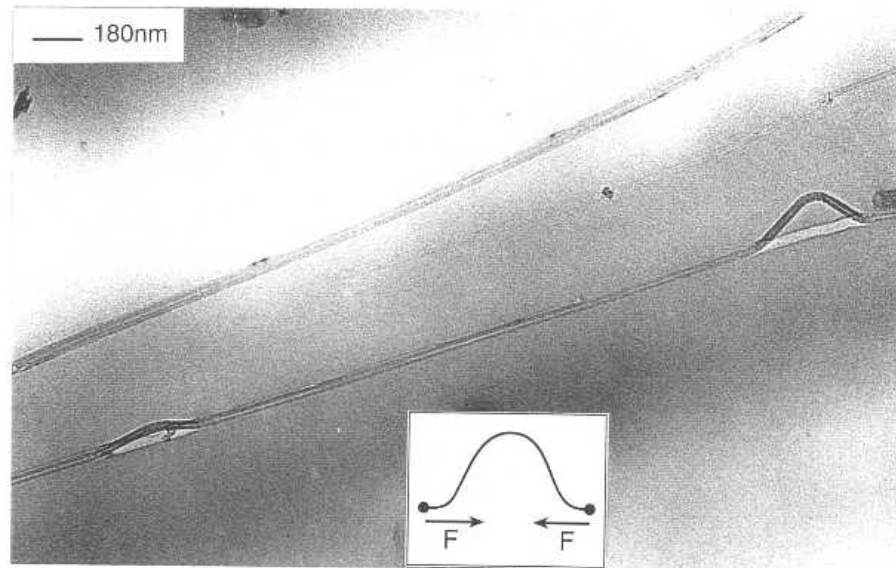


Figure 1.3 Planar Post-buckling of Nanotube [Wagner 1999]

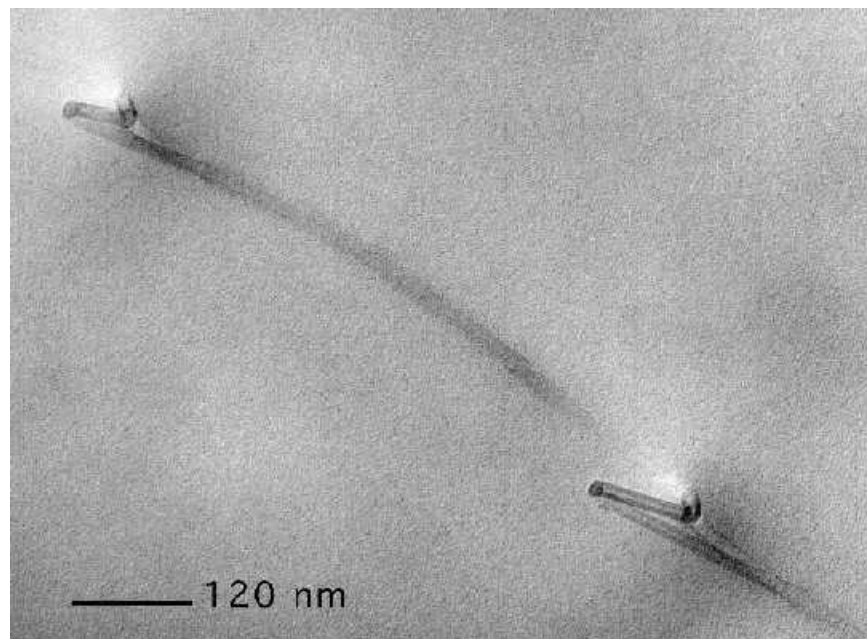


Figure.1.4 Spatial Post-buckling of Nanotube [Wagner 1999]

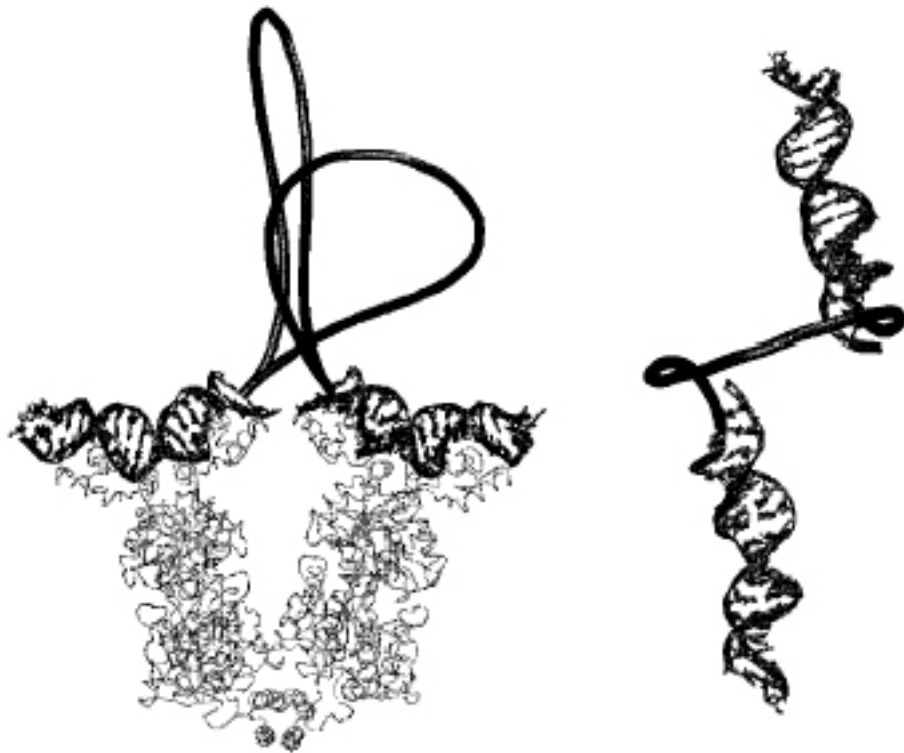


Figure 1.5 DNA modeling using elastic rod [Balaeff 1999]

In modeling the supercoiled structure of DNA, most works are done by assuming DNA as a naturally straight, inextensible elastic rod. An interesting model has been proposed by Kratky and Porod in 1949. The model describes all states between the two extreme models of the perfectly flexible chain with free rotation and perfectly rigid rod-shaped chain. It is known as the worm-like chain. Zhang et.al provided a model for DNA, and used Monte-Carlo simulations to study the elasticity of DNA structure [Zhang 2000]. These models include entropy as an important factor, but they are not within the scope of this work. However, the static equilibrium conformations of DNA are also of great importance. For example, Balaeff and his coworkers studied the *lac* repressor, one of the key enzymes in the lactose digestion chain of *E. coli* bacteria, using the theory of elasticity [Balaeff 1999]. The *lac* repressor works only through clamping two out of the three DNA sites. And between these sites,

the DNA must form a loop to interfere with reading the genes by another protein, the RNA polymerase. This is demonstrated in Figure.1.5. Shi and Hearst [Shi 1994] have obtained a closed form solution for time-independent, non-contact, one dimensional circular super-coiled DNA.

Elastica is also known as nonlinear splines in the industrial design context. The curve with functional form $\int(\alpha\kappa^2 + \beta)ds$, where κ is curvature of the curve, minimizes energy. The actual computation of nonlinear spline usually turns out to be quite difficult. Accordingly, simpler polynomial splines or rational curves, such as NURBS, are used to address the problem of shape design. On the other hand, it is also applicable to generate a discrete version of curve. Another application is the inpainting process. Inpainting is a set of techniques for making undetectable modifications to images. It can be used to reverse deterioration (e.g., cracks in photographs, scratches and dust spots in film), or to add or remove elements from a digital image. To a certain extent, the inpainting process can be viewed as a boundary value problem.

Not only rod itself can be related to elastica, some thin wall structures are closely related to elastica as well. For example, a long duct with circular cross-section subject to external load or self weight is closely related to the nonlinear curve after deformation. A sheet under different boundary condition is also within the scope of elastica. These problems also involve the contact phenomena. For example, the long pipe or duct as cylindrical shell usually rests on rigid ground. This category of problem is studied by Wang and Plaut et.al in [Wang 1981] and [Plaut 1999]. Another example in bio-engineering is the study of liposome, a kind of drug delivery structure. Liposome is modelled as an initial spherical membrane and subjected to point loads at antipodes [Pamplona 1993]. Assuming axis-symmetry, study of sphere will reduce to the planar revolution curve that generates the spherical surface.

From the above examples, we can see the importance of the study of this old problem even today. And the configuration of elastica is a necessity to our further comprehension of specific problems.

1.4 Scope and objective

This work is trying to investigate the post-buckling behaviours of elastica under various boundary conditions in a different perspective. An elastica is discretized to N rigid segments. Then this structural system is treated as a minimization problem subjected to different geometric constraints. We try to find out the post-buckling configurations of this system. Corresponding reaction forces can be obtained in terms of Lagrange multipliers. However, only static equilibrium configuration is computed and discussed. Dynamics is not within the scope of this work. Self contact is also not included in this text.

This work attempts to treat the post-buckling problem of elastica in a more straight-forward manner. It will be shown that the energy method developed here is efficient, universal and can be easily applied to problems with non-uniform system. As the numerical tools utilized are widely available, they can also be modified to meet specific requirement.

Main examples are trying to search the planar configurations. They will give the solutions under most geometric boundary conditions that encountered in applications. To demonstrate the capability of the energy based method proposed in this work, spatial configurations of both end clamped elastica are also addressed.

1.5 Organization of thesis

In this chapter, both historical background and literatures concerning elastica has been introduced. Then the significance of this topic and potential applications are

discussed. In chapter 2, the model of discretized planar elastica is defined and justified. Based on the model in chapter 2, numerical techniques employed are introduced in chapter 3. Genetic algorithm, sequential quadratic programming and shooting method will be presented separately. The framework of algorithm is then developed. In chapter 4, configurations of elastica with various geometric boundary conditions are computed. Their corresponding behavior is also discussed. Numerical examples include planar elastica and spatial elastica. Planar elastica comprise three mostly encountered cases: pin-pin elastica, clamp-pin elastica, and clamp-clamp elastica. When both ends of elastica are clamped, and the system is not confined in a plane, the elastica can deform out of plane at a certain stage. Therefore, we also study the spatial elastica whose both ends are clamped. Two different cases will be studied. One is that the tangents of both ends are located on one axis, x axis in this work. Another case is that the two tangents of both ends are parallel with each other while x -axis cannot connect them. In chapter 5, conclusions will be reached and suggestions for further study will be discussed.

CHAPTER 2 Modeling: Continuum and Discrete Models

In this chapter, we consider a slender rod, which possesses the material property of linear elasticity. For simplicity, the rod will be taken to be inextensible, unshearable and initially straight (no intrinsic curvature). It can be uniform or non-uniform, but we firstly model this structure with uniform cross-section and bending stiffness EI , where E denoting Young's modulus and I the moment of inertia of the cross-section. The total length of the rod is normalized to 1 without losing generality. The rod is subjected to end load P , whose load line passes through ends. The boundary conditions can be various: both ends simply supported; both ends clamped; one end-clamped while the other simply supported. Here, we will first demonstrate the more classical and well studied case: both ends simply supported. The other boundary conditions will be discussed in the following sections. In the last section of this chapter, we will also discuss the planar elastica constrained between two side walls. The aim of this chapter is to develop discrete models of elastica for the later search of configurations. Configuration of a structural system is defined as the simultaneous positions of all the material points of the system. Dynamic effect is neglected throughout this work. Only modelling of planar elastica is introduced in this chapter. Spatial elastica can be considered as extension of planar one. The modeling of spatial elastica will be given in chapter 4 as an example.

2.1 Continuum model

2.1.1 Formulation based on equilibrium

Euler provided an essentially complete analysis of the classical problem [Euler 1774], which will be summarized below.

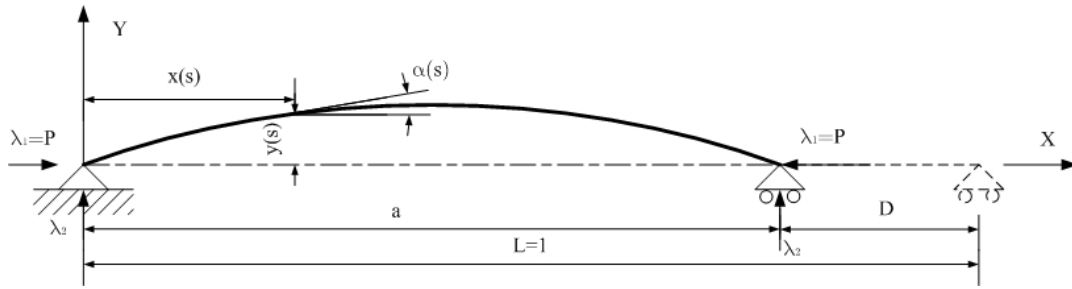


Figure 2.1 Geometry of Euler strut

As shown in Figure 2.1, the deformed configuration of Euler strut is modeled by a plane curve $(x(s), y(s))$ parameterized by the arc length $s \in [0,1]$. Assuming that the structure has infinite shear and axial stiffness, which implies the rod is inextensible and unshearable, the equilibrium equations may be reduced to the single second-order

ODE in terms of the slope $\alpha = \tan^{-1}\left(\frac{dy}{dx}\right)$:

$$EI\alpha'' + P \sin \alpha = 0 \tag{2.1}$$

, where $(\)'$ denotes d/ds . The boundary conditions for this simply supported case are zero moment at both ends:

$$\alpha'(0) = 0 = \alpha'(1) \tag{2.2}$$

As pointed out in [Kirchhoff 1859], the elastica equilibrium problem is analogous to the pendulum equation. The analogy suggests that the results for the dynamic initial value problem can be used in studying continuous model of the static boundary value problem.

2.1.2 Formulation based on energy method

Instead of using equilibrium to obtain governing equation, a classical way to obtain (2.1) is energy method. As stated in Bernoulli's principle, such a nonlinear elastic system possesses stationary potential energy when in static equilibrium configuration. The total potential energy of the system, neglecting dynamic effect, is

$$V = \frac{1}{2} \int_0^1 EI \alpha'^2 ds - PD \quad (2.3)$$

$$D = 1 - \int_0^1 \cos \alpha ds \quad (2.4)$$

$\alpha(s)$ is treated here as a function of arc length along the elastica, $s \in [0, 1]$. However, we require that $\alpha(s)$ satisfies the relationship

$$\int_0^1 \sin \alpha ds = 0 \quad (2.5)$$

, which express the equal ordinates of the two ends.

Using (2.3), (2.4) and (2.5), we can construct the functional

$$\Pi = \frac{1}{2} \int_0^1 EI \alpha'^2 ds - P(1 - \int_0^1 \cos \alpha ds) + \lambda_2 \int_0^1 \sin \alpha ds = 0 \quad (2.6)$$

, where λ_2 is a Lagrange multiplier. Set the first variation of (2.6) equal to zero, we get:

$$EI \alpha'' + P \sin \alpha + \lambda_2 \cos \alpha = 0 \quad (2.7)$$

, with the boundary conditions (2.2). If we integrate (2.7) and take (2.5) and boundary conditions (2.2) into account, we obtain

$$\lambda_2 \int_0^1 \cos \alpha ds = 0 \quad (2.8)$$

Equation (2.8) is satisfied with the following three cases:

$$\lambda_2 = 0, \quad \int_0^1 \cos \alpha ds \neq 0 \quad (\text{case A}) \quad (2.9)$$

$$\lambda_2 = 0, \quad \int_0^1 \cos \alpha ds = 0 \quad (\text{case B}) \quad (2.10)$$

$$\lambda_2 \neq 0, \quad \int_0^1 \cos \alpha ds = 0 \quad (\text{case C}) \quad (2.11)$$

Note that $\int_0^1 \cos \alpha ds$ has the meaning of $1 - D$ or a , thus case A is when the two ends of elastica don't meet. While case B and case C are when two supports meet. For case A, (2.7) and (2.1) unifies.

The solutions to the above continuum model can be found in two ways as presented in chapter 1. One is via elliptic integration. The other can be obtained by numerical solution of the Sturm-Liouville problem. [Kuznetsov 2002]

2.2 Discrete model

Although the solutions of closed form to continuums model are well studied and available, when the problems are non-uniform or other extra constraints exist, a discrete model for computational convenience is necessary. The discretized model is also convenient to obtain numerical results.

2.2.1 Discrete system based on energy principle

The elastica illustrated in Figure 2.1 can be discretized into n rigid segments, joined by linear rotational spring as in Fig 2.2. The length of each segment is s_i ($i = 1, \dots, n$). And the spring constant of elastic rotational spring connecting s_{i-1} and s_i is K_i . For a simply supported case, K_1 is zero. We adopt the variables, slopes at each node with respect to x axis, as ψ_i ($i = 1, \dots, n$). With all the variables determined, the configuration of elastica is determined. The convention of sign of each variable is illustrated in Figure 2.2.

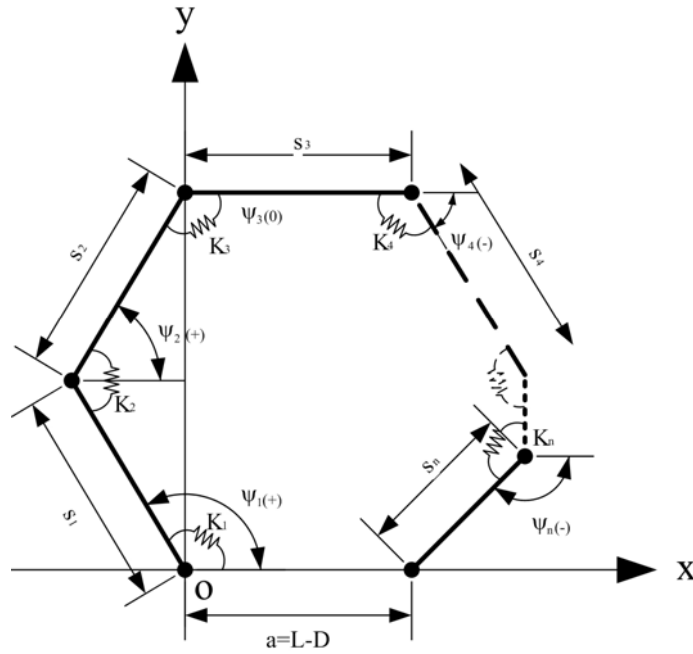


Fig 2.2 Geometry of discretized model

From solid mechanics, we know that the relationship between bending moment and the change of curvature is

$$M = EI\kappa \tag{2.12}$$

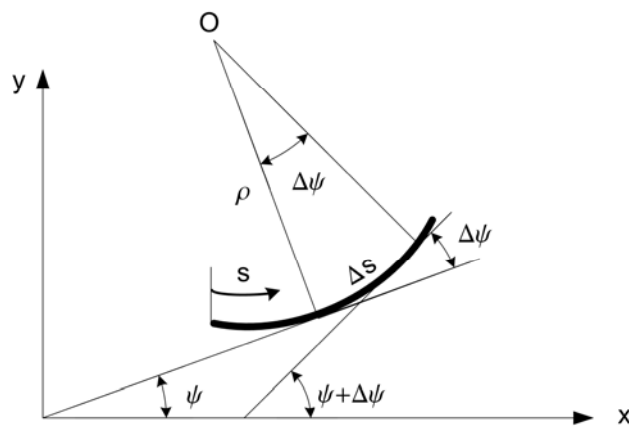


Figure 2.3 Curvature

EI is the bending stiffness of the rod, while $\kappa = \frac{1}{\rho} = \frac{d\psi}{ds}$ is curvature for a continual

bar as shown in Figure 2.3. s is the arc length measured from a starting point, and

$\Delta\psi$ is the change of inclination angle with respect to x axis.

The expression (2.12) can be therefore approximated in the form of finite difference:

$$M = EI \frac{d\psi}{ds} = EI \lim_{\Delta s \rightarrow 0} \frac{\Delta\psi}{\Delta s} \simeq EI \frac{\Delta\psi}{\Delta s} = \frac{EI}{\Delta s} \Delta\psi \quad (2.13)$$

We can define the stiffness of the elastic moment spring as

$$K_i \simeq \frac{EI}{\Delta s} = \frac{2EI}{(s_{i-1} + s_i)} \quad (2.14)$$

Finally, we can write the strain energy of the system as the sum of elastic energy in each linear moment spring

$$U_m = \sum_{i=1}^{n-1} \frac{1}{2} K_i \Delta\psi_i^2 = \sum_{i=2}^n \frac{1}{2} K_i (\psi_i - \psi_{i-1})^2 \quad (2.15)$$

Compare the above expression for a discrete system with the strain energy expression for a continuous system, we can see

$$U_m = \sum_i^n \frac{1}{2} K_m \Delta\psi_i^2 = \sum_i^n \frac{1}{2} EI \left(\frac{\Delta\psi_i}{\Delta s} \right)^2 \Delta s \rightarrow \int \frac{1}{2} EI (\psi')^2 ds \quad (2.16)$$

when $\Delta s \rightarrow 0$ and $n \rightarrow \infty$.

Different from the continuum model, we treat the nonlinear elastic system with discrete model as a minimization problem subjected to geometric constraints. Under the same geometric constraints, such a nonlinear system may possess different configurations corresponding to different energy levels. With a specified end displacement D , which will be considered a geometric constraint, we hope to find various configurations based on energy method. The reaction forces at ends will also be obtained. Setting the origin at the left side of the initial straight elastica, two geometric constrains are expressed in terms of Cartesian coordinates of the other end: $x_{n+1}(s) = a$, and $y_{n+1}(s) = 0$. As we start from origin, x_{n+1} and y_{n+1} depend on all the variables ψ_i ($i = 1, \dots, N$).

Now we express the objective function and geometric constraints in the standard form, i.e.:

$$obj: U = \frac{1}{2} \sum_{i=2}^n K_i (\psi_i - \psi_{i-1})^2 \tag{2.17}$$

$$s.t.: \begin{aligned} h_{1e} &= -a + \sum_{i=1}^n s_i \cos(\psi_i) = 0 \\ h_{2e} &= \sum_{i=1}^n s_i \sin(\psi_i) = 0 \end{aligned} \tag{2.18}$$

U is the strain energy we want to minimize, h_{1e} and h_{2e} are the equality constraints we need to be satisfied. Both objective function and constraints are nonlinear, therefore, an efficient nonlinear constraints satisfying optimization method is needed. SQP will be employed to tackle this nonlinear minimization problem. GA will also be an assistant method. They will be introduced in chapter 3.

2.2.2 Mechanical analogue of the discrete system based on equilibrium

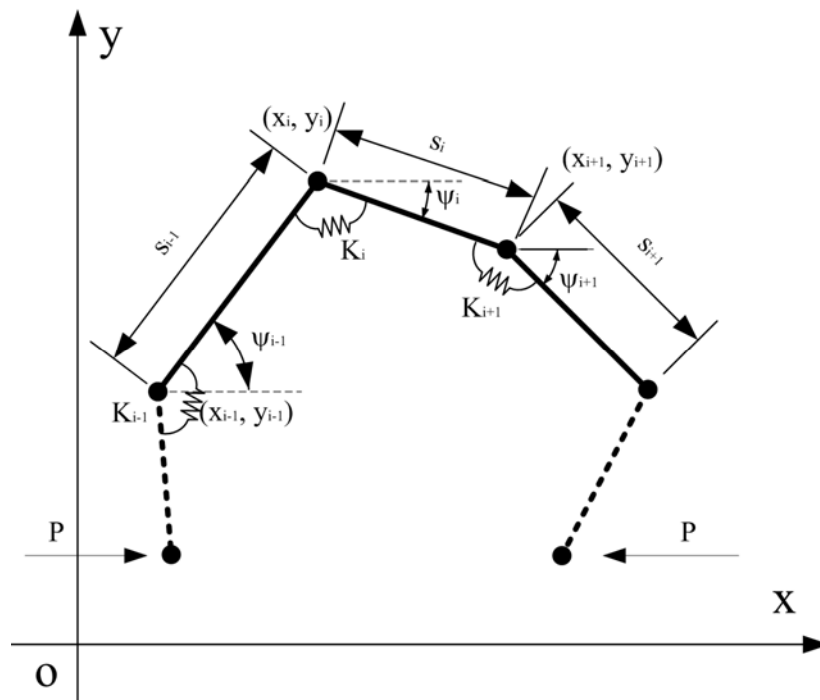


Figure 2.4 Free body of discretized pin-pin elastica

Using the discrete model illustrated in Figure 2.2, we may solve this system from equilibrium as well. This method is not the main concern of this work. But it is useful to study elastica under higher mode. For complete reason, it will be discussed here.

We take any segment s_i out of the simply supported discrete elastica. From equilibrium condition, and noticing that at each nodal point, the force in x direction is P , while the force in y direction is zero, we can write:

$$y_{i+1} = y_i + s_i \sin \psi_i \quad (2.19)$$

$$K_i(\psi_{i+1} - \psi_i) + Py_{i+1} = 0 \quad (2.20)$$

Substitute (2.19) into (2.20) and rearrange, we get

$$\psi_{i+1} = \psi_i - \frac{P}{K_i}(y_i + s_i \sin \psi_i) \quad (2.21)$$

(2.21) can be viewed as an implicit euler scheme to integrate forward with step-size s_i .

Considering the whole system illustrated in Figure.2.2, boundary conditions are stated as

$$y_1 = 0 = y_{n+1} \quad (2.22)$$

Since one end of elastica is set at origin of x - y coordinate, we can solve this two-point boundary value problem as an initial value problem. Shooting method is applicable.

2.3 Castigliano's first theorem and Lagrange multipliers

To solve a constrained optimization problem such as shown in (2.17) and (2.18), the main strategy is to turn the constraint satisfying problem (CSP) into unconstraint problem. One can construct either a weighted penalty function or a Lagrangian function. As will be discussed in the next chapter, Lagrangian function is

adopted in solving the problem. We demonstrate here the physical meaning of Lagrange multipliers.

To our interests, the Lagrange multiplier method is preferred due to the physical meaning of Lagrange multipliers. The Lagrangian function is constructed:

$$\mathcal{L}(\boldsymbol{\psi}, \boldsymbol{\lambda}) = U(\boldsymbol{\psi}) - \lambda_1 h_{1e}(\boldsymbol{\psi}) - \lambda_2 h_{2e}(\boldsymbol{\psi}) \quad (2.23)$$

The necessary condition for a local minimum is that the first order gradient of Lagrange function at a local minimum equals to zero, i.e.

$$\nabla_{\boldsymbol{\psi}} \mathcal{L}(\boldsymbol{\psi}^*, \boldsymbol{\lambda}^*) = U_{\boldsymbol{\psi}}(\boldsymbol{\psi}^*) - \mathbf{h}_{\boldsymbol{\psi}}(\boldsymbol{\psi}^*) \boldsymbol{\lambda} = 0 \quad (2.24)$$

where the subscript $(\)_{\boldsymbol{\psi}}$ denotes differentiation; $\boldsymbol{\psi}^*$ and $\boldsymbol{\lambda}^*$ are the local optimum and corresponding Lagrange multipliers. Comparing (2.24) with (2.7), we can see that they agree exactly in form. From the analogue, λ_1 and λ_2 apparently have the physical meaning of reaction forces at supports in x and y direction respectfully. In another strict manner, we can prove with Castigliano's first theorem.

Cotterill-Castigliano's first theorem: Differentiating the internal work of a system with respect to the deformation at a certain point gives the singular force at the same point.

Let $\boldsymbol{\psi}^*$ be a local minimum, the differential of the objective function is then:

$$dU(\boldsymbol{\psi}^*) = \sum_{i=0}^{n+1} \frac{\partial U}{\partial \psi_i} d\psi_i = U_{\boldsymbol{\psi}}(\boldsymbol{\psi}^*) d\boldsymbol{\psi} \quad (2.25)$$

From Eq (2.24), we have $U_{\boldsymbol{\psi}}(\boldsymbol{\psi}^*) = \mathbf{h}_{\boldsymbol{\psi}}(\boldsymbol{\psi}^*) \boldsymbol{\lambda}$, which can be substituted into Eq (2.25) to give:

$$dU(\boldsymbol{\psi}^*) = d\mathbf{h}(\boldsymbol{\psi}^*) \boldsymbol{\lambda} \quad (2.26)$$

In this case, the function U is the strain energy, while the constraints \mathbf{h} can be related to the displacements in x and y directions. Therefore, the Lagrange multipliers

λ should be the forces needed for the system to satisfy the corresponding displacement constraints or, in other words, the reaction forces. Unless stated otherwise, λ_1 will be associated with the reaction force in x direction; while λ_2 will be associated with the reaction force in y direction.

2.4 Alternative model

Different from the discrete model in Figure.2.2, we can set the unknowns as the relative change of angle from previous segment.

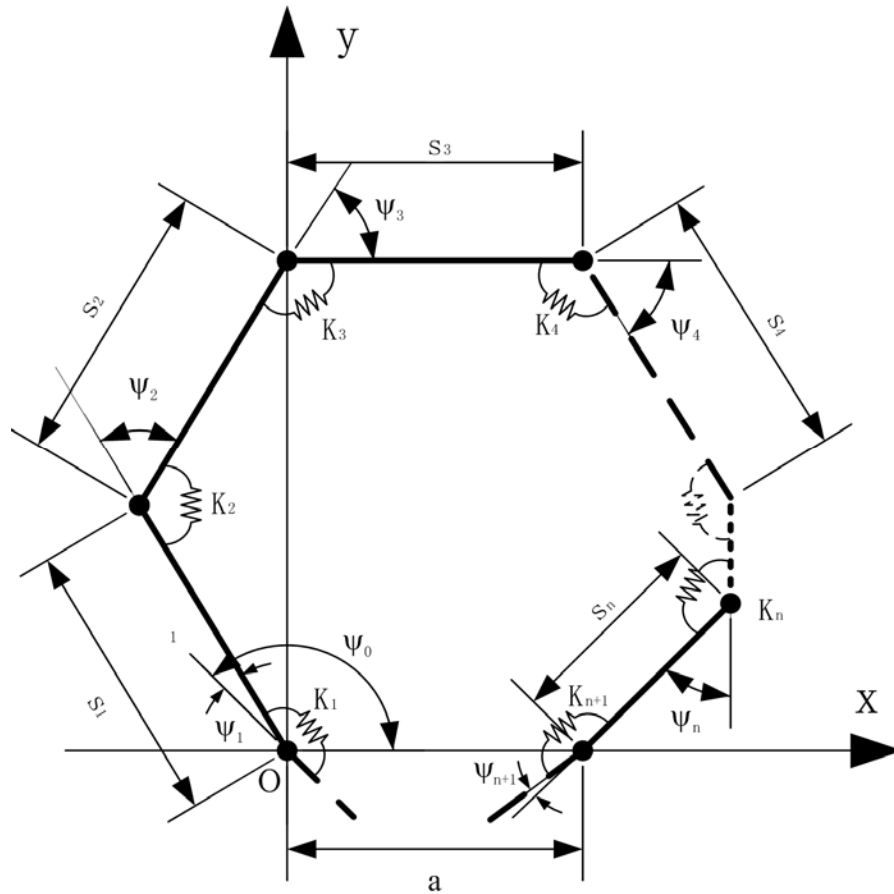


Figure.2.5 Geometry of alternative discrete model

We can see that $\psi_1, \dots, \psi_{n+1}$ are the relative angle of adjacent two segments s_i and s_{i-1} . ψ_0 is however the initial angle with respect to x axis. And two fictitious

segments are added at two ends. For this model, we can express the problem in standard form of optimization as:

$$obj: U = \frac{1}{2} \sum_{i=1}^{n+1} K_i \psi_i^2 \quad (2.27)$$

$$s.t.: \quad h_{1e} = -a + \sum_{i=1}^n s_i \cos\left(\sum_{j=0}^i \psi_j\right) = 0$$

$$h_{2e} = \sum_{i=1}^n s_i \sin\left(\sum_{j=0}^i \psi_j\right) = 0 \quad (2.28)$$

The key difference between this model and the previous model is the physical meaning of variables. Because the relative angles are small in magnitude, the searching procedure will be more susceptible to perturbations. If the aim is to find as many local optima as possible under the same boundary conditions and constraints, this model is preferable. In addition, it is more convenient to describe the boundary conditions. However, it is apparent from a comparison between equations (2.18) and (2.28) that the latter equality constraints are more complicated in form. Therefore, it is likely that the numerical error will be higher.

With Eqns (2.27) and (2.28), a Lagrangian function can also be constructed. Since the two equality constraints have the same meaning as (2.17) and (2.18), the Lagrange multipliers has the same meaning as proved in section 2.3.

2.5 Boundary conditions

In the above models, boundary conditions are not directly included. For equilibrium considerations, we need to check the boundary conditions. For a pin-pin case, if we include the boundary conditions directly as constraints, additional constraints will cause computational difficulty, and it may not be efficient to do so. Because there are no constraints to confine rotation at the two ends for pin-pin case, the solutions obtained, which are the local minima under current geometrical equality

constraints, should have lower energy than the ones of elastica with one end or both clamped. The boundary conditions should already be fulfilled.

For the model illustrated in Figure.2.5, we can check the boundary conditions for a pin-pin case:

$$\psi_1 \leq \varepsilon; \quad \psi_{n+1} \leq \varepsilon; \quad \lambda_2 / \lambda_1 \leq \varepsilon \quad (2.29)$$

where ε is a small number. The first two terms in (2.29) ensure that the moments at both ends are zero. The third term checks if the reaction force at support is zero.

The other boundary conditions are studied in this work as well, and they are summarized below:

Clamped-Clamped:

$$\psi_0 = 0; \quad \sum_{i=0}^{n+1} \psi_i = 2k\pi \quad (k = 0, \pm 1, \pm 2, \dots) \quad (2.30)$$

Clamped-Pin:

$$\psi_0 = 0; \quad \psi_{n+1} \leq \varepsilon \quad (2.31)$$

The boundary condition for a clamp-free case is:

$$\psi_0 = 0 \quad (2.32)$$

Note that the geometric constrains stated in (2.18) or (2.28) should be revised. Since one end is fixed at origin, and we still have the moving end displacement D as control parameter, the constraint is only in x direction but not in y direction. Different from the pin-pin end condition, wherever the clamp end condition is to be imposed, (2.30) or the first expression in (2.31) should be included as geometric constraints. ψ_0 is not necessary 0, but can be arbitrary angle according to how the coordinate system is defined.

2.6 Extra constraints by sidewalls

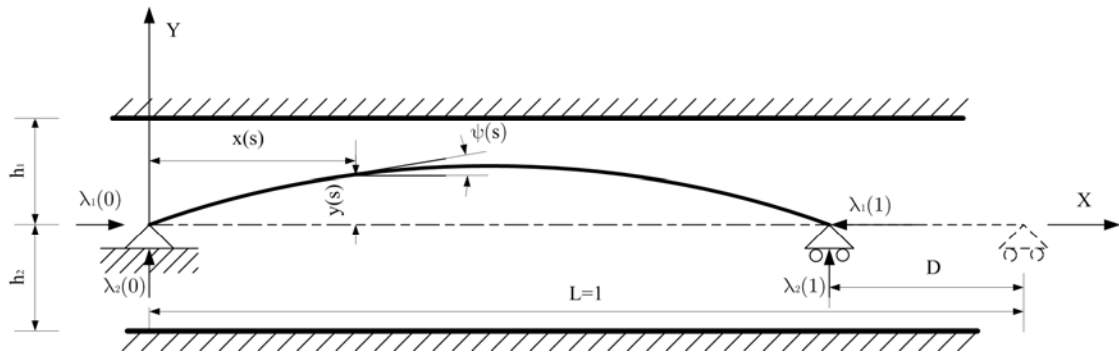


Figure 2.6 Elastica with sidewall constraints

In engineering application, elastica may be subjected to constraints from sidewalls. The sidewall may be either on one side or on both sides. If only one sidewall exists, elastica is free to deflect to the side where no sidewall exists. We will demonstrate the use of numerical strategy to approximate the solution.

The geometry of this problem is illustrated in Figure 2.6. The sidewall on either side of x axis has distance h_1 and h_2 from x respectively. The other notations have exactly the same meaning stated in preceding sections. It is pointed out that due to the existence of sidewalls, $\lambda_2(0)$ may not equal to $\lambda_2(1)$. Detailed discussion can be found in Chapter 4.

Generally, the sidewall is assumed rigid and frictionless. But an approximation is made by constructing a penalty function of (2.17):

$$obj: U = \frac{1}{2} \sum_{i=2}^n K_i (\psi_i - \psi_{i-1})^2 + \sum_{i=2}^n \left(\frac{b}{y_i + h_1} - \frac{b}{y_i - h_2} \right) \tag{2.33}$$

in which b can be considered a characteristic of the sidewall. The sidewall is no longer perfectly rigid, but “soft”. And b describes how “soft” or how “hard” the sidewalls are.

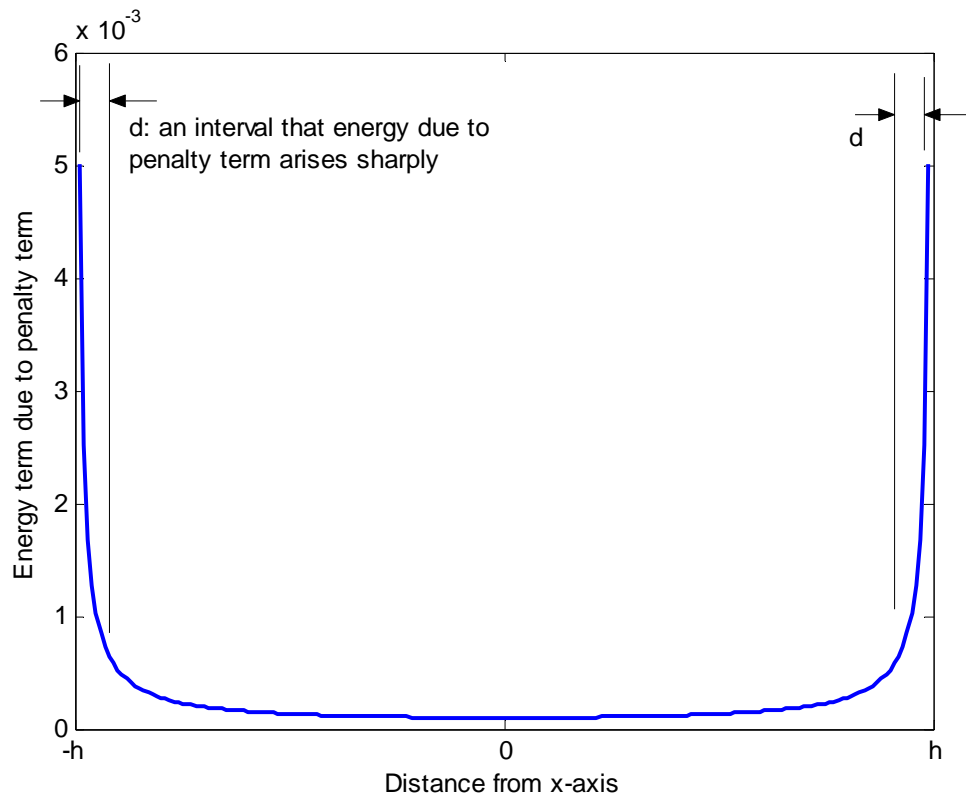


Figure 2.7 Characteristics of the added penalty term

Figure.2.7 demonstrates the effect of the added penalty term on the objective function. When the deformed elastica approaches either or both sides of the sidewalls, the potential energy, which is the objective function to be minimized, will arise sharply. In such a way, the configurations of elastica searched are still based on the energy principle.

Nevertheless, it is apparent that the characteristic parameter, b , is critical to how close equation (2.33) approximates the real situation. The smaller in magnitude b is, the closer equation (2.33) approximates to rigid wall. On the other hand, if we set b too small, the computation will be difficult to continue. As we evaluate the potential energy at each nodal point, there will be a number of segments affected. If within a certain interval d the potential energy arises largely, while the discrete segment length s_i is not small enough, the solution may show that the elastica can penetrate into the

sidewalls. For example, when s_i is more than twice the interval d , the “penetration” can happen. The penalty term can only force the points away from the sidewall, but cannot prevent the penetration if the segment length is not small enough. Therefore, the parameter b needs to be tuned according to the number of segments. Another unsatisfactory comes from the approximation itself. The elastica is never impossible to contact the sidewalls. The point contact, line contact and secondary buckling happen at a fictitious wall with a distance h smaller than the real one. Consequently, if we require a better approximation concerning the distance of sidewall, we need to adjust the h in equation (2.33) slightly larger than what we expect. It may be necessary for us to fine-tune this constant to achieve what we expect.

CHAPTER 3 Numerical Techniques

The problem of elastica can be presented in two manners. One is based on Bernoulli's principle, while the other is based on equilibrium of the system. To study the system using a discrete model, we employ genetic algorithm and sequential quadratic programming as the numerical techniques to minimize the total potential energy. Concerning the equilibrium of the system, Kirchhoff's analogue suggests that we can handle this boundary value problem as an initial value problem. Naturally, the shooting method will be the choice. First, in this chapter, these three numerical techniques are briefly introduced. Then they are associated with the model described in the Chapter 2.

3.1 Sequential quadratic programming (SQP)

The sequential quadratic programming is widely accepted as one of the most efficient optimization techniques for constrained nonlinear optimization problems. SQP outperforms other optimization approach especially when constraints are nonlinear, which is the characteristic of the model presented in chapter 2. Before the overall framework of algorithm is depicted, we revisit some basic concepts on optimization and constraints satisfaction that related to the discrete model of elastica.

3.1.1 Necessary and sufficient conditions

From Taylor's series expansion including only the linear term, we can have the approximate expression of function $f(\mathbf{x})$ about a local minimum \mathbf{x}^* :

$$f(\mathbf{x}) \approx f(\mathbf{x}^*) + \nabla f(\mathbf{x}^*)(\mathbf{x} - \mathbf{x}^*) \quad (3.1)$$

For \mathbf{x}^* to be a local minimum, the following expression must be satisfied for all \mathbf{x} in the small neighborhood of \mathbf{x}^* :

$$f(x) - f(x^*) \geq 0 \quad (3.2)$$

Substitute the approximation of $f(\mathbf{x})$ in (3.1) into (3.2), and define $\mathbf{d} = \mathbf{x} - \mathbf{x}^*$ to get:

$$\nabla f(\mathbf{x}^*)^T \mathbf{d} \geq 0 \quad (3.3)$$

Since \mathbf{d} can be either positive or negative, in order to satisfy the above condition, the gradient of $f(\mathbf{x})$ at \mathbf{x}^* , $\nabla f(\mathbf{x}^*)$, must be zero. Thus, the first order necessary condition is

$$\nabla f(\mathbf{x}^*) = 0 \quad (3.4)$$

However, following the above procedure, one can derive the same necessary condition even if \mathbf{x}^* is a maximum or inflection. Therefore, to ensure one point in the solution space to be a local minimum, sufficient condition must be satisfied as well.

Again, expand $f(\mathbf{x})$ about \mathbf{x}^* using Taylor's series, but in quadratic form this time:

$$f(x) \approx f(\mathbf{x}^*) + \nabla f(\mathbf{x}^*)^T (\mathbf{x} - \mathbf{x}^*) + \frac{1}{2} (\mathbf{x} - \mathbf{x}^*)^T \nabla^2 f(\mathbf{x}^*) (\mathbf{x} - \mathbf{x}^*)$$

or

$$f(x) = f(\mathbf{x}^*) + \nabla f(\mathbf{x}^*)^T \mathbf{d} + \frac{1}{2} \mathbf{d}^T \nabla^2 f(\mathbf{x}^*) \mathbf{d} \quad (3.5)$$

Substitute (3.5) into (3.2):

$$\nabla f(\mathbf{x}^*)^T \mathbf{d} + \frac{1}{2} \mathbf{d}^T \nabla^2 f(\mathbf{x}^*) \mathbf{d} \geq 0 \quad (3.6)$$

From necessary condition derived above, which states that $\nabla f(\mathbf{x}^*) = 0$, (3.6) yields:

$$\frac{1}{2} \mathbf{d}^T \nabla^2 f(\mathbf{x}^*) \mathbf{d} \geq 0 \quad (3.7)$$

In the quadratic form on the left hand side of (3.7), the sign is decided by the Hessian matrix $\nabla^2 f(\mathbf{x}^*)$. Corresponding to different status of Hessian matrix, one can write the corresponding sufficient conditions:

- a) \mathbf{x}^* is a local minimum, if Hessian matrix $\nabla^2 f(\mathbf{x}^*)$ is positive definite;
- b) \mathbf{x}^* is a local maximum, if Hessian matrix $\nabla^2 f(\mathbf{x}^*)$ is negative definite;
- c) \mathbf{x}^* is a inflection point, if Hessian matrix $\nabla^2 f(\mathbf{x}^*)$ is indefinite;
- d) status of \mathbf{x}^* cannot be determined at this order, if Hessian matrix $\nabla^2 f(\mathbf{x}^*)$ is semidefinite.

3.1.2 Karush-Kuhn-Tucker conditions

In the previous section, the necessary and sufficient conditions of optimization problems are summarized briefly. However, the discrete model of elastica should be viewed as a constraints-satisfying minimization problem with (2.17) subject to (2.18). The two geometric constraints are equality constraints. Thus, it is necessary to introduce *Lagrangian* function and *Karush-Kuhn-Tucker* conditions (KKT conditions).

The constraint satisfying optimization has the standard form of

$$\begin{aligned} \min \quad & f(x) \\ \text{s.t.} \quad & \begin{cases} h_i(x) = 0, & i \in \mathcal{E} \\ h_i(x) \leq 0, & i \in \mathcal{I} \end{cases} \end{aligned} \quad (3.8)$$

Considering the optimization problem of (3.8), Lagrangian function is expressed as:

$$\mathcal{L}(\mathbf{x}, \boldsymbol{\lambda}) = f(\mathbf{x}) - \sum_{i \in \mathcal{E} \cup \mathcal{I}} \lambda_i h_i(\mathbf{x}) \quad (3.9)$$

In the above equation, \mathbf{x} is the vector of unknowns, $\boldsymbol{\lambda}$ is the vector of Lagrange multipliers, $f(\mathbf{x})$ is the objective function, \mathcal{E} is the set of equality constraints, \mathcal{I} is the set of inequality constraints, while $h_i(\mathbf{x})$ and λ_i are the constraint and the corresponding Lagrange multiplier. The active set $\mathcal{A}(x)$ is the union of the equality constraints set \mathcal{E} with the indices of the active inequality constraints: $\mathcal{A}(\mathbf{x}) = \mathcal{E} \cup \{i \in \mathcal{I} \mid h_{i'}(\mathbf{x}) = 0\}$. If the set of active constraint gradients

$\{\nabla h_i(\mathbf{x}^*), i \in A(\mathbf{x}^*)\}$ is linearly independent, we say that \mathbf{x}^* at active set $\mathcal{A}(\mathbf{x}^*)$, the linear independence constraint qualification holds.

Suppose that \mathbf{x}^* is a local solution of (3.8), and the linear independence constraint qualification holds, there is a Lagrange multiplier vector $\boldsymbol{\lambda}^*$, with components λ_i^* , $i \in \mathcal{E} \cup \mathcal{I}$, such that the following conditions are satisfied at $(\mathbf{x}^*, \boldsymbol{\lambda}^*)$

$$\begin{aligned} \nabla_x \mathcal{L}(\mathbf{x}^*, \boldsymbol{\lambda}^*) &= 0, \\ h_i(\mathbf{x}^*) &= 0, \quad \text{for all } i \in \mathcal{E}, \\ h_i(\mathbf{x}^*) &\leq 0, \quad \text{for all } i \in \mathcal{I}, \\ \lambda_i^* &\geq 0, \quad \text{for all } i \in \mathcal{I}, \\ \lambda_i^* h_i(\mathbf{x}^*) &= 0, \quad \text{for all } i \in \mathcal{E} \cup \mathcal{I} \end{aligned} \tag{3.10}$$

As in our model of (2.17) and (2.18), only the equality constraints are of our interests. The next sections develop algorithm address only equality constraints. The methods are, however, not only restricted to equality constraints problems. When inequality constraints are necessary to meet, the basic idea is to transform the inequality constraints into equality constraints by relaxation coefficients. [Nocedal 1999]

3.1.3 Quasi-Newton approximation

Bearing in mind that SQP is an iterative optimization technique for smooth problem, we need to find the search direction and step length at each iteration utilizing the derivative information of Lagrangian function. Steepest descent method is a line search method that utilizes only the gradients, but not the second derivatives. This brings the disadvantage of slow convergence. Newton's direction is preferred, but it uses the second derivatives, *Hessian*. And when $\nabla^2 f_k$ or $\nabla^2 \mathcal{L}_k$ is not positive definite, the Newton direction cannot even be defined, since $\nabla^2 f_k^{-1}$ may not exist. Quasi-Newton method is invented to avoid the excessive computational cost of Hessian.

Quasi-Newton method approximates the Hessian with the information gained at each step. There are several updating schemes. Named after its inventors, *Broyden*, *Fletcher*, *Goldfarb*, and *Shanno*, BFGS formula is defined as

$$B_{k+1} = B_k - \frac{B_k s_k s_k^T B_k}{s_k^T B_k s_k} + \frac{y_k y_k^T}{y_k^T s_k} \quad (3.11)$$

In (3.11), k is the current iterate index, B_k is the approximation of Hessian, while y_k and s_k are defined as

$$s_k = x_{k+1} - x_k \quad (3.12)$$

$$y_k = \nabla f_{k+1} - \nabla f_k \quad (3.13)$$

The initial approximation B_0 must be chosen by the user. To satisfy the equality constraints, (3.13) need to be modified using Lagrangian function:

$$y_k = \nabla_x \mathcal{L}(x_{k+1}, \lambda_{k+1}) - \nabla_x L(x_k, \lambda_k) \quad (3.14)$$

3.1.4 Framework of SQP

We denote Jacobian matrix of the constraints in (3.9) as

$$J(x) = [\nabla h_1(x), \nabla h_2(x), \dots, \nabla h_m(x)]^T \quad (3.15)$$

Since only equality constraints are considered, i.e., only the terms involving equality constraints in KKT conditions (3.10), we can obtain a system of $n + m$ equations with n and m standing for the number of unknowns and constraints respectively:

$$F(x, \lambda) = \begin{bmatrix} \nabla f(x) - J(x)^T \lambda \\ h(x) \end{bmatrix} = 0 \quad (3.16)$$

Denote the Hessian of the Lagrangian with:

$$W(x, \lambda) = \nabla_{xx}^2 \mathcal{L}(x, \lambda) \quad (3.17)$$

Jacobian of (3.16) is:

$$\begin{bmatrix} W(x, \lambda) & -J(x)^T \\ J(x) & 0 \end{bmatrix} \quad (3.18)$$

The Newton step from the iterate (x_k, λ_k) is thus given by

$$\begin{bmatrix} x_{k+1} \\ \lambda_{k+1} \end{bmatrix} = \begin{bmatrix} x_k \\ \lambda_k \end{bmatrix} + \begin{bmatrix} p_k \\ p_\lambda \end{bmatrix} \quad (3.19)$$

, where p_k and p_λ can be found by solving the KKT system

$$\begin{bmatrix} W(x, \lambda) & -J(x)^T \\ J(x) & 0 \end{bmatrix} \begin{bmatrix} p_k \\ p_\lambda \end{bmatrix} = \begin{bmatrix} -\nabla f(x) + J(x)^T \lambda \\ -h(x) \end{bmatrix} \quad (3.20)$$

Both x_k and λ_k are updated simultaneously until the convergence criterion is reached.

The convergence criterion is set as

$$\nabla f_k < \varepsilon, \quad \text{and} \quad h_{ik} < \varepsilon \quad (3.21)$$

In (3.21), ε is a user-defined small number. The framework of the algorithm is depicted in the following flowchart.

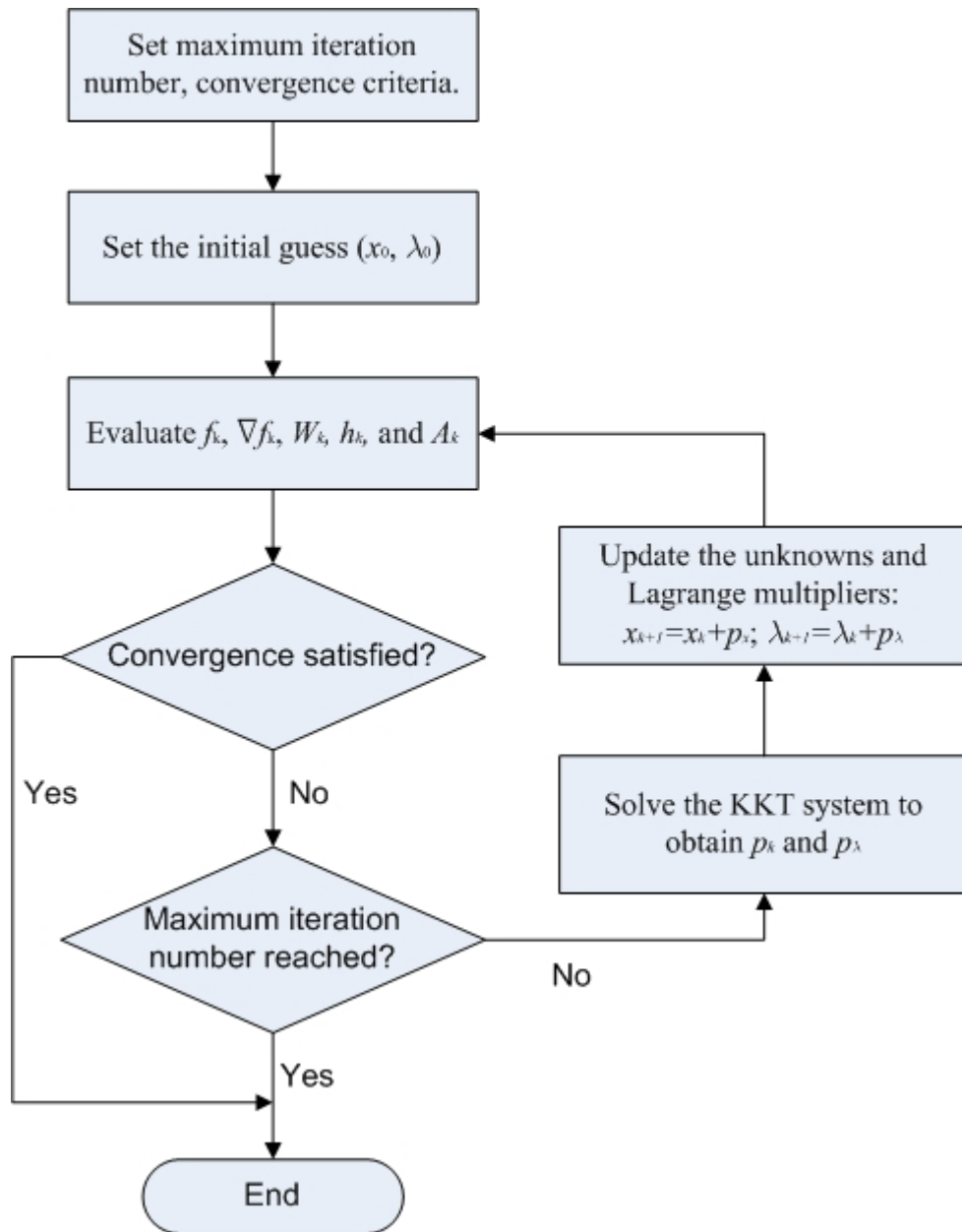


Figure 3.1 Flowchart of SQP

Powell suggested that Hessian should be kept positive definite even though the Hessian might be positive indefinite at a local solution. A positive definite Hessian is maintained providing $y_k^T s_k$ is positive at each update and that B_k is initialized with a positive definite matrix. When $y_k^T s_k$ is not positive, y_k is modified on an element-by-element basis so that $y_k^T s_k > 0$. At the initial stage, the smallest element of $y_k^T s_k$ is

halved until $y_k^T s_k > \varepsilon$, with ε being a small number. If $y_k^T s_k$ is still not positive, we modify y_k in the following way:

$$y_k = y_k + wv \quad (3.22)$$

Here, w is a scalar, while the vector v is

$$v_i = \begin{cases} \nabla h_i(x_{k+1}) \cdot h_i(x_{k+1}) - \nabla h_i(x_k) \cdot h_i(x_k), & \text{if } (y_k)_i \cdot w < 0 \text{ and } (q_k)_i \cdot (s_k)_i < 0 \\ 0, & \text{otherwise} \end{cases} \quad (3.23)$$

And we increase w systematically until $y_k^T s_k$ is positive. (cf. [Powell 1978], [MathWorks 2003])

For SQP, it may be efficient to converge to a local solution, but a good initial guess plays critical role in the searching procedure. Convergence is not guaranteed when the initial guess strays away from a local minimum.

3.2 Genetic algorithm

Inspired by the Nature, genetic algorithm (GA) embraces the doctrine that “the fittest survives”. Basically, GA is a stochastic sampling method. Unlike the descent methods, such as SQP, GA utilizes no characteristics of the problem itself to determine the next sampling point. Instead, GA utilizes the rule of selection among a population, and simulates the evolution. Two genetic operators, crossover and mutation, especially the latter, play important roles in the procedure of this kind of simulated evolution. We can describe GA as a population based search strategy, because in every generation, a population is maintained with certain number of individuals. Generation by generation, the population reproduce themselves, and mutate, approaching the optimum.

Chromosome represents and describes each individual of our interests. Based on the type of chromosome, there are two versions of GA. One is binary version, which represents the individual as binary digits, i.e. 0 and 1, and operates bit by bit.

This requires the transformation of real unknowns into binary strings and manipulates the binary strings during crossover and mutation operations. Then, we need to transform the binary string back into real values to evaluate the fitness values and make the selection based on these fitness values. The other is the real version. During the simulated evolution, we maintain the real value unknowns as they are, and utilize specially designed crossover and mutation operations. Michalewicz has done extensive numerical experimentations to compare real-valued and binary GA [Michalewicz 1994]. His work demonstrates that real value GA outperforms its counterpart in terms of CPU time required. Accordingly, we choose the real value GA in this work.

Since we employ GA as a mechanism to provide reasonable initial guess, only the operations we exercised in this work are introduced. But before that, the following figure is a simple flowchart that involves the entire essential elements in GA. More detailed introduction and discussion are available in these references: [Goldberg 1989], [Michalewicz 1994], and [Haupt 1997].

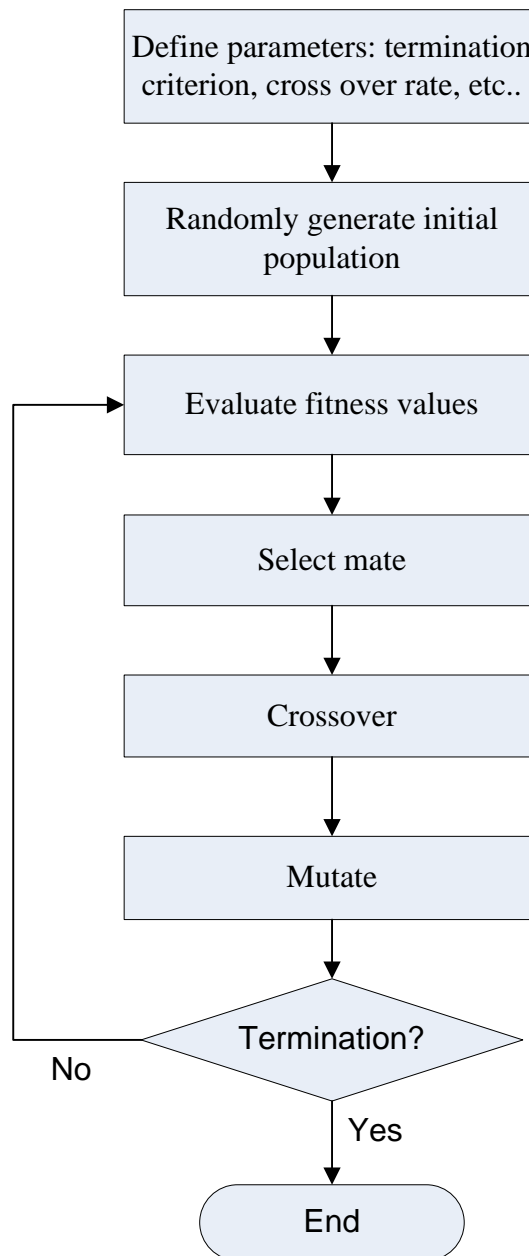


Figure 3.2 Flowchart of Genetic Algorithm

3.2.1 Selection

Since GA lets the strongest individuals to survive and to have higher possibility to reproduce, the selection function is undoubtedly critical to the success of GA optimization. There are several types of selection function: the roulette wheel selection, scaling techniques, tournament and ranking methods. [Goldberg 1989; Michalewicz 1994]

First developed by Holland [Holland 1975], the roulette wheel selection is used in this work. The probability of each individual in population is defined as:

$$p_i = \frac{F_i}{\sum_{j=1}^m F_j} \quad (3.24)$$

where m is the population size, F_i is the i th individual's fitness value. Then, the cumulative probability is calculated:

$$cp_i = \sum_{j=1}^i p_j \quad (3.25)$$

where cp_i is the cumulative probability for the i th individual. Each time, we select a single chromosome for a new population in this way:

- Generate a random number r within the range $[0, 1]$;
- If $r < cp_1$, then select the first chromosome; otherwise, select the i th chromosome such that $cp_{i-1} < r < cp_i$.

Note that we must make sure the fitness values being positive. Otherwise, we should utilize the scaling mechanism.

3.2.2 Genetic operators

Genetic operators are used to manipulate the chromosomes selected by the selection function to generate the new population. We call the new population as offspring and the former selected chromosomes as parents. As the real value GA is used, the crossover may not be identical to the biology concept of “crossover” as in binary GA. A simple arithmetic crossover operator is used and defined as

$$\begin{aligned} X' &= crX + (1-cr)Y \\ Y' &= (1-cr)X + crY \end{aligned} \quad (3.26)$$

where X' and Y' are the offspring, X and Y are the parents, and $cr \in (0, 1)$ is the crossover rate chosen by the user. Another plausible crossover operation is heuristic crossover. Heuristic crossover applies a linear extrapolation to create new offsprings. By exploring new area to check whether a point with better fitness value exists, offspring produced by this method may exceed the boundary set by parents. The extrapolation direction is decided by the fitness value of parents. If X outperforms Y , the fitness value tends to decrease in the direction from Y to X . Hence this direction should be tried. The heuristic crossover is expressed as below:

$$X' = X + cr(Y - X) \quad (3.27)$$

$$Y' = X \quad (3.28)$$

We choose 0.6 as the crossover rate and the uniform mutation schedule, which randomly selects one variable, k , and sets it equal to an uniform random $U(a_i, b_i)$:

$$x_i' = \begin{cases} U(a_i, b_i), & \text{if } i = j \\ x_i, & \text{otherwise} \end{cases} \quad (3.29)$$

Here, x_i is a real value unknown of the problem, a_i and b_i are lower and upper bound of x_i respectively.

3.2.3 Initialization and termination

An initial population must be provided for GA to start. Since we assume that we have no prior knowledge toward the optimum, the initial population is just generated randomly within the bounds of each unknown.

Termination criterion is generally set as either maximum generation number or an anticipated fitness value that the problem should converge to. However, it will be too costly to do so. Because the aim to utilize GA is to provide a good initial guess for SQP, we set the criterion as the lack of improvement. That is, when the evolution does

not improve further in terms of fitness value within a pre-defined generation number, the search will be terminated.

3.2.4 Constraints handling

Normally, GA is efficient and widely used for unconstrained optimization problems. For constrained optimization problems, which are common in many engineering problems, one common approach is to convert the original problem into an unconstrained one by either a weighted penalty function or a Lagrangian function. Another approach is to manipulate the searching region to allow only feasible solutions in the population. The latter approach excludes infeasible solutions by either discarding the infeasible solutions whenever they appear, or using specialized operators that maintain the feasibility. This technique may be very effective on certain specialized problems. But when the infeasible solutions arise too frequently, or the portion of the infeasible searching region outnumbers that of the feasible region, it will be over costly to maintain the feasibility. The situation may be worse for a problem with nonlinear equality constraints. This is largely due to stochastic nature of GA. On the other hand, a more direct way is to transform the constrained optimization problem into an unconstrained problem by adding a penalty term. The penalty can be either constant or adaptive. If a constant penalty weight is used, the magnitude of the penalty can significantly affect the search procedure. When the penalty weight is too “heavy”, many individuals in the mating pool that are not strictly compatible with the constraints will become extinct too early in the GA evolution. The population will lose diversity and premature convergence will result. Penalty will also cause the searching region being too “rugged” to find a good solution in. In contrast, if the weight is too “light”, the searching procedure will be very hard to converge to the correct solution. Therefore, the choice of weight depends largely on the user’s experience and judgment.

It is almost sure that re-tuning of the weight either before or during searching procedure is inevitable.

In this work, an adaptive penalty function is utilized. The fitness evaluation function is composed of the gradient of the Lagrangian function and the constraints; the Lagrange multipliers are evaluated from the least squares condition of the local minimum [Moerder and Pamadi, 1994]. Following the same approach, we construct the fitness evaluation function based on the model presented in chapter 2. From (2.17) and (2.18), but not limited to them, we construct the Lagrangian function as:

$$\mathcal{L}(\boldsymbol{\psi}, \boldsymbol{\lambda}) = U(\boldsymbol{\psi}) - \mathbf{h}\boldsymbol{\lambda} \quad (3.30)$$

in which U , $\boldsymbol{\psi}$, \mathbf{h} , $\boldsymbol{\lambda}$ are the objective function, vector of variables, vector of equality constraints, and vector of Lagrange multipliers respectively. If $(\boldsymbol{\psi}^*, \boldsymbol{\lambda}^*)$ is a local solution, the following equation can be obtained from KKT condition (3.10):

$$\nabla_{\boldsymbol{\psi}} \mathcal{L}(\boldsymbol{\psi}^*, \boldsymbol{\lambda}^*) = U_{\boldsymbol{\psi}}(\boldsymbol{\psi}^*) - \mathbf{h}_{\boldsymbol{\psi}}(\boldsymbol{\psi}^*)\boldsymbol{\lambda}^* = 0 \quad (3.31)$$

where the subscript indicates differentiation with respect to $\boldsymbol{\psi}$. In this approach, the Lagrange multipliers are not treated as independent variables as in SQP. From (3.31), we estimate the value of Lagrange multipliers at each evaluation by:

$$\begin{pmatrix} \lambda_1 \\ \lambda_2 \\ \vdots \\ \lambda_m \end{pmatrix} = \begin{pmatrix} h_{1\psi_1} & h_{2\psi_1} & \cdots & h_{m\psi_1} \\ h_{1\psi_2} & h_{2\psi_2} & \cdots & h_{m\psi_2} \\ \vdots & \vdots & \ddots & \vdots \\ h_{1\psi_n} & h_{2\psi_n} & \cdots & h_{m\psi_n} \end{pmatrix}^{\dagger} \begin{pmatrix} U_{\psi_1} \\ U_{\psi_2} \\ \vdots \\ U_{\psi_n} \end{pmatrix} \quad (3.32)$$

in which $h_j(\boldsymbol{\psi})$ ($j=1, \dots, m$) is the j -th equality constraint, m is the number of equality constraints, and n is the number of variables. The operator \dagger denotes Moore-Penrose inversion or pseudo-inversion defined as:

$$\mathbf{h}^{\dagger} = (\mathbf{h}_{\boldsymbol{\psi}}^T \mathbf{h}_{\boldsymbol{\psi}})^{-1} \mathbf{h}_{\boldsymbol{\psi}}^T \quad (3.33)$$

The fitness evaluation function is constructed as follows:

$$F(\boldsymbol{\psi}, \boldsymbol{\lambda}) = \sum_{i=1}^n |\mathcal{L}_{\psi_i}(\boldsymbol{\psi}, \boldsymbol{\lambda})| + \sum_{j=1}^m |h_j(\boldsymbol{\psi})| \quad (3.34)$$

Once the Lagrange multipliers are estimated using (3.32), the fitness evaluation function is only a function of $\boldsymbol{\psi}$. This constructed fitness evaluation function has the advantage that we know the anticipated fitness value for a local solution should be zero. Even though, we cannot afford to have GA terminated when the fitness values approaches zero. This is because of the nonlinearity in both the objective function and equality constraints. Numerical experiments also demonstrate that it is inefficient to do so.

3.3 Framework of energy based search strategy

Two numerical techniques have already been introduced in the preceding sections. We can find that both techniques have their own advantages and disadvantages. SQP is efficient to produce a satisfying local solution provided that it starts from a promising initial guess. However, SQP does not guarantee the convergence. If we want to find the global minimum, SQP is well known for its easily being trapped at a local minimum. On the other hand, due to its stochastic nature, the results of GA search are often not satisfactory for problems with a large number of unknowns and nonlinear constraints, such as the problem studied in this work. The difficulty is actually twofold: firstly, the search with GA alone can hardly yield a reasonable result when the number of unknowns is large; secondly, if the resolution of the searching space is high, which is a necessary condition for getting reasonable results, the computation cost will be prohibitive.

The advantages of SQP and GA are what we want to utilize. By utilizing the gradient information of the objective function and constraints, SQP is effective and efficient for searching a local optimum. GA has two advantages. One is that we do not

need to know the characteristics of the solution and can start with randomly selected initial guesses and then let GA evolves toward the solution. The other advantage is that it can possibly jump out of a local minimum and find the global minimum. This latter advantage benefits from GA's population-based search strategy.

Viewing these attributes, we can combine the two methods and utilize them at different stage of our search. We first use GA to roughly optimize the model with a randomly generated start point. When GA cannot achieve the improvement for a certain generations, we let SQP take over. The result obtained by GA is then set as the initial guess for SQP. If the aim is just to find one local optimum, this will be all. If more local optima are required under the same constraints, we can start GA again with a newly randomly generated initial population. To avoid GA generating results close to those have been obtained, a penalty term can be added to the fitness evaluation function defined in (3.34):

$$F(\boldsymbol{\psi}, \boldsymbol{\lambda}) = \sum_{i=1}^n |\mathcal{L}_{\psi_i}(\boldsymbol{\psi}, \boldsymbol{\lambda})| + \sum_{j=1}^m |h_j(\boldsymbol{\psi})| + C\zeta \quad (3.35)$$

where C is a user-defined penalty weight, ζ is defined as

$$\zeta = \begin{cases} 1 & \text{if } \boldsymbol{\psi} \in \mathcal{N} \\ 0 & \text{otherwise} \end{cases} \quad (3.36)$$

where \mathcal{N} is the neighborhood of the set \mathcal{R} containing all existing solutions. \mathcal{R} is a long-term memory including the randomly generated initial population for GA, terminated population of GA, and the solutions obtained after SQP is terminated successfully. This set will be updated continually.

Assume that we do not know the characteristics of solutions; direct search is performed using the following flow chart.

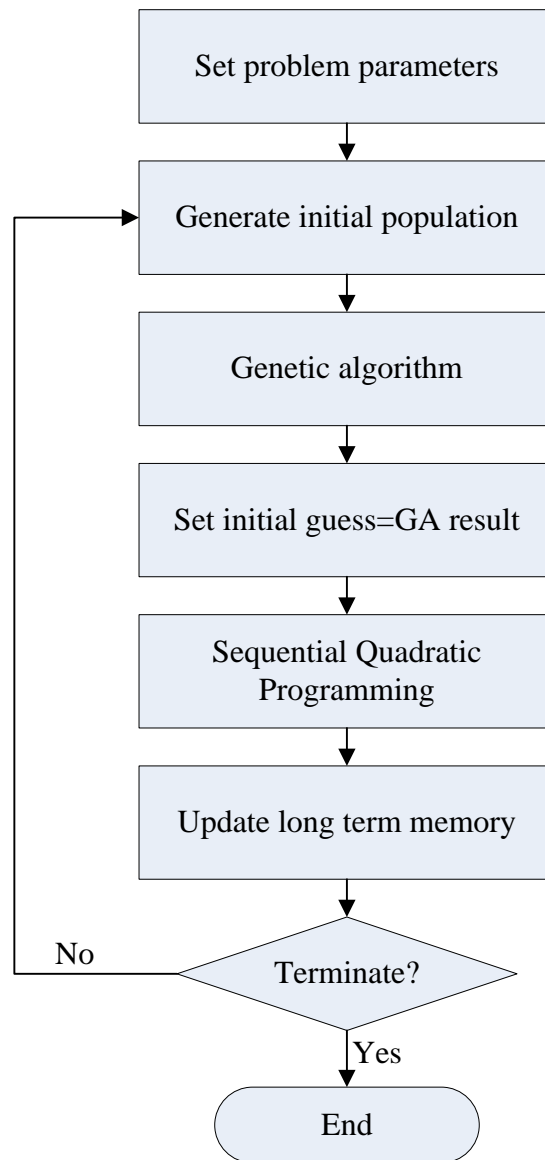


Figure 3.3 Framework of direct search using energy principle

Comparing with the shooting method introduced in the next section, this method will be more universal and especially suitable for elastica under different the boundary conditions or subject to other constraints are involved.

3.4 Shooting method

In chapter 2, the analogue of a discrete system based on the equilibrium condition suggests that we can utilize shooting method to solve this problem. The idea of shooting method is to use the numerical method of initial value problem to integrate

forward from one boundary and check the boundary conditions when the other boundary is reached. Various special techniques have been invented to solve different problems. We only adopt the simple and straightforward “pure shooting”. The pure shooting is to start “shoot” from one point with an initial guess of one or more variables of the differential equations. The setting of the starting point is manipulated to satisfy the boundary conditions at the start point. Then the integration proceeds from the start point employing one of the numerical methods in IVP. In this study the implicit Euler’s method is used as the analogue suggested. After the other point is reached, we must adjust our initial guess of variables for another “shoot” if boundary conditions are not satisfied. The adjustment is made to eliminate the difference between the boundary values obtained in the current “shoot” and the boundary conditions at this point. These procedures are repeated until the boundary conditions at the second point are satisfied. To produce a new initial guess based on the information gathered from the previous “shoot”, iterative method is employed. Suppose that at the starting point, there are N unknowns and n_1 boundary conditions. The number of unknowns to be specified is $n_2 = N - n_1$. The problem remaining now is to find the root of a nonlinear system with n_2 unknowns. Generally, there are three types of updating scheme: bisection, Newton-Raphson’s method, and secant method. Bisection method is stable but with a slow convergence rate. Newton-Raphson’s method is the most widely used. Secant method can be viewed as a kind of Newton’s method, which is easy to implement when $n_2 = 1$.

For example, if a pin-pin elastica is studied, the system is summarized in (2.19), (2.21) and (2.22). Global equilibrium path is to be plotted as diagram of ψ_0 v.s P , where ψ_0 is the initial angle at starting point of the “shoot”, and P is the applied load.

If we take ψ_0 as the controlling parameter, it can be set from 0 to π . P is then the parameter needs to be guessed. Using the secant method, two guesses of P are first made. Denoting the boundary value obtained with $y(P_{k-1})$ and $y(P_k)$, P_{k+1} are updated using:

$$P_{k+1} = P_k - \frac{P_k - P_{k-1}}{y(P_k) - y(P_{k-1})} y(P_k) \quad (3.37)$$

Apparently, with different guessed value of P , the obtained configurations might be at different mode. This example will be computed in chapter 4.

3.5 Path following strategy

In the previous discussion, we are trying to form a strategy that directly searches the configuration of elastica given certain boundary conditions and constraints. However, if we want to get a better understanding of the elastica's post-buckling behavior, the complete solution family of a certain class is necessary to be generated.

Throughout this work, the complete solution family of a class solution is obtained by changing (increasing or decreasing) the geometric constraints: the end displacement D for energy based method; initial angle ψ_0 for shooting method. Since this procedure is performed gradually, we can view the change as a small perturbation based on the previous configuration. The geometric constraint in terms of D is also known as "hard loading" in other literatures studying elastica. As SQP and the shooting method both employ Newton's method to find solutions, it will be computationally efficient to use the previous configuration as the initial guess.

When treating the elastica as a constraint-satisfying problem, we still need to specify a configuration firstly using the algorithm in Figure 3.3. After that, the part of

GA can be taken out, and only SQP is necessary to continue. The flowchart is displayed in Figure 3.4. When solving the problem with the shooting method, we can always start from the straight configuration. If a class of the first mode configurations is to be generated, it will be easier to set the well known Euler critical buckling load as the first initial guess. After the shooting method is terminated successfully, the corresponding P_k can then be set as the next initial guess to generate new configuration with larger ψ_0 .

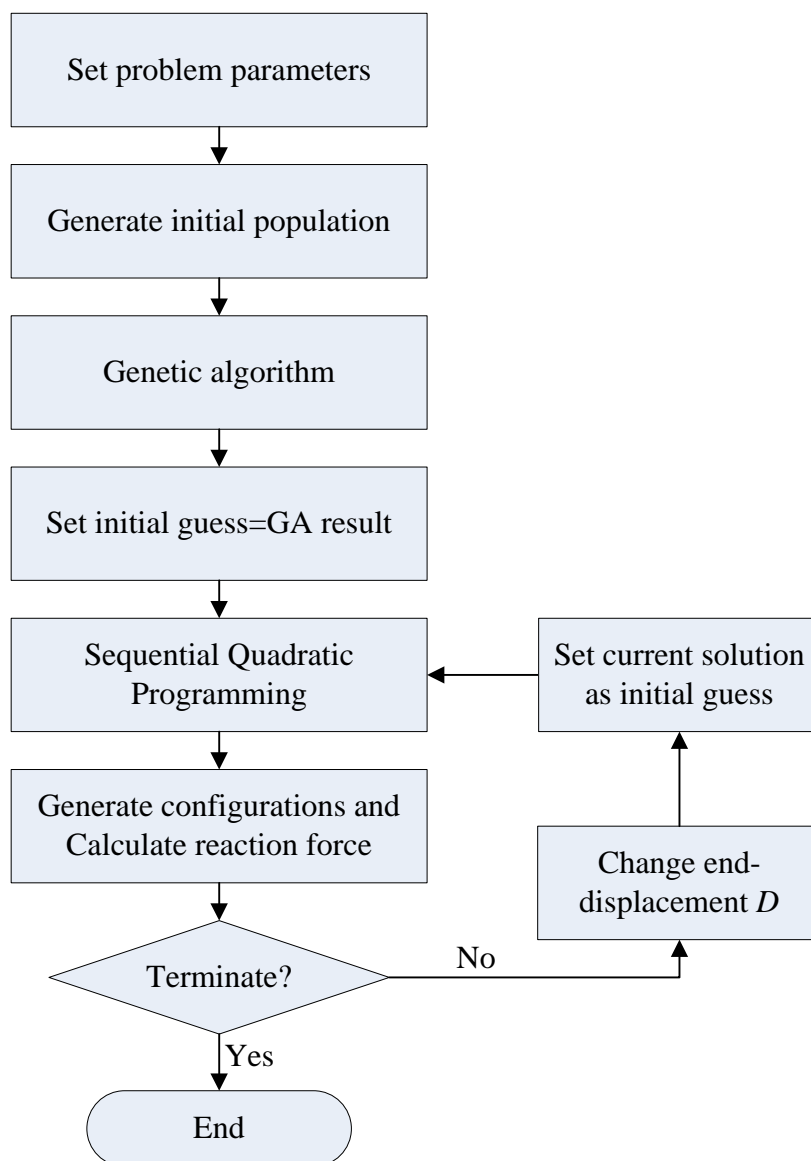


Figure 3.4 Framework of path following strategy using energy principle

CHAPTER 4 Numerical Examples and Applications

In this chapter, we will demonstrate the use of the numerical techniques introduced in chapter 3 to solve the problems of chapter 2. The first section will cover the pin-pin elastica. Since this simple elastica has been studied using other methods, we can use the widely available solution to compare and verify our numerical results. The other sections will deal with different geometric boundary conditions. Using path-following strategy, the quantitative characteristics of several typical or critical configurations of the first mode will be discussed. To demonstrate the universality of the energy method, spatial elastica and elastica with side walls are also studied. Formulation of spatial clamp-clamp elastica is firstly developed. Their configurations and qualitative behavior will be discussed.

4.1 Elastica with two ends simply supported

When an elastica is simply supported at two ends as shown in Figure.2.1, both energy based method and shooting method are used. First, we identify the configurations corresponding to several critical points and compare the results with the available analytical solutions.

4.1.1 Comparison study with analytical results

To compare the results with the analytical ones obtained by Kuznetsov *et al.* and by Timoshenko's method using the elliptical integration, we compute four basic configurations. Let $a = L - D$, and set $a = 0.3879$. Divide the elastica into 50 segments, that is $N = 50$, $s_i = 0.02$. The stiffness of the elastic moment spring $K = 1$. The value of K only affects the magnitude of the end load, but not the planar configurations. For

the convenience of comparison, λ_1 and λ_2 with the physical meaning of reaction forces in x direction and y direction respectively are normalized with respect to Euler

buckling load P_{cr} . For this example, $P_{cr} = \frac{\pi^2 EI}{L^2}$, where EI can be obtained as $s_i K$.

The maximum displacement in y direction is denoted as w . Again, we normalize this result as $\frac{w}{L}$. After the direct search method is implemented, we have the results shown

in Figure.4.1 and Table.4.1. In this chapter, the X and Y in the configuration plot denote the rectangular coordinates of the system.

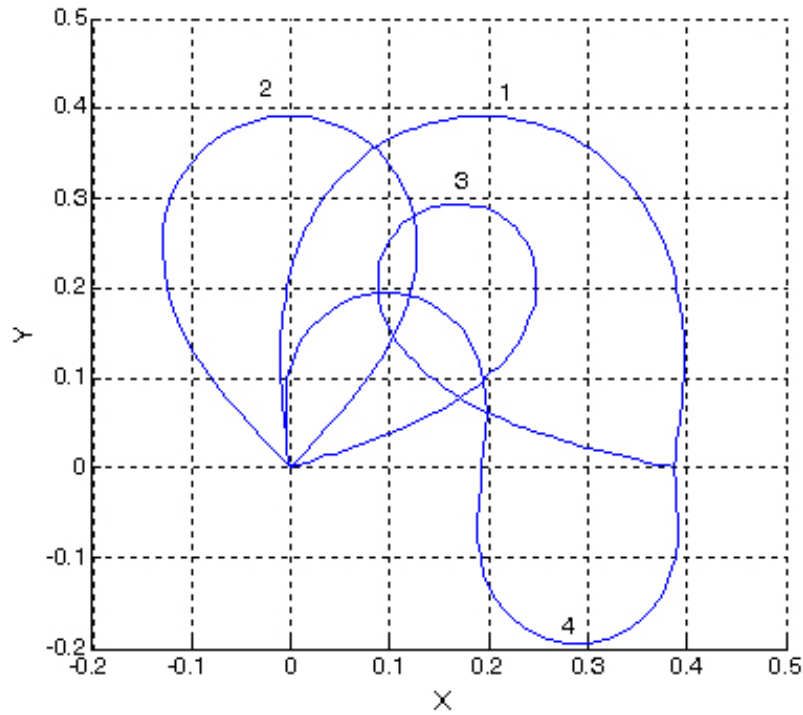


Figure 4.1 Basic Configurations with $a=0.3879$ (1,3,4) and $a=0$ (2)

Table 4.1 Comparison with analytical solutions

Configuration	Solutions by Kuznetsov <i>et al</i> (2002) and Timoshenko (1963)			Solutions using energy based direct search		
	λ_1 / P_{cr}	λ_2	w/L	λ_1 / P_{cr}	λ_2	w/L
1	1.47129	0	0.39159	1.4707	-7.2588e-006	0.3935
2	2.18338	0	0.39159	2.1819	3.2904e-017	0.3917
3	4.56625	0	0.29494	4.5697	5.9309e-005	0.2943
4	5.87698	0	0.19569	5.8770	-0.0011	0.1954

From the results listed in Table.4.1, it is observed that the proposed approach of combining GA and SQP, can produce accurate result. The algorithm is also efficient. It takes less than 30 seconds to obtain one configuration. If only SQP is employed with a reasonable initial guess, the computation time needed for each configuration is within 5 seconds on a Pentium-4 1.4GHz computer.

We can use this method to directly obtain different configurations under same boundary conditions and constraints. The results are shown in Figure 4.2.

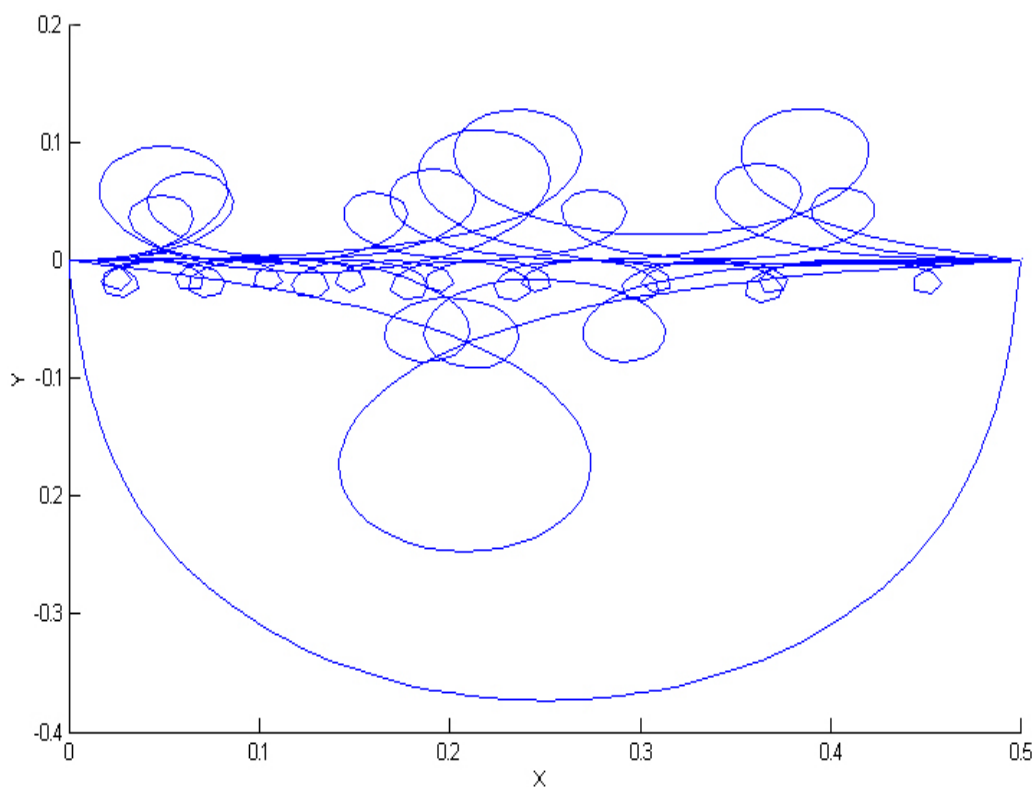


Figure 4.2 Configurations of elastica with $a=0.5$, both ends simply supported

4.1.2 Path following study of the pin-pin elastica

To the applications interests, the most important mode is the first mode. It is generally more stable than the other modes. This enables us to follow its path easily. Since the coordinate system can be defined as will, we fix the left end A of the initially straight elastica at origin, while the other end B is moved toward A before both ends

meet. If the moving end is allowed to continue moving along the x axis away from origin, a loop will eventually form. Let D denotes the displacement of the moving end, we can divide the full path into two stages: $D \in [0, 1]$ and $D \in (1, 2]$. In the second stage, the configuration is defined as the 7th class by *Euler*.

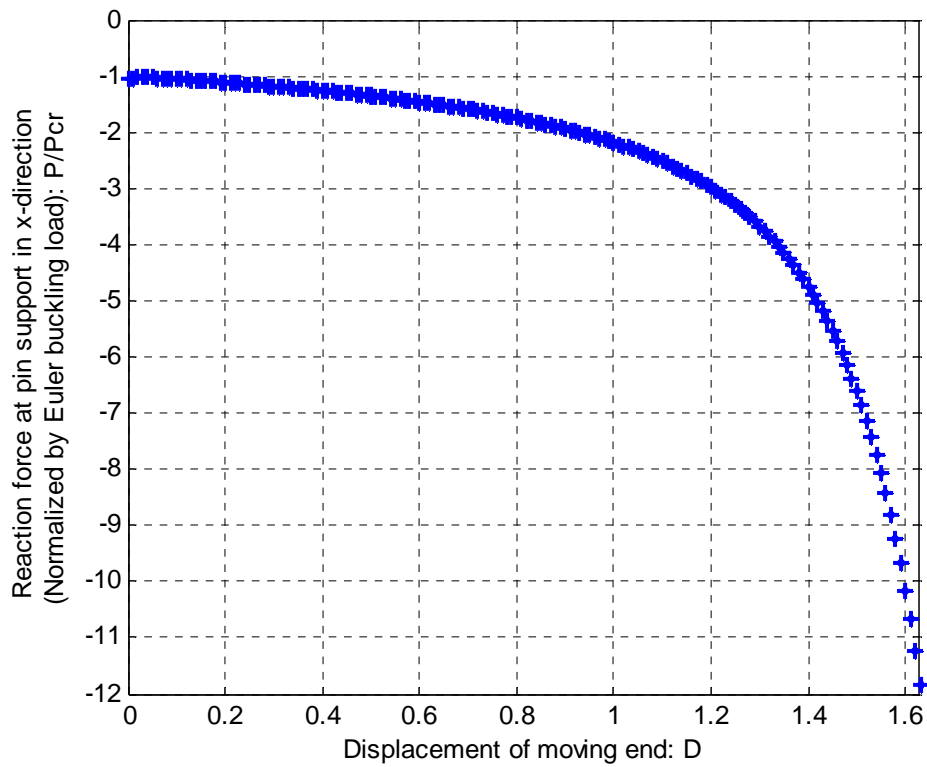


Figure 4.3 Diagram of $D - \lambda_1 / P_{cr}$ (pin-pin elastica)

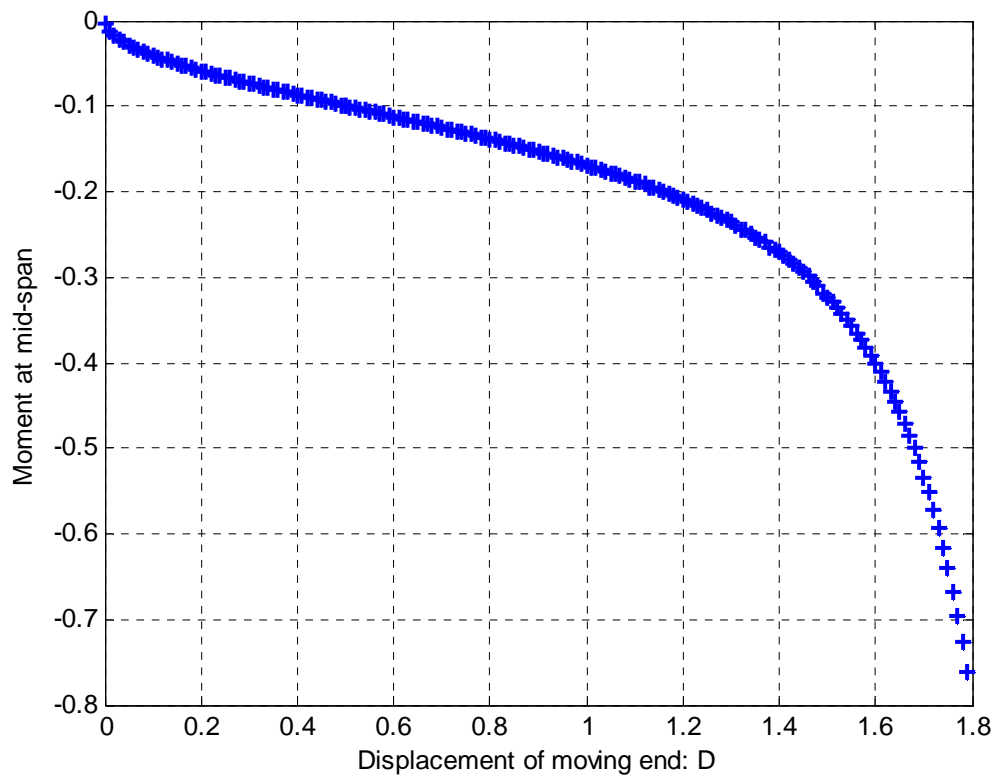


Figure 4.4 Diagram of $D - M$ (pin-pin elastica)

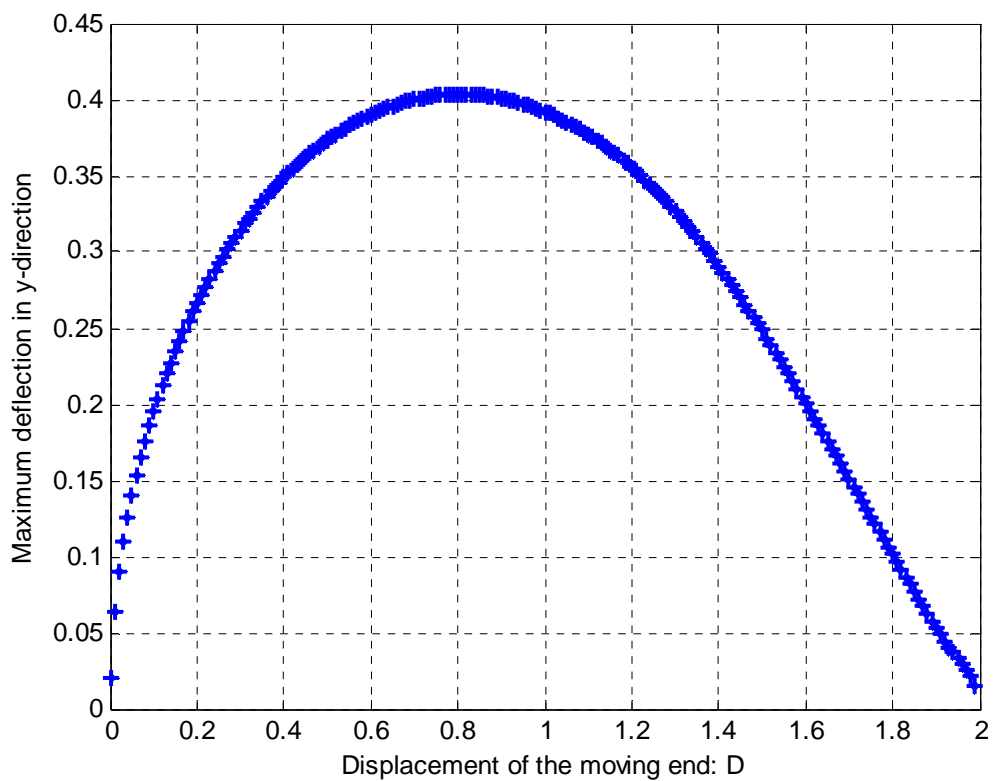


Figure 4.5 Diagram of $D - w/L$ (pin-pin elastica)

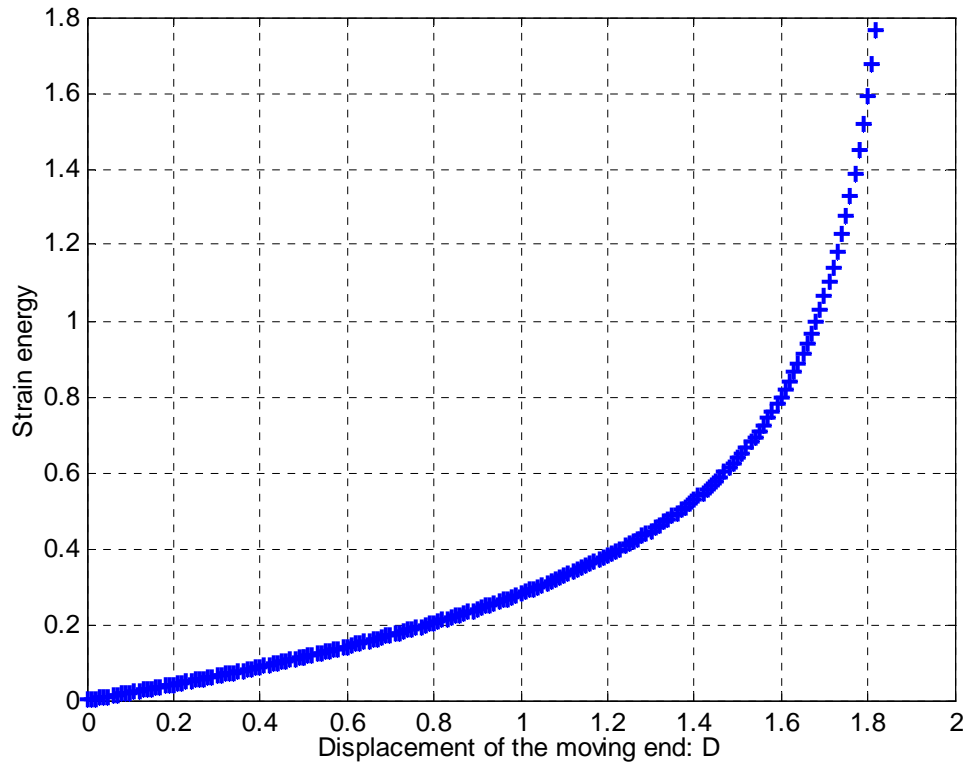


Figure 4.6 Diagram of D – Strain Energy (pin-pin elastica)

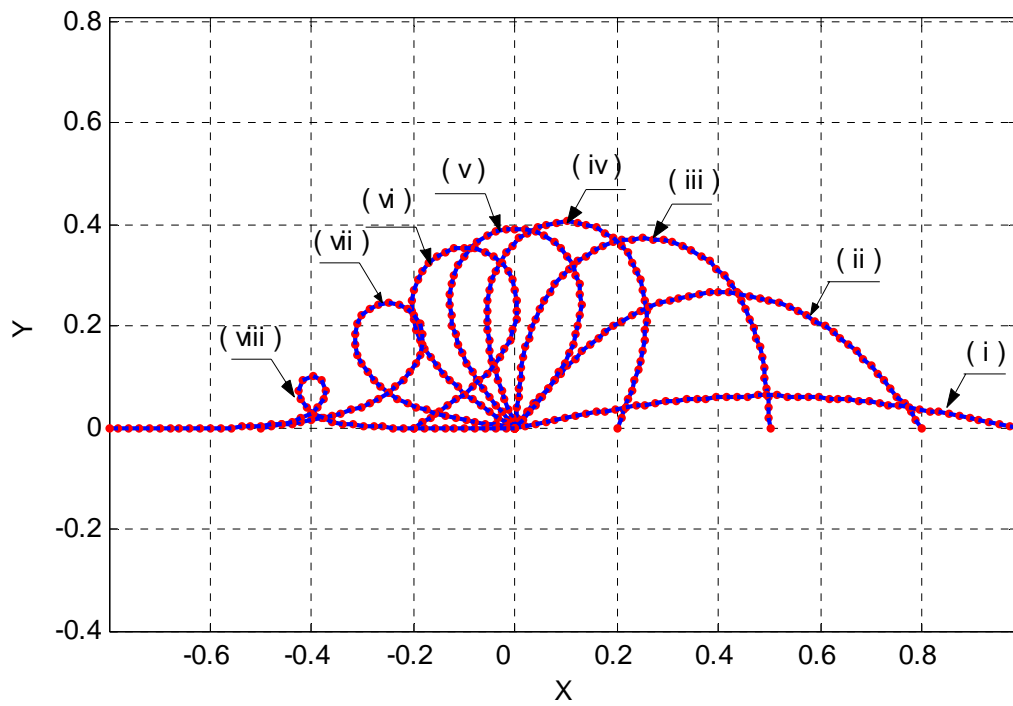


Figure 4.7 Several typical configurations of pin-pin elastica

Table 4.2 Numerical results at configurations shown in Figure 4.7 (pin-pin)

Configuration	D	λ_1 / P_{cr}	λ_2 / P_{cr}	w/L	M	PE
(i)	0.01	-1.0091	-2.07e-7	0.0631	-0.0125	0.0020
(ii)	0.2	-1.1146	9.57e-6	0.2664	-0.0585	0.0416
(iii)	0.5	-1.3517	3.54e-4	0.3734	-0.0994	0.1140
(iv)	0.8	-1.7425	9.71e-4	0.4033	-0.1383	0.2043
(v)	1	-2.1867	7.63e-4	0.3918	-0.1688	0.2810
(vi)	1.2	-2.9810	2.77e-4	0.3550	-0.2085	0.3811
(vii)	1.5	-6.6007	1.63e-5	0.2477	-0.3221	0.6379
(viii)	1.8	-40.0661	2.25e-6	0.1014	-0.8001	1.5929

The results shown as configurations and diagrams as we change D step by step are illustrated from Figure 4.3 to Figure 4.7. The numerical results in terms of reaction forces, maximum deflection, moment, and strain energy are listed in Table 4.2. One critical configuration is configuration (iv), at which the deflection w/L reaches its maximum, 0.4033. When the two ends of pin-pin elastica meet, the reaction force in x direction is $2.1867P_{cr}$. This is also a critical point where the structural system demonstrates instability. The instability will be discussed in next section.

To display how elastica evolves from $D = 0$ to $D = 2$, each configuration with step size 0.01 is superimposed in Figure 4.8.

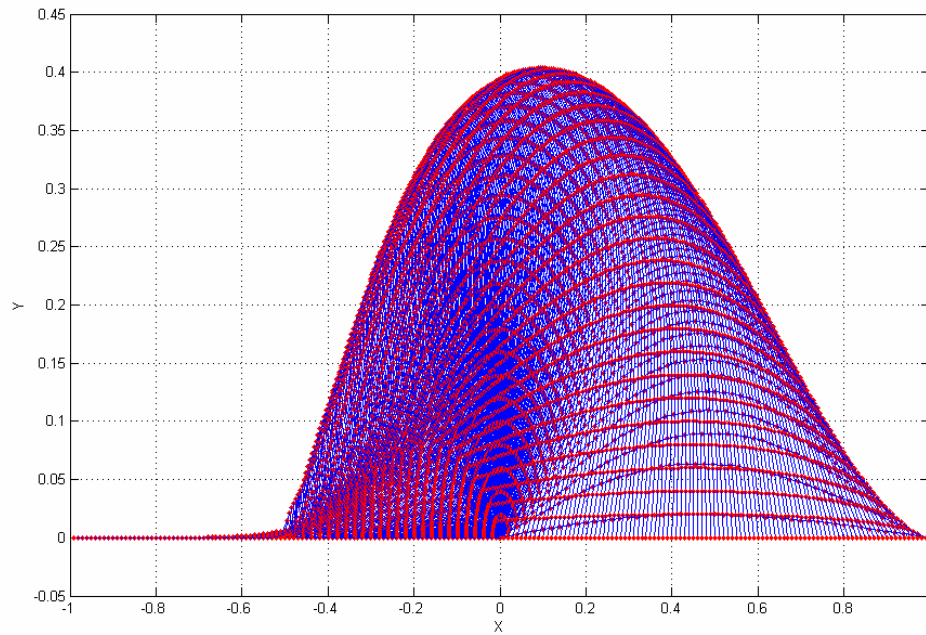


Figure 4.8 Superimposition of configurations of pin-pin elastica

4.1.3 Stability of post-puckling region

The previous section has shown the results obtained using the path-following strategy. These results are obtained using the model in Figure 2.2. However, when the two ends coincide, rigid rotation of the whole system around pin supports is possible. If the instability is to be studied, this model is no longer suitable. In path-following strategy, the configuration before two ends coincide is used as initial guess. But the previous configuration is stable and symmetric about the perpendicular bisect line of a . In this model, each variable ψ_i is the angle with respect to x axis. When rigid rotation happens, each variable will change greatly in magnitude. Therefore, small perturbation is not likely to produce rigid rotation of the whole system. This model is inadequate to describe the real situation. Hence, the alternative model illustrated in Figure 2.5 is preferred.

In the alternative model, only perturbation to the first variable ψ_1 will introduce rotation of the whole system when two ends coincide. The other variables with the meaning of relative change of angle from previous segment will not change. The configurations are similar; only their planar positions are different. This phenomenon is illustrated in Figure 4.9. Corresponding diagram of $D - \lambda_1 / P_{cr}$ is shown in Figure 4.10. It shows λ_1 , or P , can change within the range $[-2.1867P_{cr}, 2.1867P_{cr}]$. Accordingly, the reaction force in y direction is also within the range $[-2.1867P_{cr}, 2.1867P_{cr}]$ at $D=1$. We also superimpose these configurations in Figure 4.11 to show how this procedure evolves.

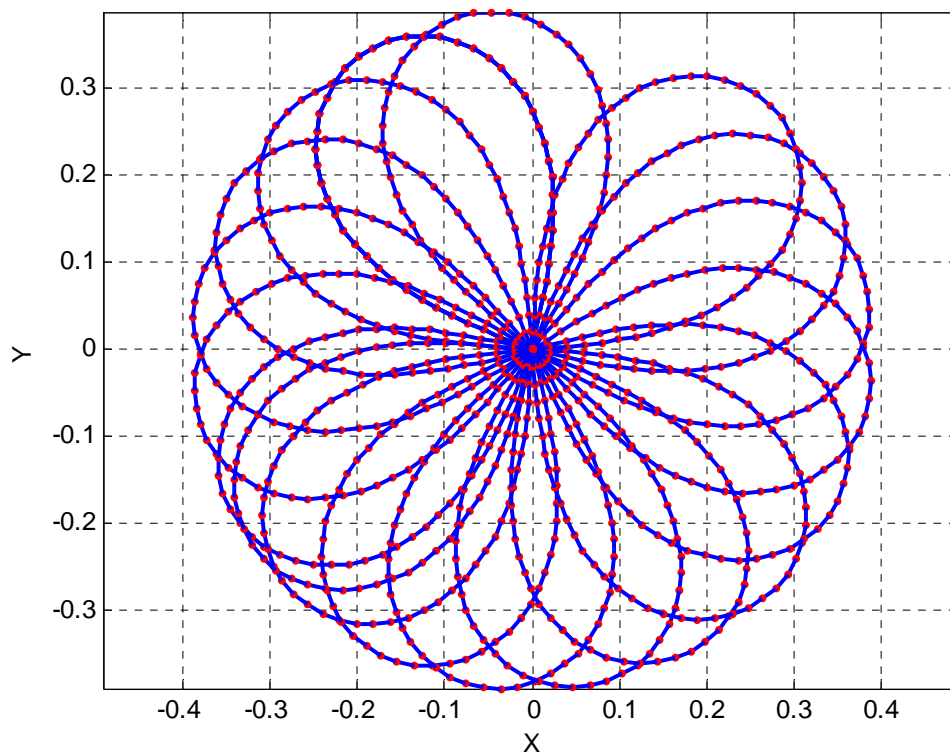


Figure 4.9 Several configurations of pin-pin elastica when two ends coincide

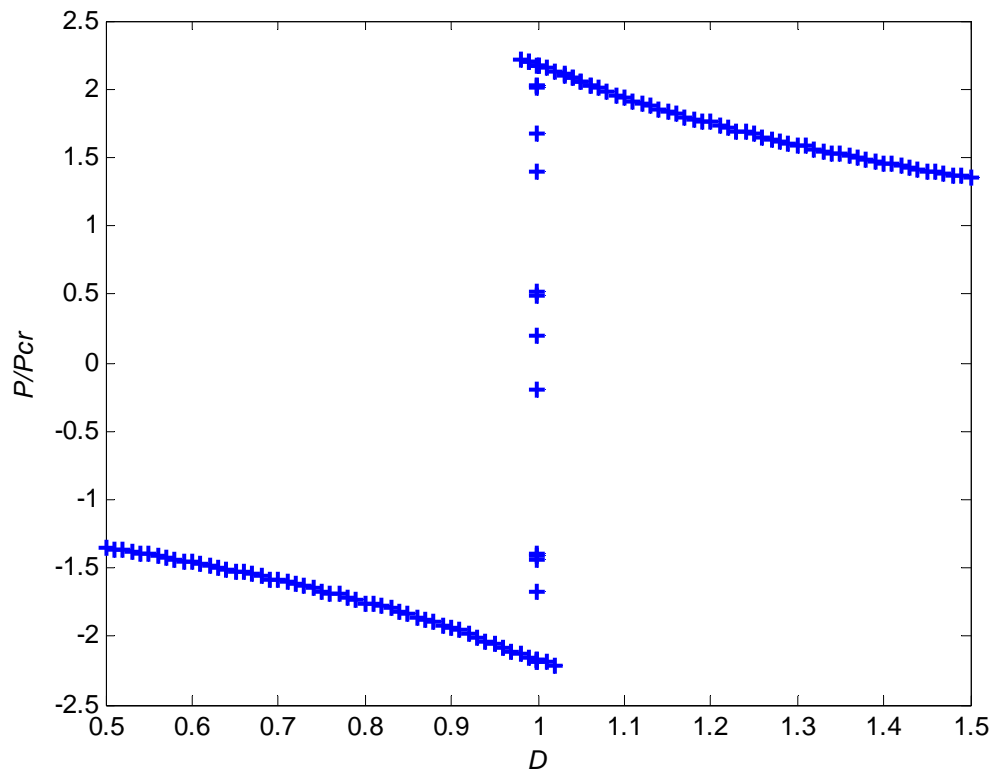


Figure 4.10 Diagram of $D - P/P_{cr}$ (pin-pin elastica, snap through happens when $D=1$)

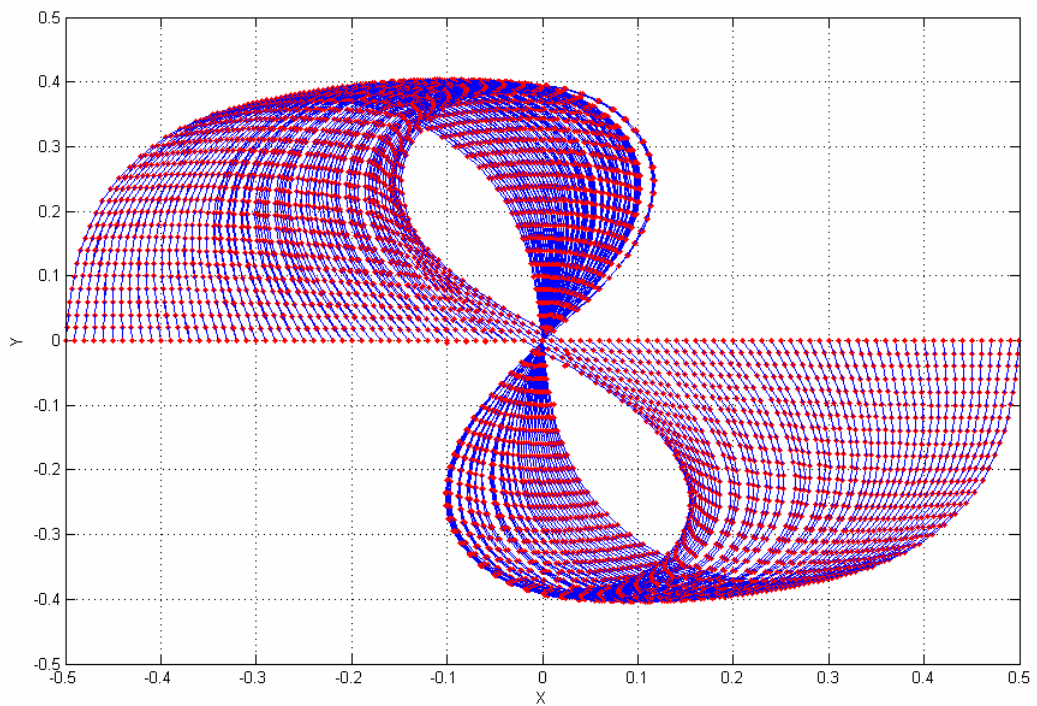


Figure 4.11 Superimposition of configurations of pin-pin elastica $D \in [0.5, 1.5]$ (Snap-through when $D = 1$)

4.1.4 Shooting method

In Chapters 2 and 3, the shooting method is introduced as a complementary numerical technique to solve the geometric nonlinear structure of elastica. For the example in this section, the shooting method is utilized for the model introduced in Section 2.2. It has been shown that the modelling of discrete elastica is analogous to the implicit Euler integration in shooting method. And the implicit Euler method has the advantage that it will guarantee convergence provided the step-size is small enough. Another advantage of shooting method to solve this problem is that it is easy to obtain the configurations at higher modes. As stated in Sections 2.2 and 3.4, the control parameter is taken as ψ_0 , the “shooting” angle at the start point. Then an initial guess needs to be given to the corresponding P . Because we can start from the straight configuration, the initial guess of P can be set as the critical Euler buckling load. Starting with different buckling load at different mode, higher mode configurations can be obtained. The elastica is also divided into 50 segments. In the path-following procedure, control parameter ψ_0 is changed from 0 to π . The increment is set as 0.01π . The configurations and global behaviour demonstrated as diagram of $P/P_{cr} - \psi_0$ are plotted in Figures 4.12 to 4.15. The 9 configurations are plotted at $\psi_0 = 0.1\pi, 0.2\pi, \dots, 0.9\pi$. In this model, the instability occurring when two ends coincide cannot be simulated. Since the shooting method is not the focus of this work, it will not be employed in the following sections.

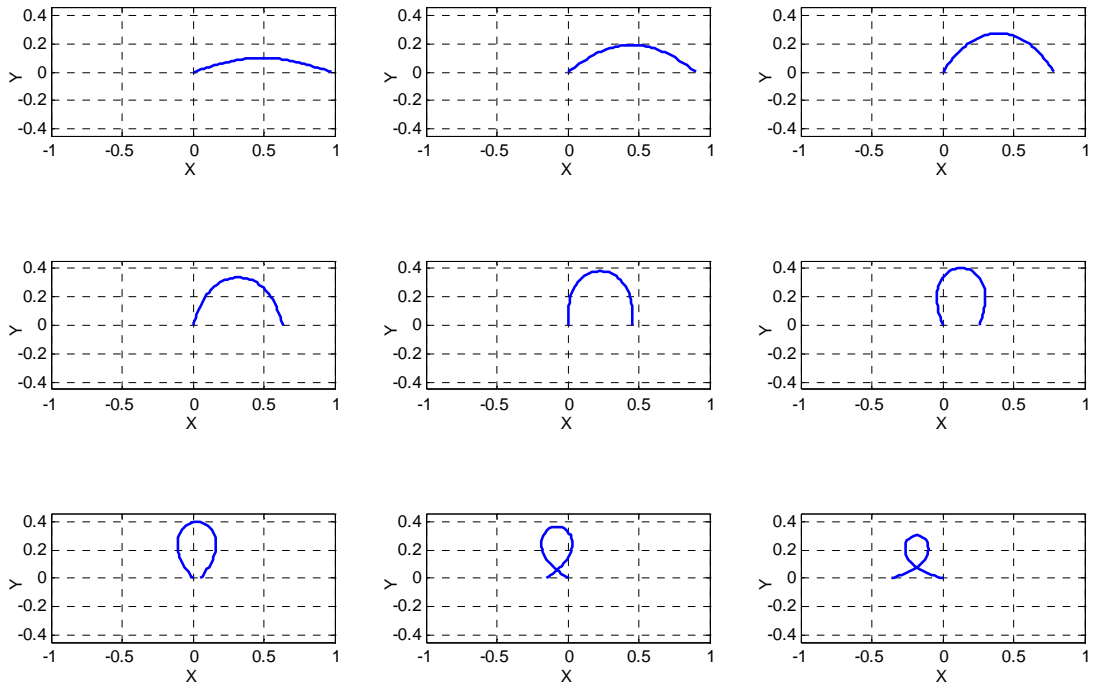


Figure 4.12 Configurations at first mode

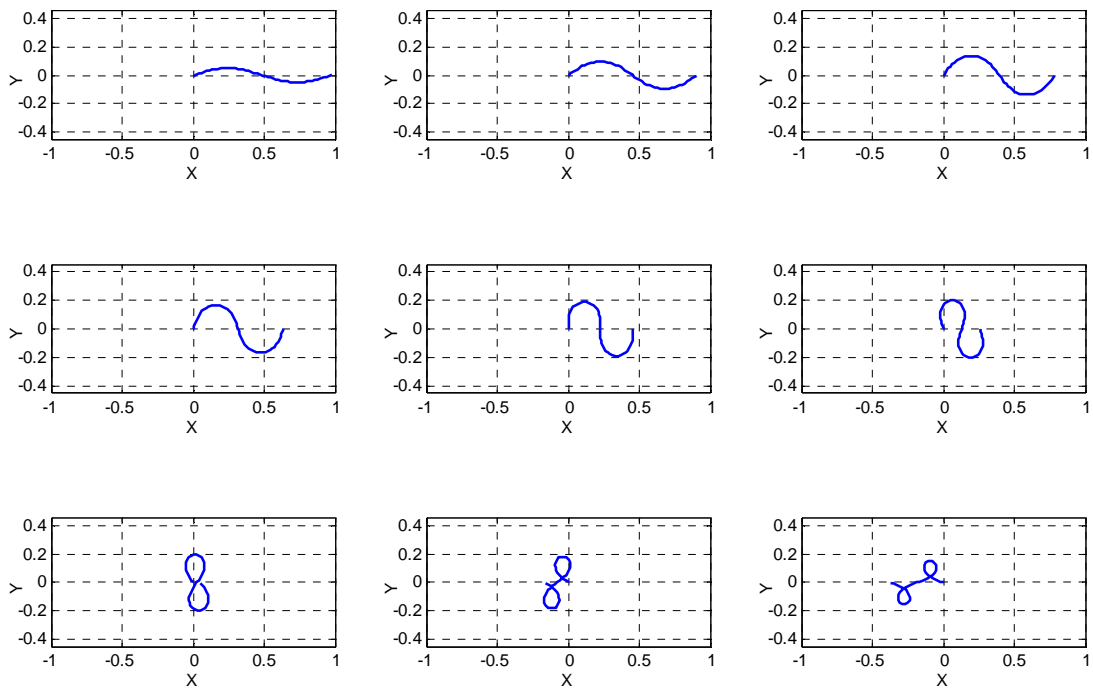


Figure 4.13 Configurations at second mode

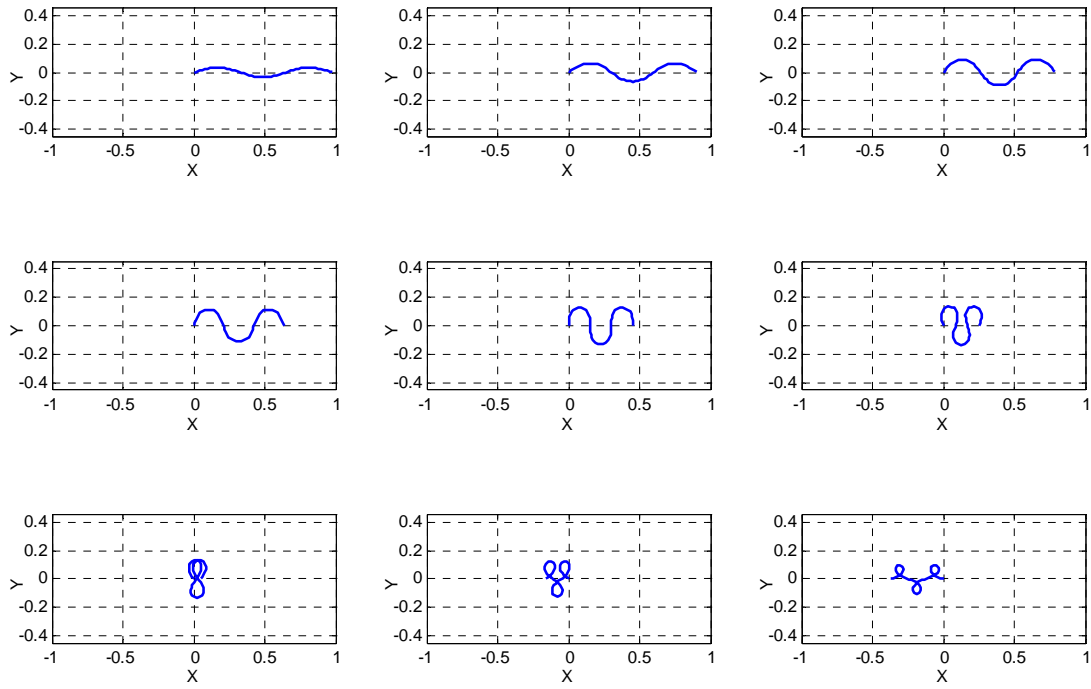


Figure 4.14 Configurations at third mode

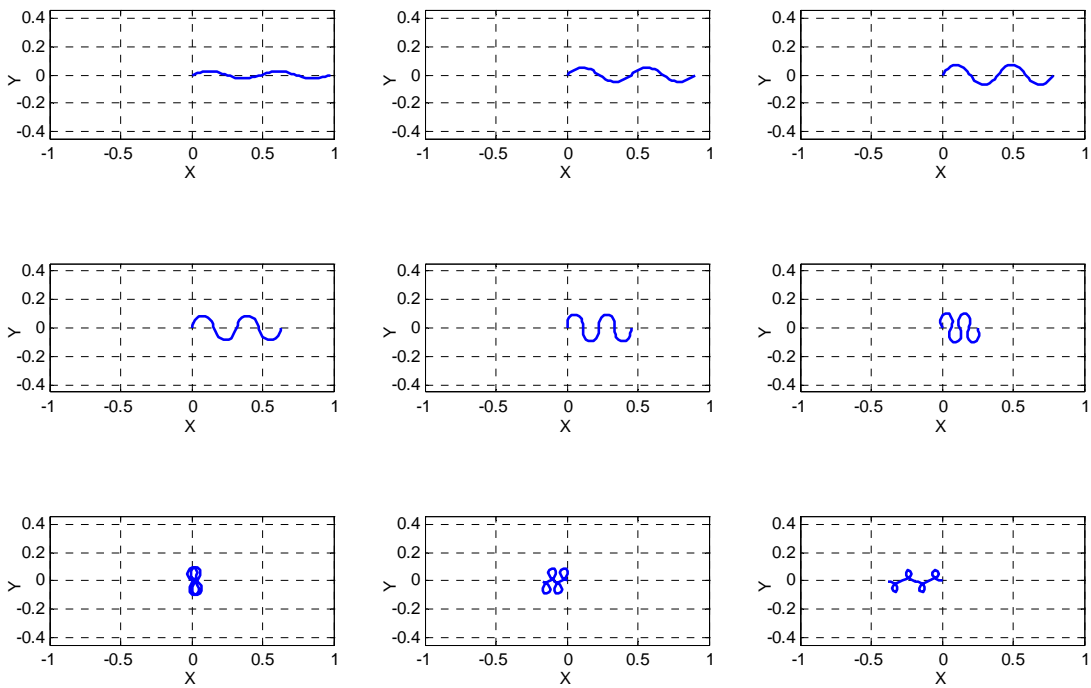


Figure 4.15 Configurations at fourth mode

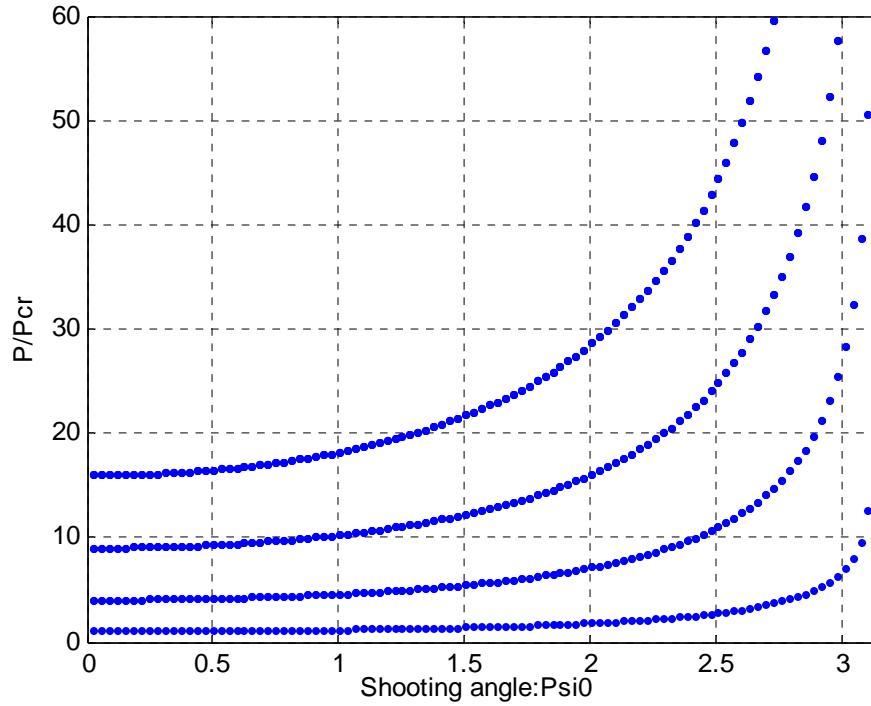


Figure 4.16 Diagram of $\psi_0 - P/P_{cr}$ (shooting method)

4.2 Elastica with one end clamped, one end pinned

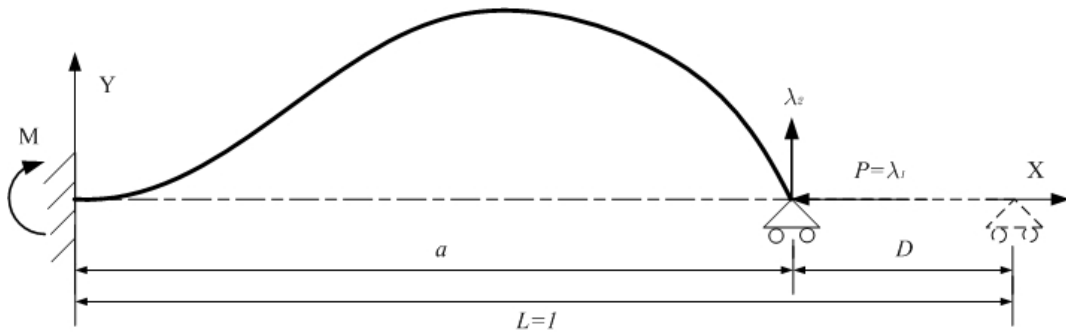


Figure 4.17 Geometry of Clamp-pin elastica

In the numerical example of this section, we utilize the energy-based algorithm to study elastica with one end clamped and the other pinned as illustrated in Figure 4.17. When the end load P is equal to the critical buckling load P_{cr} , lateral buckling happens. And the reaction force λ_2 in y -direction at the pin support appears; it will

balance the moment M at the clamped end. The critical Euler buckling load is given by

Timoshenko (1961): $P_{cr} = \frac{\pi^2 EI}{(0.699l)^2}$. In the setting of our example, i.e. l is

normalized to 1, and divided into $N = 50$ segments, the critical buckling load has the magnitude of 0.404. Therefore, the obtained reaction forces at supports can be normalized to 0.404; M is calculated by $\lambda_2 a$. The numerical results are plotted in the following figures. Note that the moment at the clamped end is only normalized with L . Strain energy is not normalized. The magnitudes of these two results only demonstrate the quality characteristics and show the global path. The clamp condition at O is fulfilled by confining $\psi_1 = 0$.

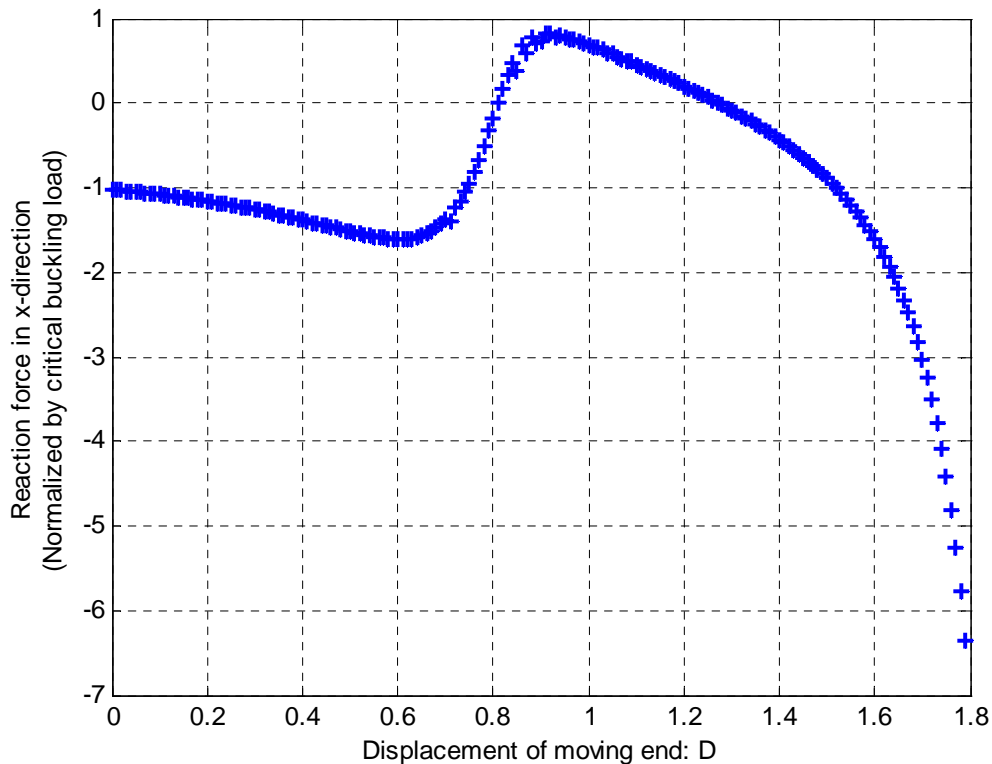


Figure 4.18 Diagram of $D - P/P_{cr}$ (clamp-pin elastica)

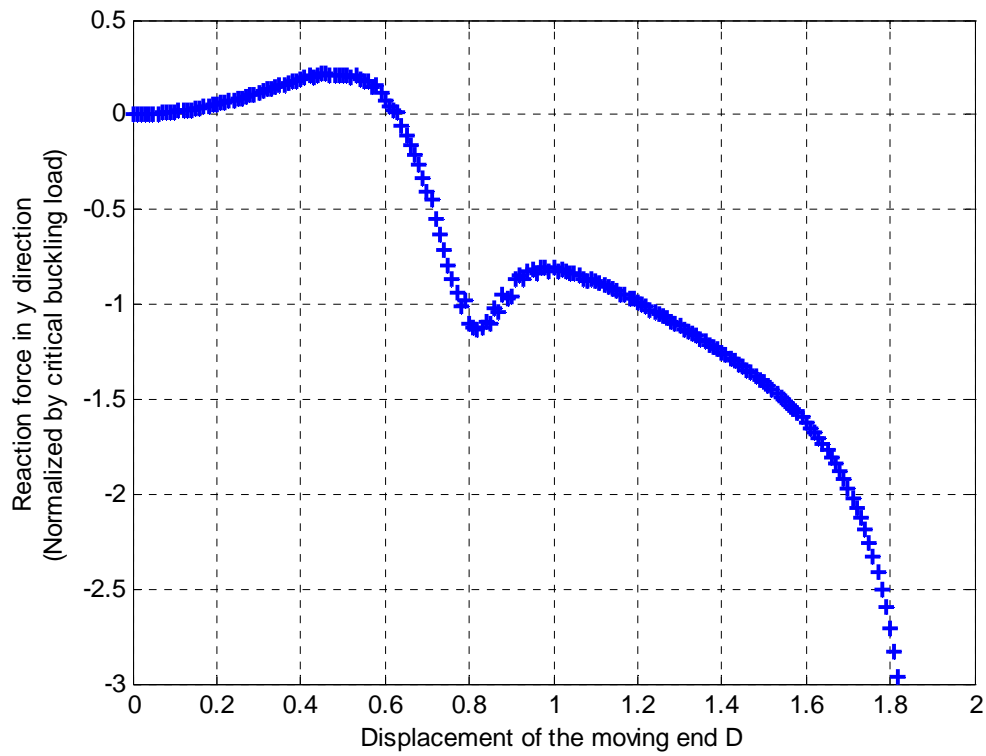


Figure 4.19 Diagram of $D - \lambda_2 / P_{cr}$ (clamp-pin elastica)

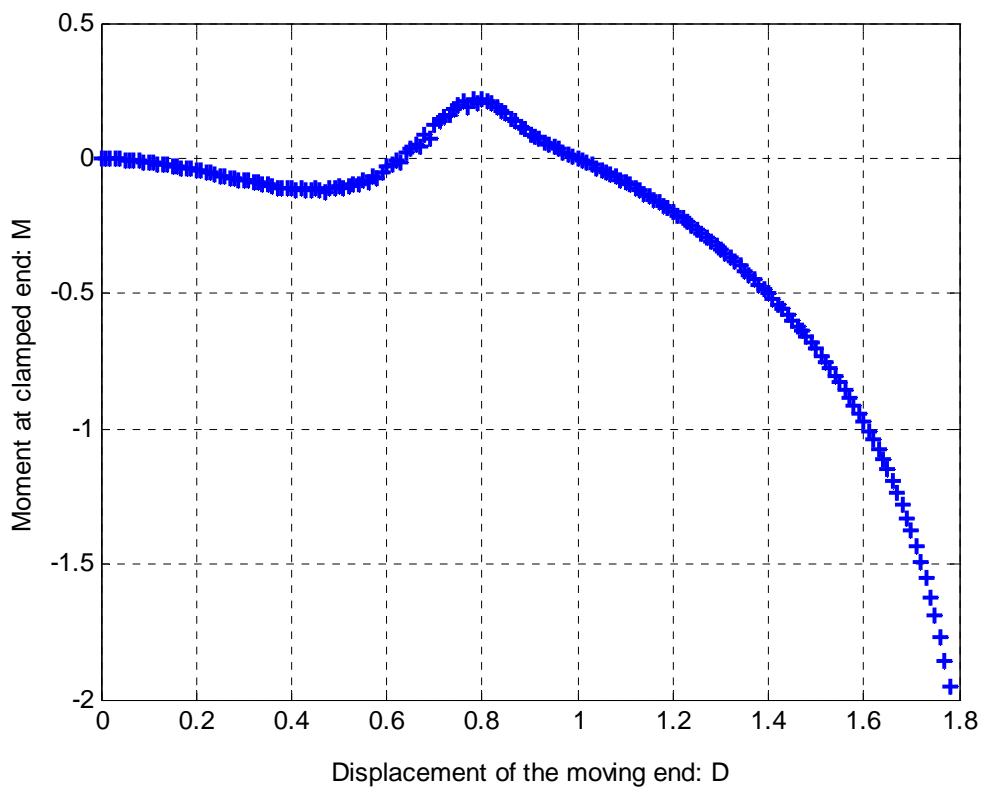


Figure 4.20 Diagram of $D - M$ (clamp-pin elastica)

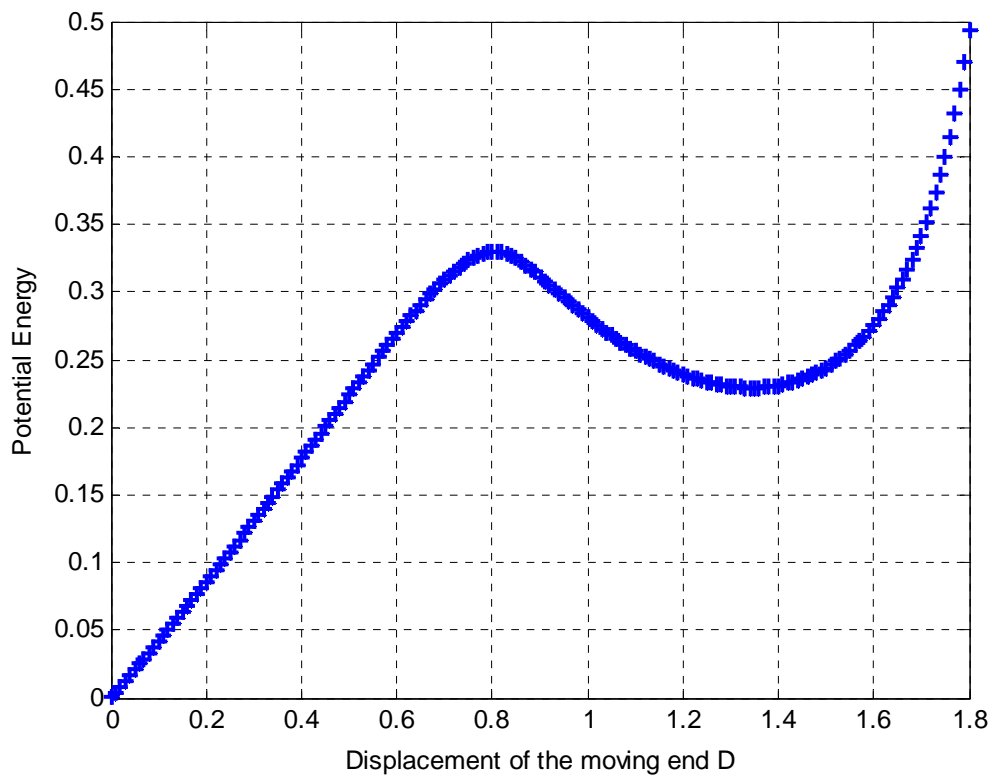


Figure 4.21 Diagram of $D-PE$ (clamp-pin elastica)

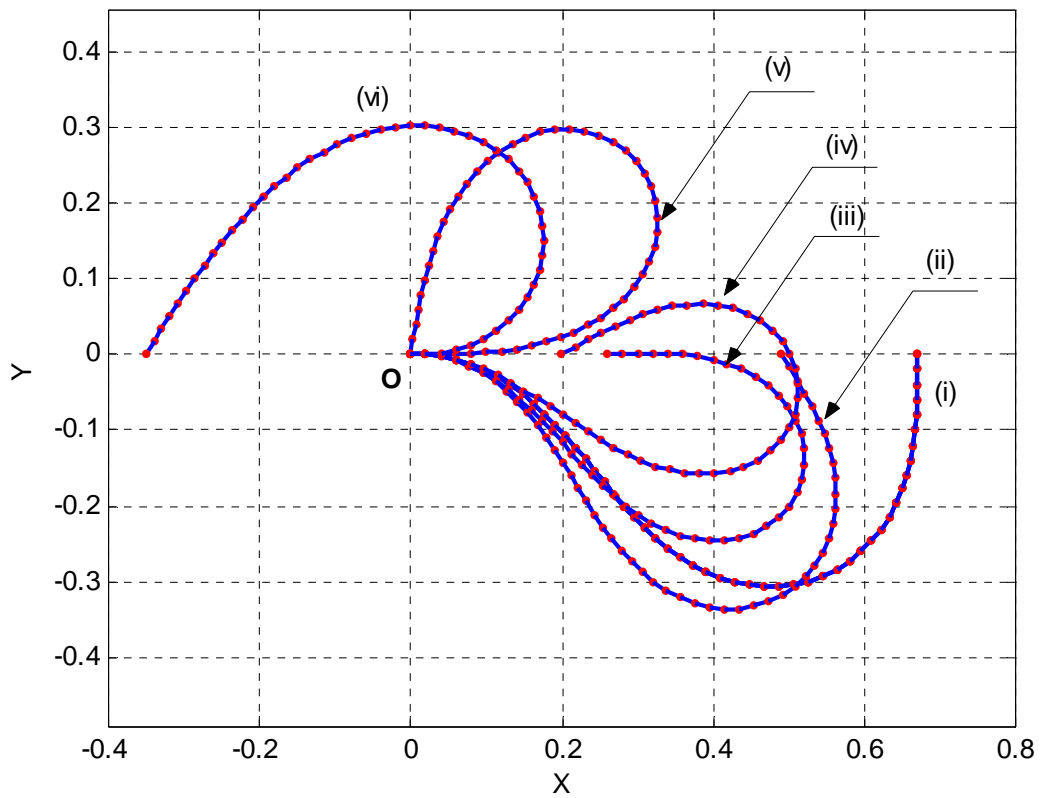


Figure 4.22 Several critical configurations of clamped-pin elastica

Table 4.3 Numerical results at configurations shown in Figure 4.22 (clamp-pin)

Configuration	D	λ_1 / P_{cr}	λ_2 / P_{cr}	w/L	M	PE
(i)	0.33	-1.2915	0.1393	0.3075	0.0377	0.1444
(ii)	0.51	-1.5393	0.2240	0.3367	0.0443	0.2285
(iii)	0.74	-1.0101	-0.7386	0.2464	-0.0776	0.3210
(iv)	0.8	-0.1895	-1.1013	0.1580	-0.0890	0.3296
(v)	1	0.6960	-0.8117	0.2972	0.000	0.2810
(vi)	1.35	-0.2458	-1.1827	0.3004	0.1672	0.2283

With all the plots and Table 4.3 above, we can now discuss the behavior of the elastica whose one end is clamped at O, while the other is pinned. As in the previous section, the discussion of the behaviour of elastica is divided to two stages: $0 < D \leq 1$ and $1 < D < 2$. First, the configuration (i) shown in Figure 4.17 is when the pin end rotates about $-\frac{\pi}{2}$. Configuration (ii) is when the elastica has the maximum deflection in y direction. The value of w/L is 0.3367. And the corresponding end-displacement D is 0.51. For configuration (iii), the moving end has rotated about the pin end for $-\pi$. As the moving end continues to move toward fixed end, an important configuration, (iv) shown in Figure 4.17, appears. When $D = 0.8$, both the potential energy and the reaction force in y -direction λ_2 reach their maximum in the first stage. It is also at this point that the moment at the clamped end is the largest within range $D \in [0, 1]$. At this point, the reaction force in x -direction changes to the opposite direction for the first time, i.e. $\lambda_2 \approx 0$ at $D = 0.8$. The fifth configuration is when the two ends coincide. Different from the pin-pin elastica, snap-through cannot happen. This is due to the clamped end, which limits free rotation of the elastica. Rigid body rotation is thus not possible. Note that when the two ends coincide, the moment at the clamp end vanishes.

The reaction forces in x and y directions are also within the range of $[-2.1867P_{cr}, 2.1867P_{cr}]$. Not surprisingly, the strain energy is same as the one of pin-pin elastica under the same geometric constraints.

If we permit the moving end to continue in the same direction, the elastica enters the second stage $D \in (1, 2]$. The only critical configuration of interest in this stage is configuration (vi). Strain energy of this system comes to a local minimum. Afterwards, the energy will increase in a rapid rate. The reaction forces in x and y directions and moment at clamped end also increase in magnitude. Figure 4.23 shows the superimposition of all configurations during the procedure when we change D from 0 to 2.

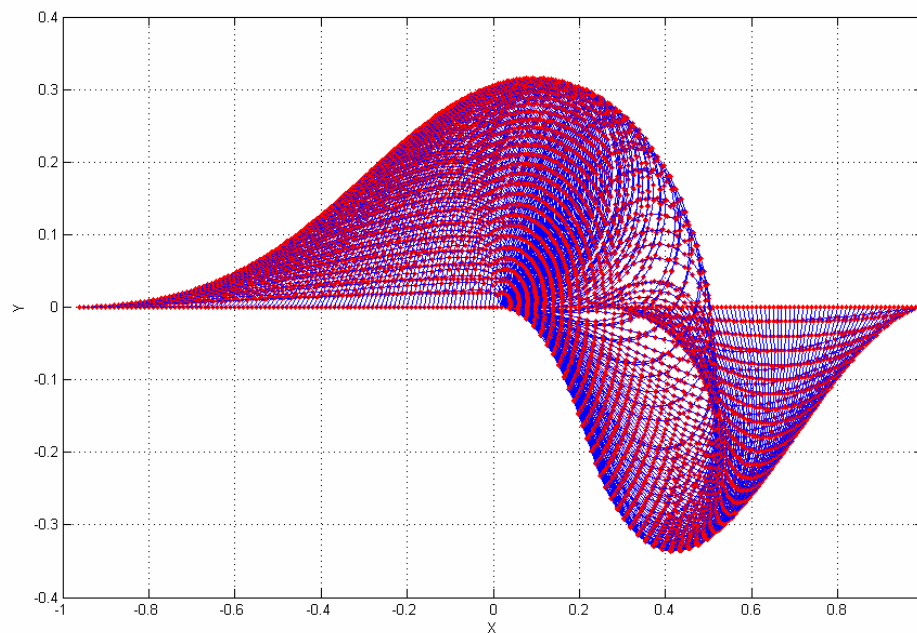


Figure 4.23 Superimposition of all configurations of clamp-pin elastica

4.3 Elastica with both ends clamped

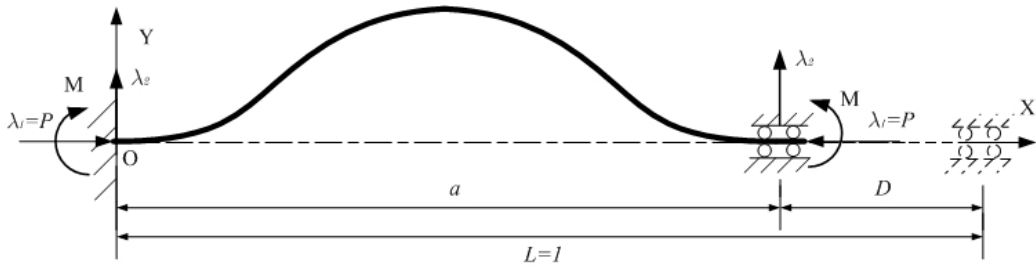


Figure 4.24 Geometry of planar clamp-clamp elastica

Apart from the two examples in the previous sections, the elastica with both ends clamped is another important situation frequently encountered in application. The geometry of this situation is drawn in Figure 4.24. The setting to solve this problem is

same as the previous examples. The critical buckling load P_{cr} is $\frac{4\pi^2 EI}{L^2}$.

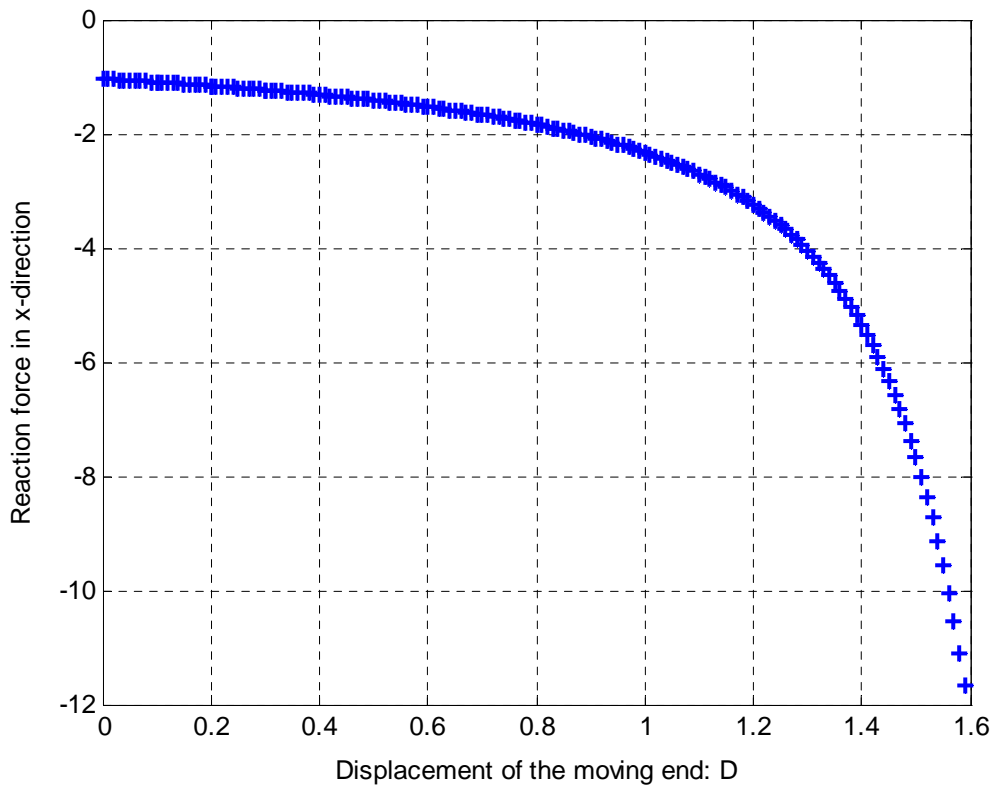


Figure 4.25 Diagram of $D - P/P_{cr}$ (clamp-clamp elastica)

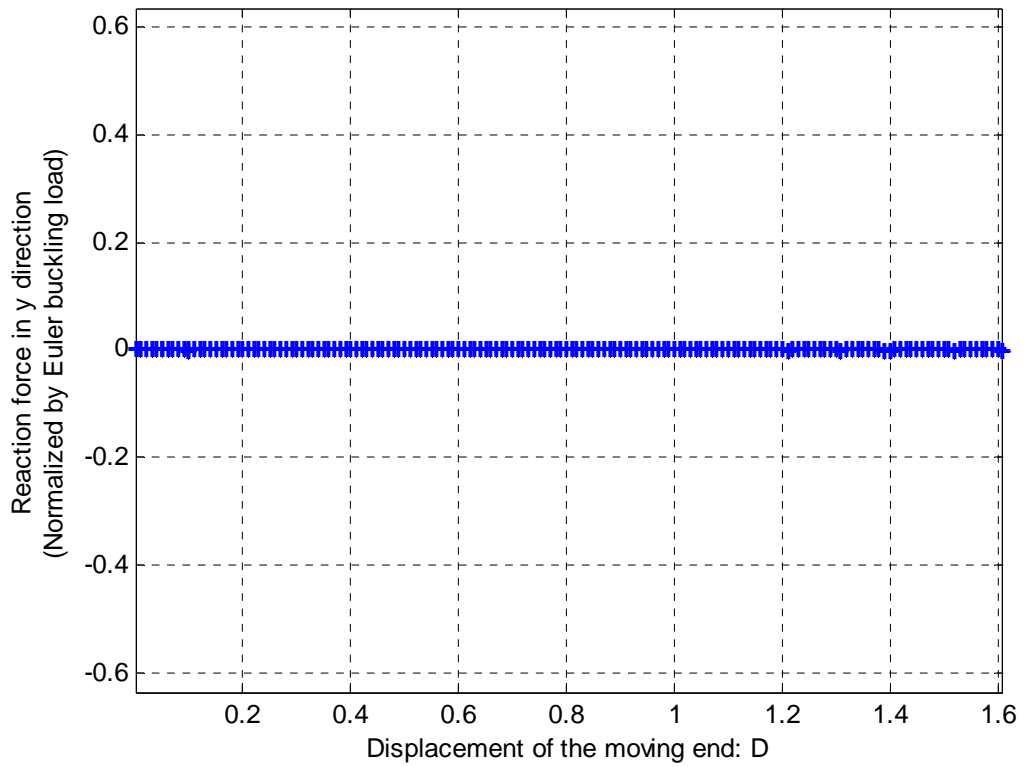


Figure 4.26 Diagram of $D - \lambda_2 / P_{cr}$ (clamp-clamp elastica)

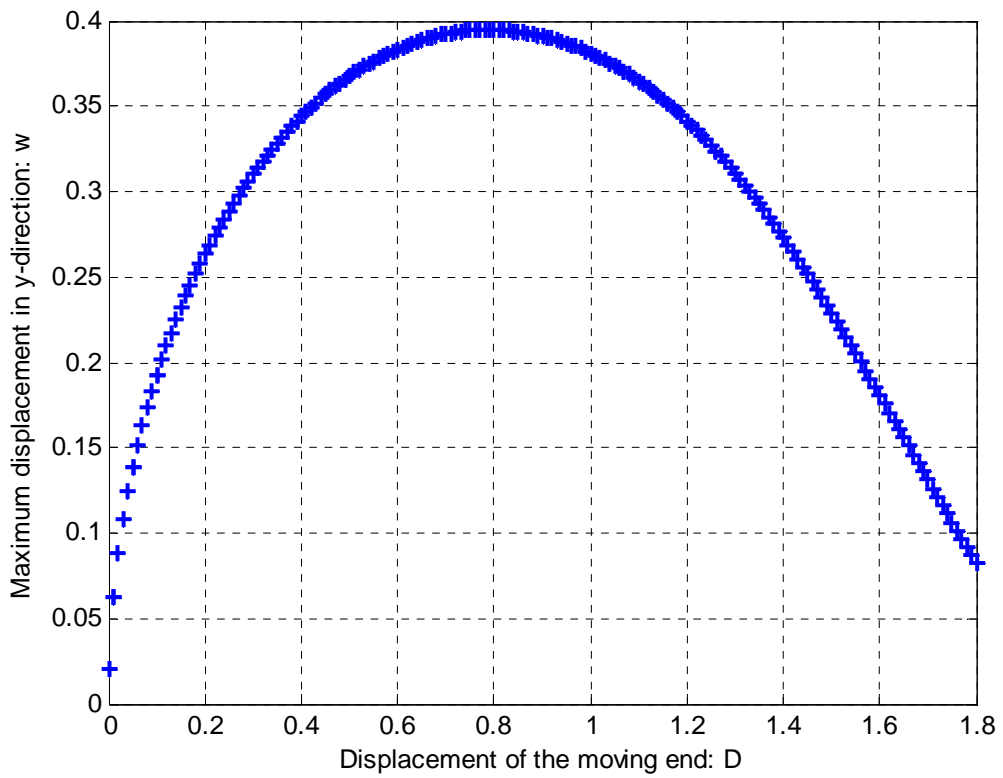


Figure 4.27 Diagram of $D - w/L$ (clamp-clamp elastica)

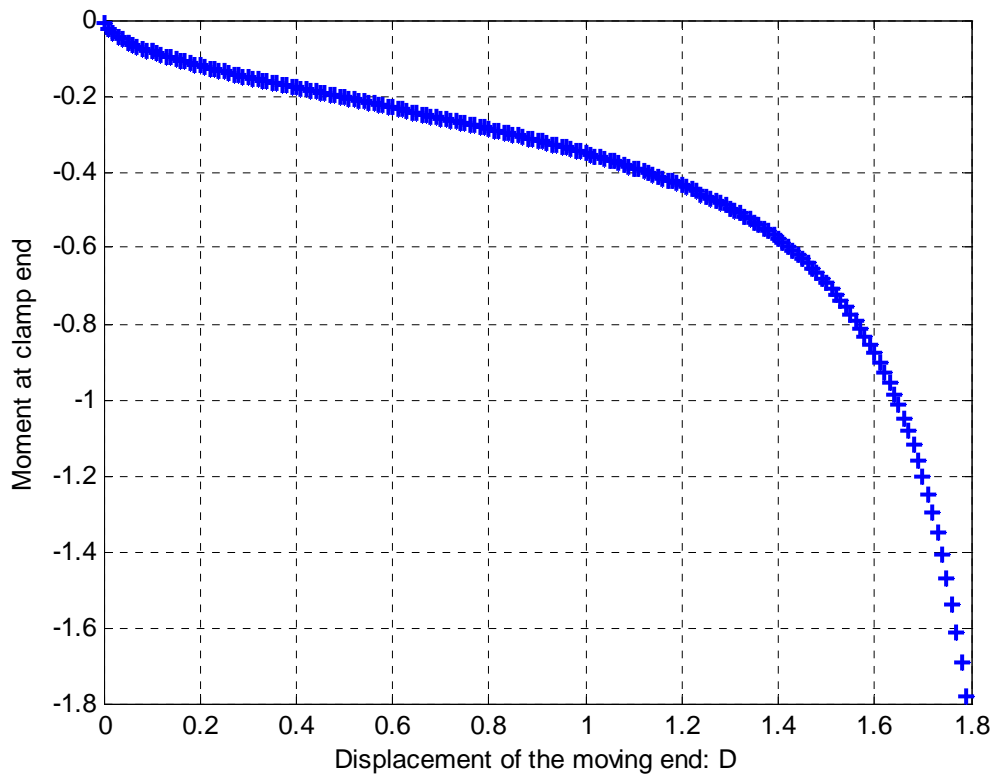


Figure 4.28 Diagram of $D-M$ (clamp-clamp elastica)

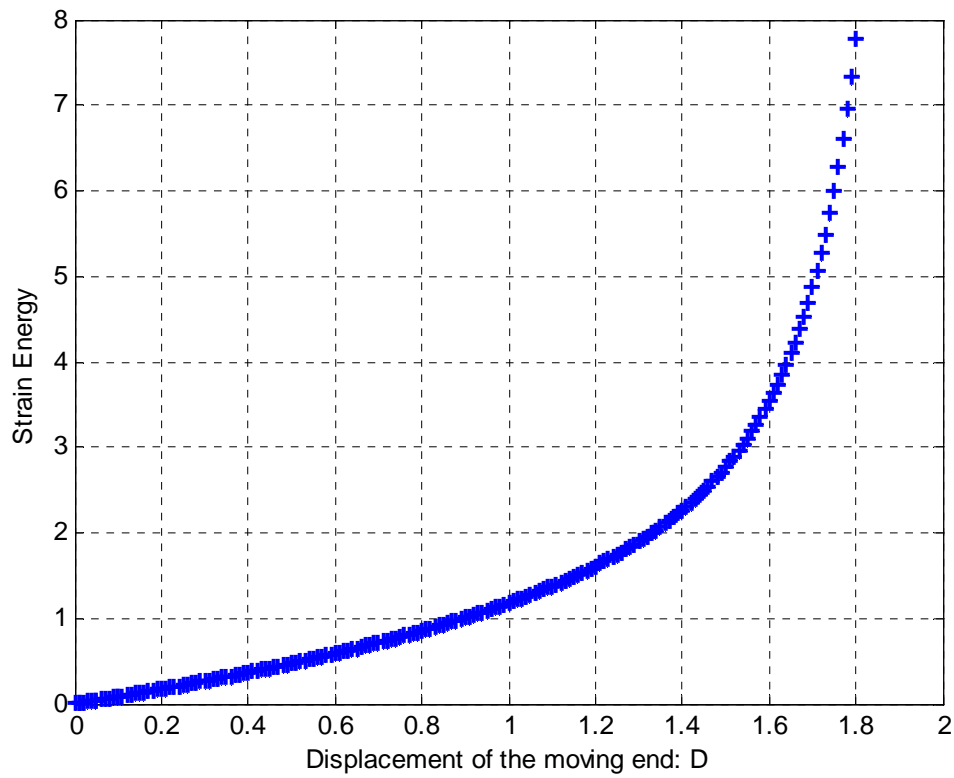


Figure 4.29 Diagram of $D-PE$ (clamp-clamp elastica)

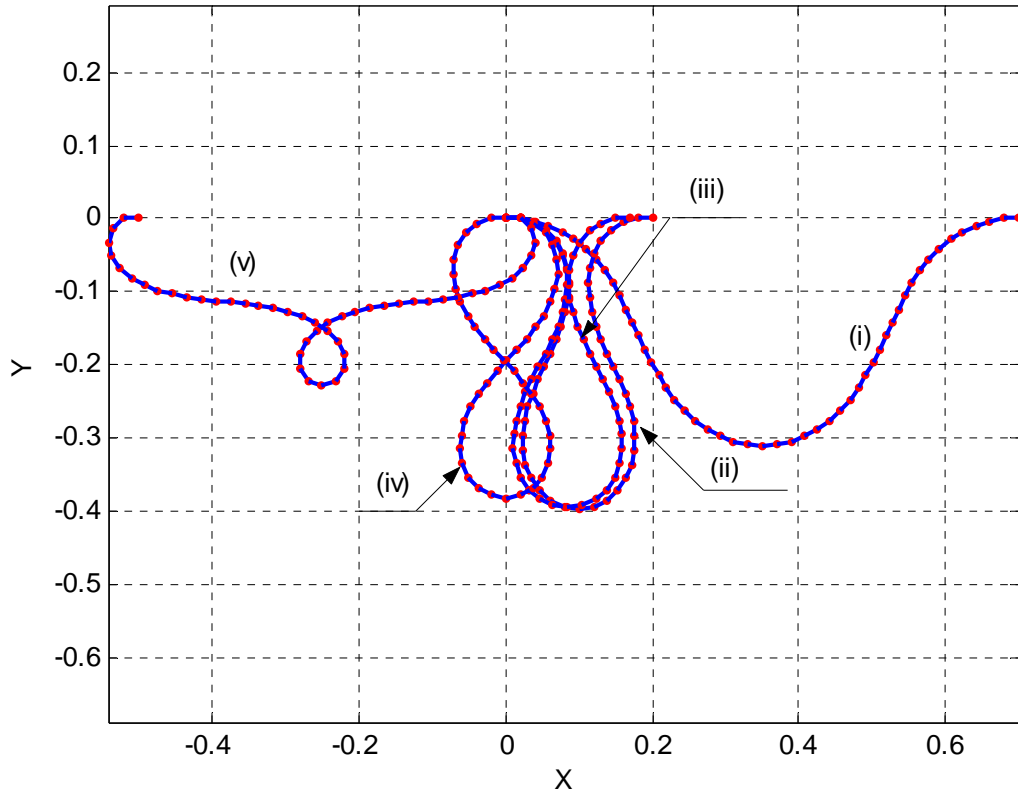


Figure.4.30 Several typical configurations of clamp-clamp elastica

Table 4.4 Numerical results at configurations shown in Figure 4.30 (clamp-clamp)

Configuration	D	λ_1 / P_{cr}	λ_2 / P_{cr}	w/L	M	PE
(i)	0.2	1.1597	0.000	0.2632	-0.1205	0.1733
(ii)	0.79	-1.821	0.0009	0.3951	-0.2841	0.8416
(iii)	0.83	-1.897	0.0006	0.3944	-0.2955	0.9003
(iv)	1	-2.332	0.0005	0.3813	-0.3510	1.1819
(v)	1.5	-7.676	0.0003	0.2288	-0.6935	2.7686

Because the elastica is approximated by rigid segments, the two ends will gradually demonstrate discontinuity. At the second stage that $D > 1$, the reaction forces at supports, potential energy and maximum displacement in y -direction all increase or decrease monotonically. Around $D=0.8$, we find the maximum deflection $w/L = 0.3951$.

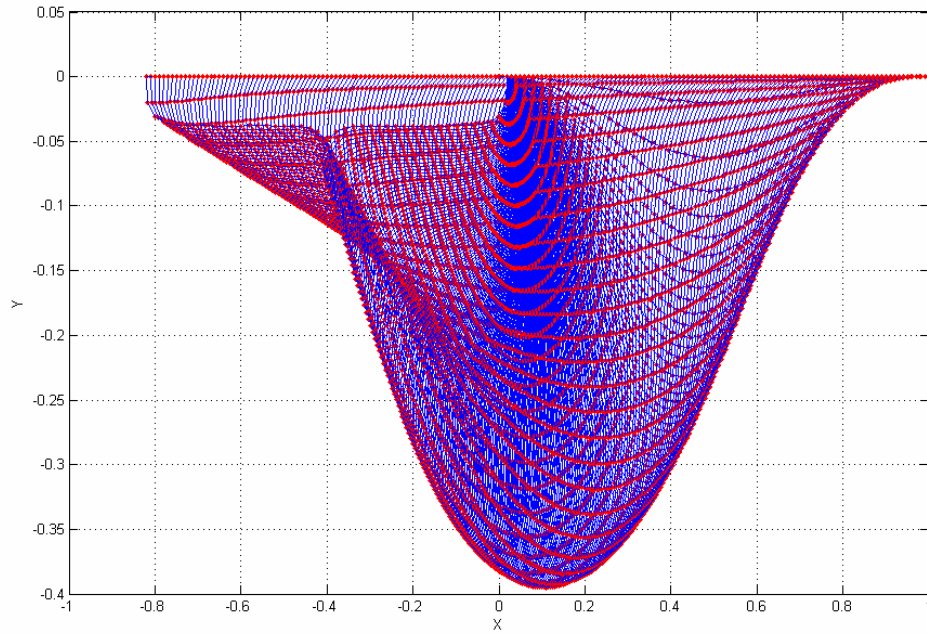


Figure.4.31 Superimposition of all the configurations of clamp-clamp elastica
 ($D \in [0,1.8]$)

4.4 Spatial elastica with both ends clamped

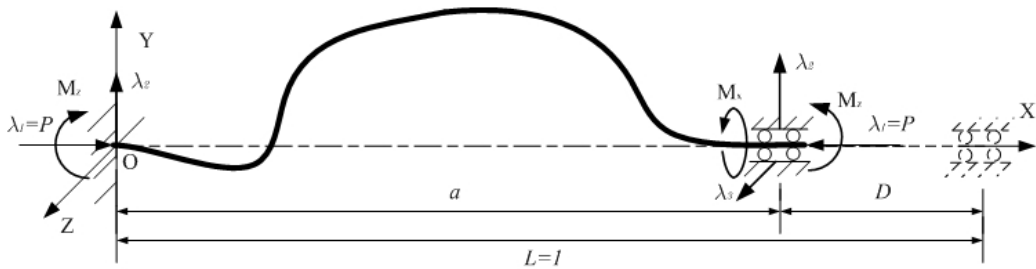


Figure 4.32 Geometry of spatial elastica with both ends clamped

The model and numerical framework proposed in this work are not limited to planar problems. They can also be extended to spatial cases. A typical example is illustrated in Figure 4.31 where clamp-clamp elastica can buckle out of the $x - y$ plane. As an extension of planar examples, we consider the elastica or the discrete elastic

chain is free to twist. The elastica is also assumed to have circular section and isotropic material. The tangents of both clamp ends locate along the x axis.

A spatial elastica's deformation is the combination of three kinds of deformations: bending, opening and twist. They are shown in Figure 4.33. We define the bending happens in $x'-y'$ plane; opening in $x'-z'$ plane; and twist in $y'-z'$ plane. The frame of $x'-y'-z'$ is the local coordinate in reference to the previous segment.

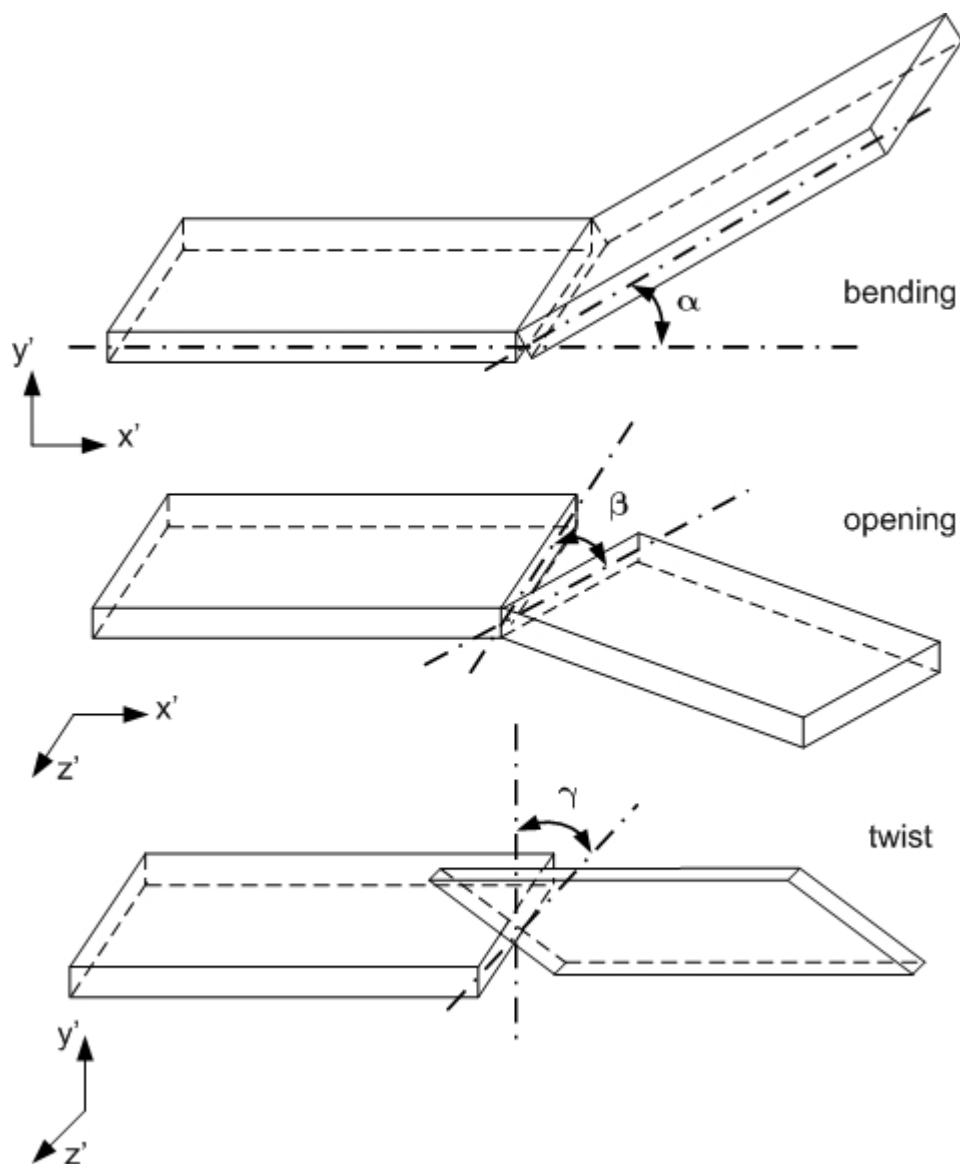


Figure 4.33 Three kinds of deformation of spatial elastica

In this example, elastica is still discretized into $N=50$ segments. Each segment is also assumed to be rigid without extensibility. If the effect of twisting is not taken into account, the frame of coordinates can be fixed. The position of each node needs two variables to be determined. These two variables can be different combinations of α_i , β_i , γ_i and θ_i as illustrated in Figure 4.34. In the figure below, α_i is the angle between x axis and projection of s_i on $x-y$ plane; β_i is the angle between x axis and projection of s_i on $x-z$ plane; γ_i is the angle between y axis and projection of s_i on $y-z$ plane; and θ_i is the spatial angle between s_i and x axis. Let s_{x-y} denote the length of the projection of s_i in $x-y$ plane and s_{y-z} be the counterpart in $y-z$ plane. Next, we derive the formulas needed in a minimization problem.

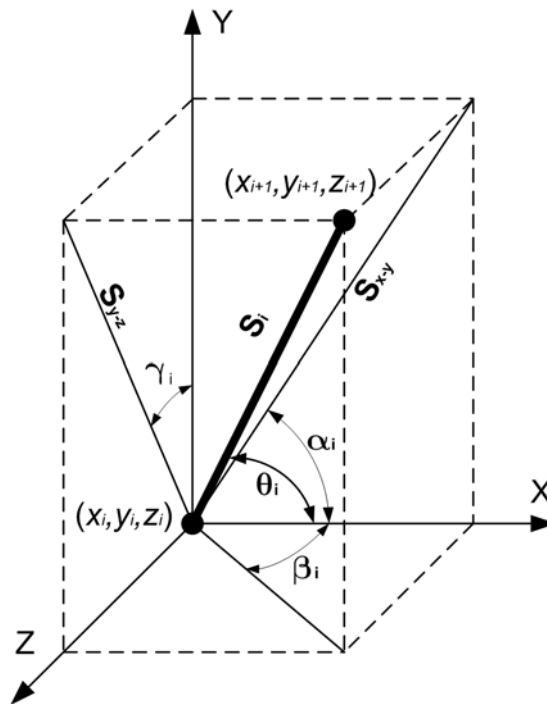


Figure 4.34 Geometry of a spatial rigid segment

It is easy to notice that

$$(x_{i+1} - x_i)^2 + (y_{i+1} - y_i)^2 + (z_{i+1} - z_i)^2 = s_i^2 \quad (4.1)$$

With the aid of Figure 4.34, we can write

$$x_{i+1} = x_i + s_{x-y} \cos \alpha_i \quad (4.2)$$

$$y_{i+1} = y_i + s_{x-y} \sin \alpha_i = y_i + s_{y-z} \cos \gamma_i \quad (4.3)$$

$$z_{i+1} = z_i + s_{y-z} \cos \gamma_i \quad (4.4)$$

From (4.1) to (4.4), s_{x-y} and s_{y-z} can be expressed by s_i . Thus we have:

$$x_{i+1} = x_i + s_i \cos \alpha_i \sqrt{\frac{\cos^2 \gamma_i}{1 - \cos^2 \alpha_i \sin^2 \gamma_i}} \quad (4.5)$$

$$y_{i+1} = y_i + s_i \sin \alpha_i \sqrt{\frac{\cos^2 \gamma_i}{1 - \cos^2 \alpha_i \sin^2 \gamma_i}} \quad (4.6)$$

$$z_{i+1} = z_i + s_i \sin \gamma_i \sqrt{\frac{\sin^2 \alpha_i}{1 - \cos^2 \alpha_i \sin^2 \gamma_i}} \quad (4.7)$$

In (4.5), (4.6) and (4.7), the terms under square root sign are always greater or equal to zero therefore guarantee x_{i+1} , y_{i+1} and z_{i+1} to be real. The signs of $(x_{i+1} - x_i)$, $(y_{i+1} - y_i)$ and $(z_{i+1} - z_i)$ are determined by α_i and γ_i . In addition, we can obtain the relationship that

$$\tan \beta_i = \tan \alpha_i \tan \gamma_i \quad (4.8)$$

With the four equations (4.5)-(4.8), and assuming the discrete elastic chain is free to twist, the problem can be expressed in standard optimization formulation:

$$\text{obj: } \frac{1}{2} \sum_{i=2}^N [K_{m1i} (\alpha_i - \alpha_{i-1})^2 + K_{m2i} (\tan^{-1}(\tan \alpha_i \tan \gamma_i) - \tan^{-1}(\tan \alpha_{i-1} \tan \gamma_{i-1}))^2] \quad (4.9)$$

$$\text{s.t.: } -a + \sum_{i=1}^N s_i \cos \alpha_i \sqrt{\frac{\cos^2 \gamma_i}{1 - \cos^2 \alpha_i \sin^2 \gamma_i}} = 0 \quad (4.10)$$

$$\sum_{i=1}^N s_i \sin \alpha_i \sqrt{\frac{\cos^2 \gamma_i}{1 - \cos^2 \alpha_i \sin^2 \gamma_i}} = 0 \quad (4.11)$$

$$\sum_{i=1}^N s_i \sin \gamma_i \sqrt{\frac{\sin^2 \alpha_i}{1 - \cos^2 \alpha_i \sin^2 \gamma_i}} = 0 \quad (4.12)$$

In these equations, K_{m1i} and K_{m2i} are elastic spring constants of x - y plane and x - z plane respectively. Equations (4.9)-(4.12) give a general nonlinear optimization description to the problem of spatial elastica that is free to twist. The formulation is straight-forward: determining the configuration of elastica by minimizing the bending energy. However, on the computational aspect, the disadvantage lies in the calculation of \tan^{-1} terms. In addition at initial stage of searching, the denominator terms may also cause problem when $\cos^2 \alpha_i \sin^2 \gamma_i$ approaches 1. With careful manipulation, the solution can still be obtained. But we will not use these formulae to solve the problem. Further simplification is made next.

If the cross-section of elastica is circular and material is isotropic, the bending stiffness EI will be consistent in every direction. Hence the bending energy at the i th node is only related to constant K_{mi} . This simplification is never trivial. Many real application problems have such characteristics. Apparently, α_i and β_i are not suitable to model the elastica. Instead, we use γ_i and θ_i . The bending curvature is now defined by $\frac{\psi_i}{s_i}$. We need to express ψ_i in terms of γ_i and θ_i .

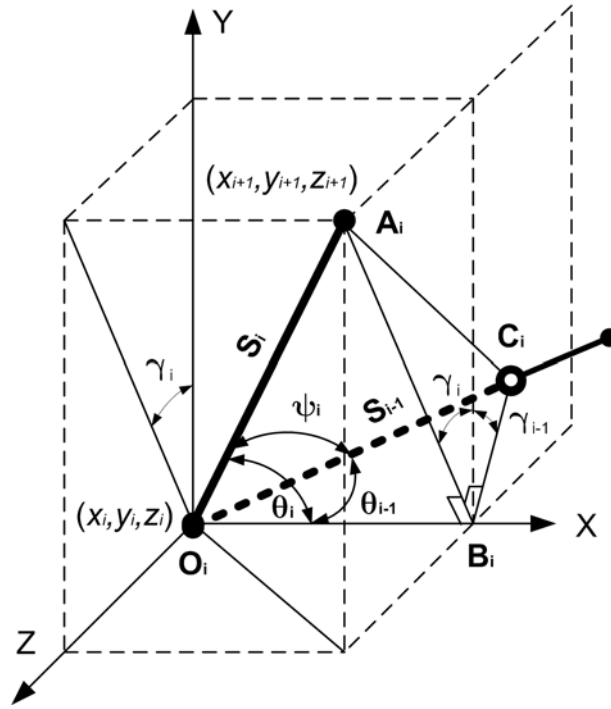


Figure 4.35 Geometry of a spatial rigid segment with circular section

As illustrated in Figure 4.35, ψ_i is the spatial angle between s_i and s_{i-1} . The segment s_i starts from O_i and points to A_i . In the above figure, extension line of S_{i-1} intersect the plane $A_i B_i C_i$, which is parallel to $y-z$ plane, at C_i . To define ψ_i , the $|\overline{O_i C_i}|$ and $|\overline{A_i C_i}|$ are necessary to be obtained first. From trigonometric formulae, they can be expressed in terms of γ_{i-1} , γ_i , θ_{i-1} and θ_i . Neglecting the detailed procedure, we can finally get these formulae:

$$x_{i+1} = x_i + s_i \cos \theta_i \quad (4.13)$$

$$y_{i+1} = y_i + s_i \sin \theta_i \cos \gamma_i \quad (4.14)$$

$$z_{i+1} = z_i + s_i \sin \theta_i \sin \gamma_i \quad (4.15)$$

and

$$\psi_i = \cos^{-1}(\cos \theta_i \cos \theta_{i-1} + \sin \theta_i \sin \theta_{i-1} \cos(\gamma_i - \gamma_{i-1})) \quad (4.16)$$

The boundary of θ_i must be set as $[0, \pi]$. This will guarantee the signs in (4.13) - (4.16) to be correct. If we set $\gamma_{i-1} = 0$ and $\gamma_i = 0$. Then equations (4.13) to (4.15) for spatial elastica will become the same equations for planar elastica. And (4.16) becomes $\psi_i = \cos^{-1}(\cos(\theta_i - \theta_{i-1})) = \theta_i - \theta_{i-1}$.

With equation (4.13) to (4.16) the standard form of this constrained optimization problem can be expressed as:

$$obj: \frac{1}{2} \sum_{i=2}^N K_{mi} \psi_i^2 \quad (4.17)$$

$$s.t.: -a + \sum_{i=1}^N s_i \cos \theta_i = 0 \quad (4.18)$$

$$\sum_i^N s_i \sin \theta_i \cos \gamma_i = 0 \quad (4.19)$$

$$\sum_i^N s_i \sin \theta_i \sin \gamma_i = 0 \quad (4.20)$$

In this example, we change the control parameter D from 0 to 1. The configurations and diagram of numerical results are plotted in the following figures.

The configurations are arranged in each figure as $\begin{bmatrix} x-y \text{ plane} & x-z \text{ plane} \\ y-z \text{ plane} & \text{perspective view} \end{bmatrix}$.

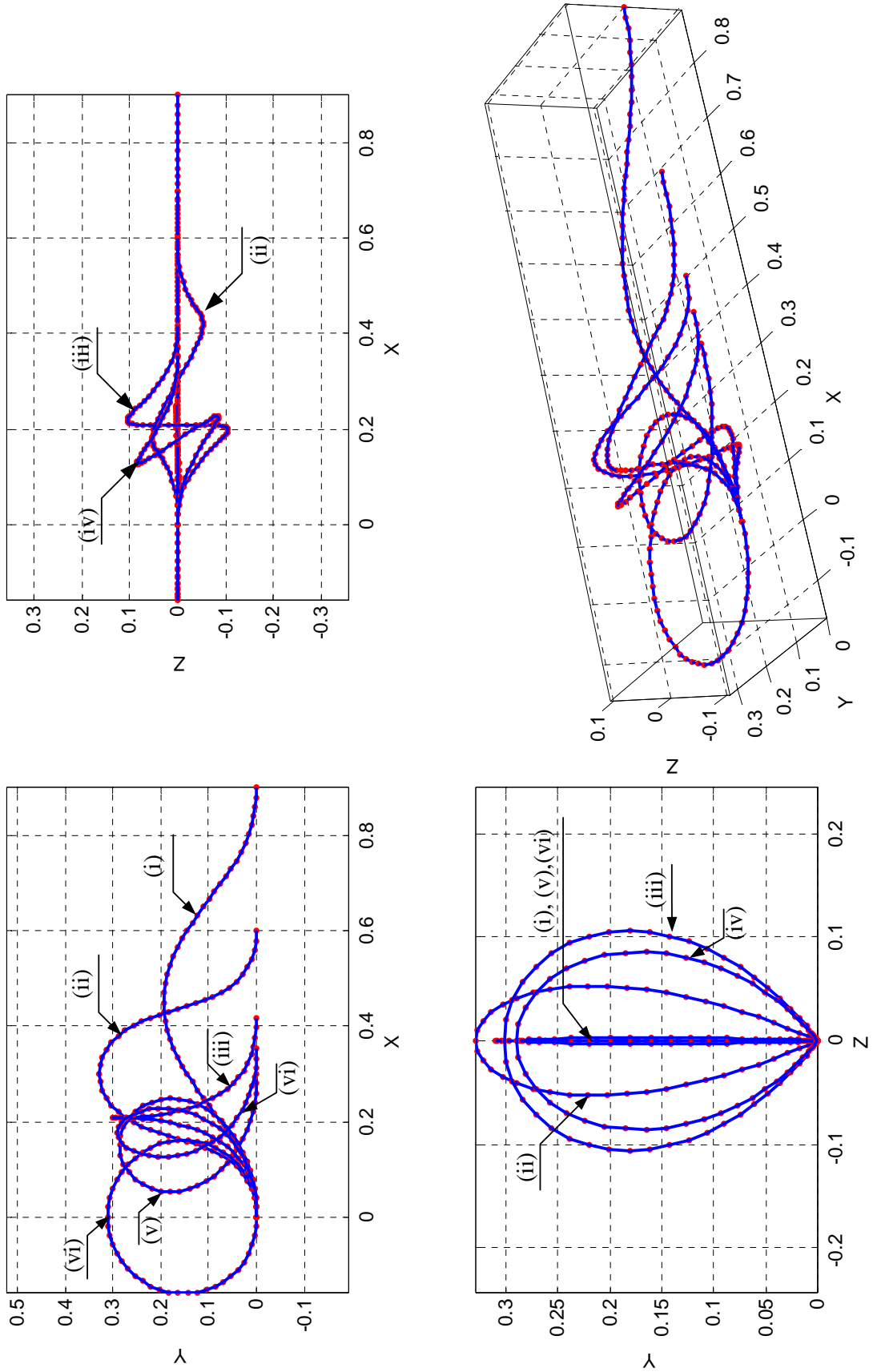


Figure 4.36 Several critical configurations of clamp-clamp elastica ($T = \pi$)

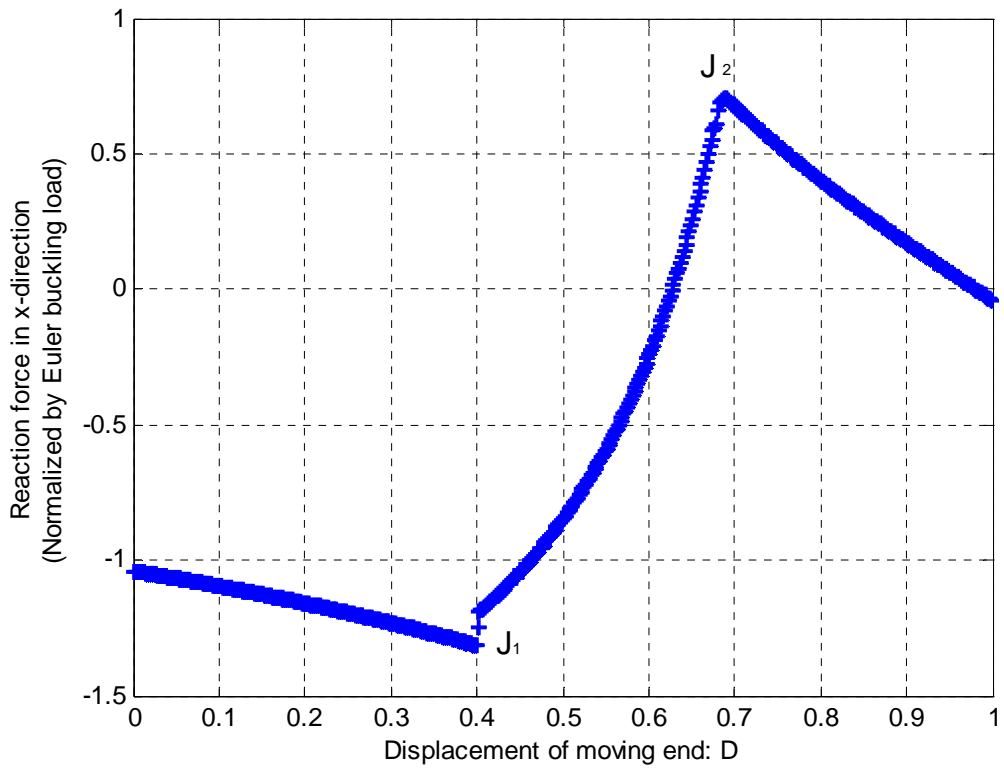


Figure 4.37 Diagram of $D - \lambda_1 / P_{cr}$ (spatial clamp-clamp elastica)

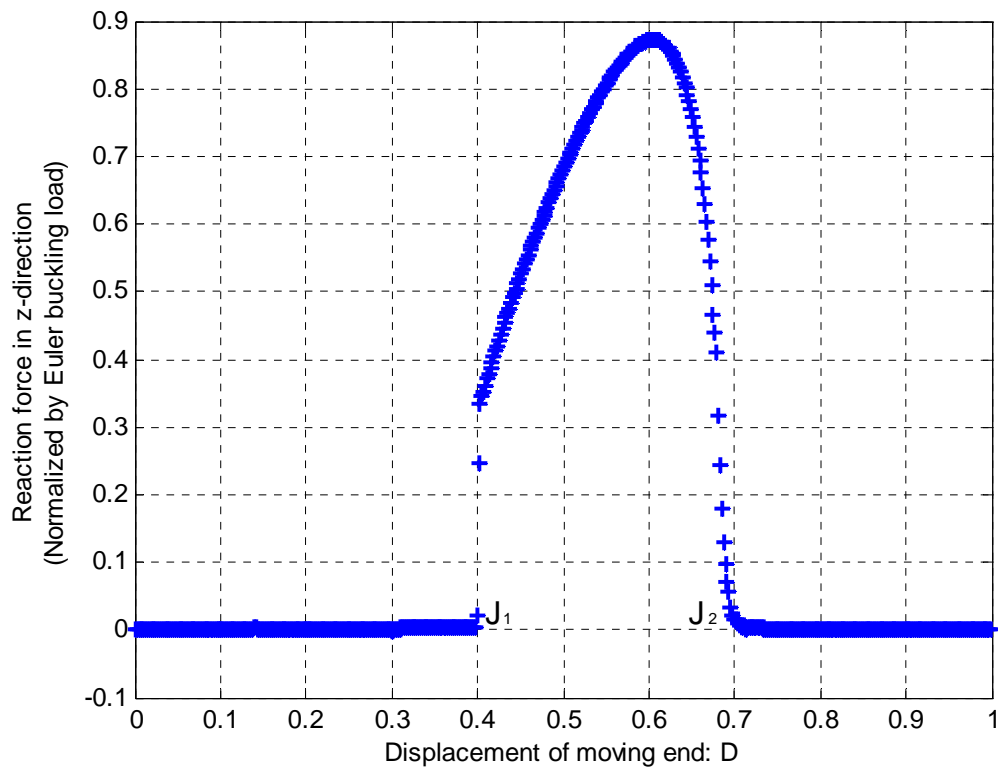


Figure 4.38 Diagram of $D - \lambda_3 / P_{cr}$ (spatial clamp-clamp elastica)

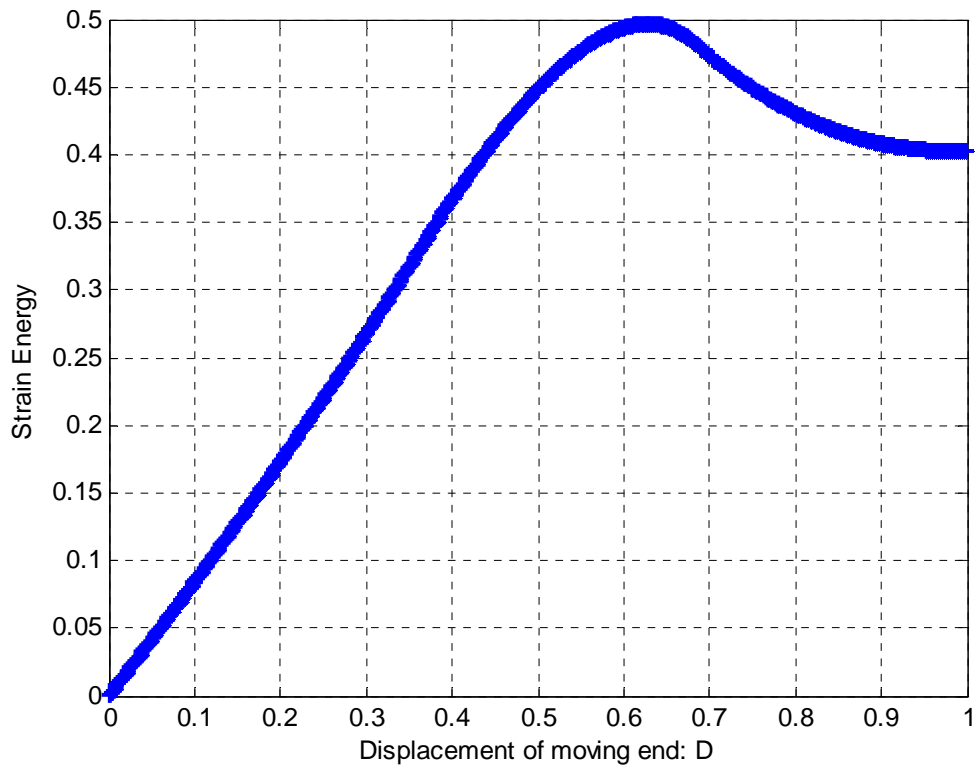


Figure 4.39 Diagram of D – Strain energy (spatial clamp-clamp elastica)

When the control parameter D starts from zero, the reaction force in x -direction starts from the critical buckling load $\frac{4\pi^2 EI}{L^2}$. Before $D=0.4$, the elastica is maintained in a planar configuration. The diagram of $D-\lambda_1/P_{cr}$ is same as the example in section 4.3. A representative configuration (i) in Figure 4.36 is when $D=0.1$. Since $D=0.4$, the path of $D-\lambda_1/P_{cr}$ does not follow the one of planar clamp-clamp elastica. This is because the out-of-plane-buckling happens. The point is marked J_1 in Figure 4.37 and Figure 4.38. The reaction force in x -direction begins to decrease in magnitude, while the reaction force in z -direction appears. Increasing D , the configuration of elastica will evolve back to a planar configuration with a loop. During this procedure, λ_1 will change direction and λ_3 will gradually change back to 0. Around $D=0.69$, the post-buckling behaviour will be in-plane. Configuration (v) is

when $D = 0.7$. Afterwards, the post-buckling will remain in the $x-y$ plane. When $D = 1$, the configuration (vi) in Figure 4.36 is obtained. Comparing Figure 4.39 and Figure 4.29, the strain energy that permitting out-of-plane buckling is lower than that the elastica is confined in $x-y$ plane.

4.5 Spatial elastica with two ends clamped but not locate on x-axis

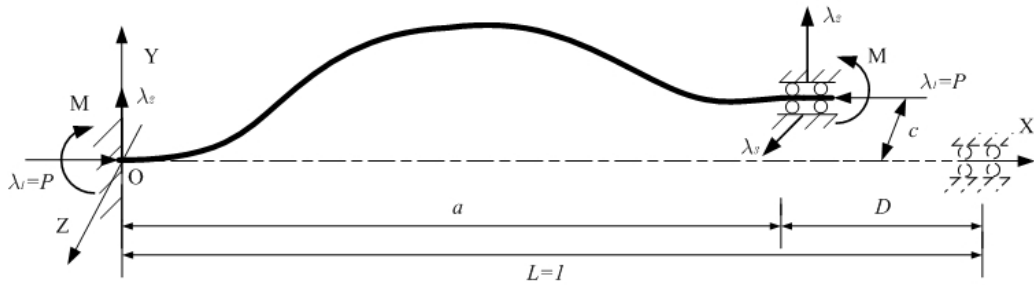


Figure 4.40 Geometry of clamp-clamp spatial elastica (two ends parallel)

The example presented in this section is similar to the problem in section 4.4. But this time we fix D , and move the end in z -direction away from x -axis. The displacement in z -direction is denoted with c as illustrated in Figure 4.40. The main settings are same as the ones in the previous section. But we fix D this time, and change c instead. Correspondingly, (4.19) will be revised as

$$\sum_i^N s_i \sin \theta_i \sin \gamma_i = c \quad (4.21)$$

The path following strategy is still used here to obtain the path of λ_1 and λ_3 . They are

also normalized by Euler buckling load $\frac{4\pi^2 EI}{L^2}$.

The first example is started from $D = 0.3$, and change c from 0 to 0.5 with increment 0.001. The numerical results as reaction forces in x , and z direction and configurations when $c=0, 0.18$ and 0.36 are plotted in Figure 4.41 to Figure 4.43.

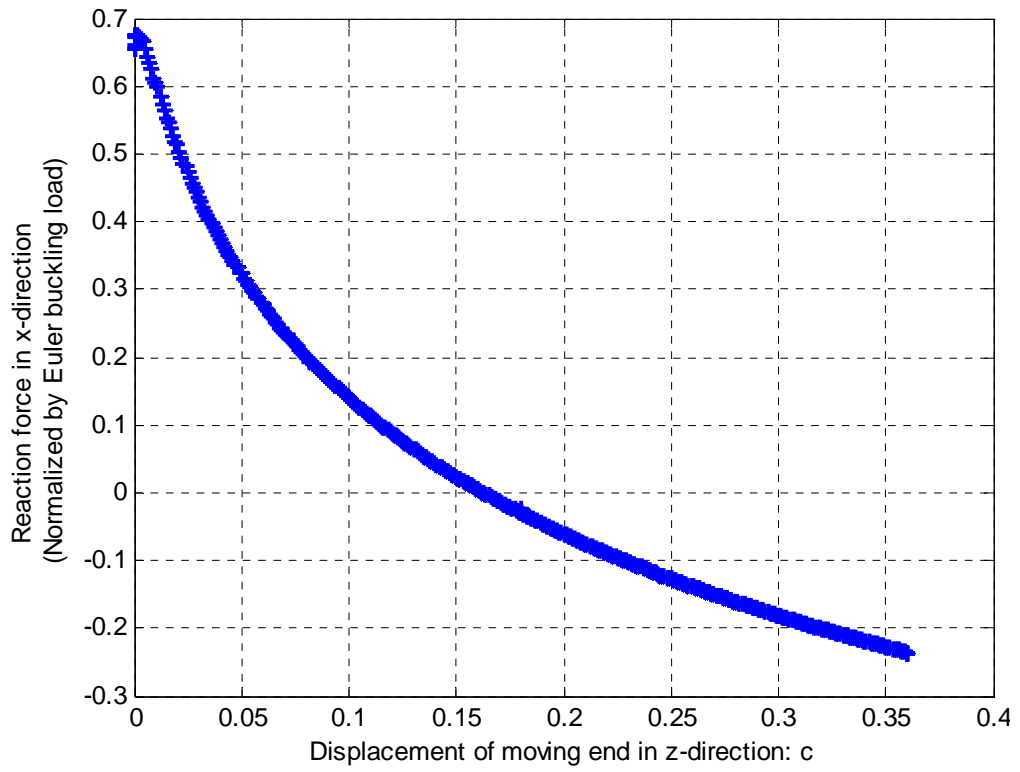


Figure 4.41 Diagram of $c - \lambda_1 / P_{cr}$ (spatial clamp-clamp elastica, $D=0.7$)

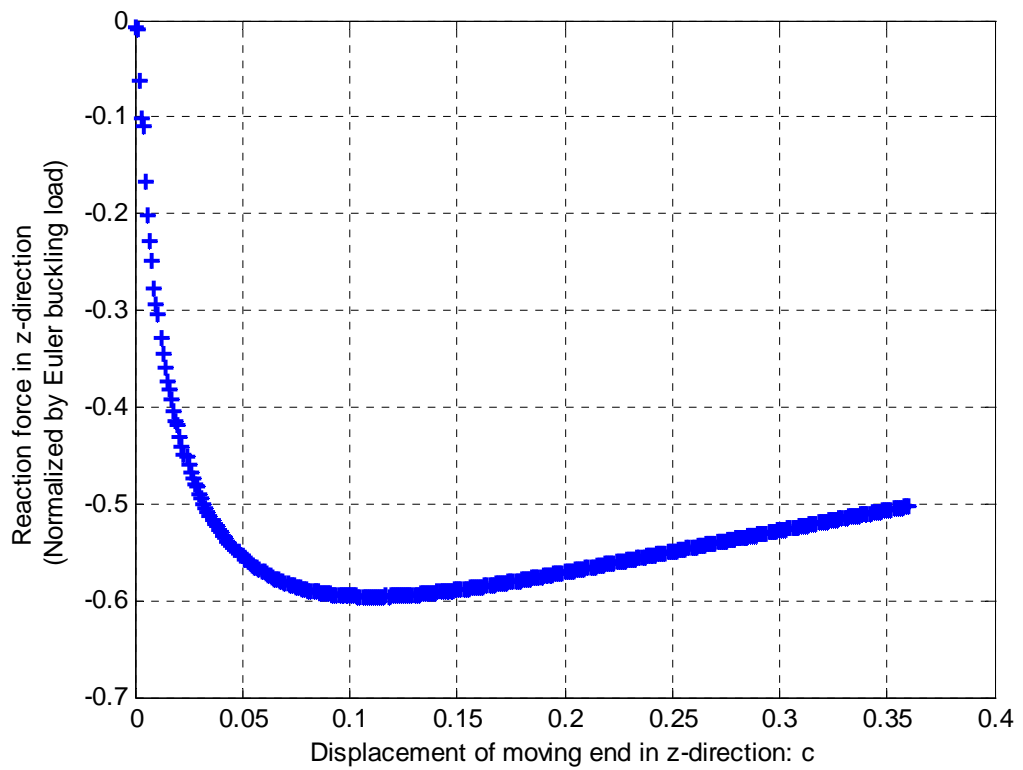


Figure 4.42 Diagram of $c - \lambda_3 / P_{cr}$ (spatial clamp-clamp elastica, $D=0.7$)

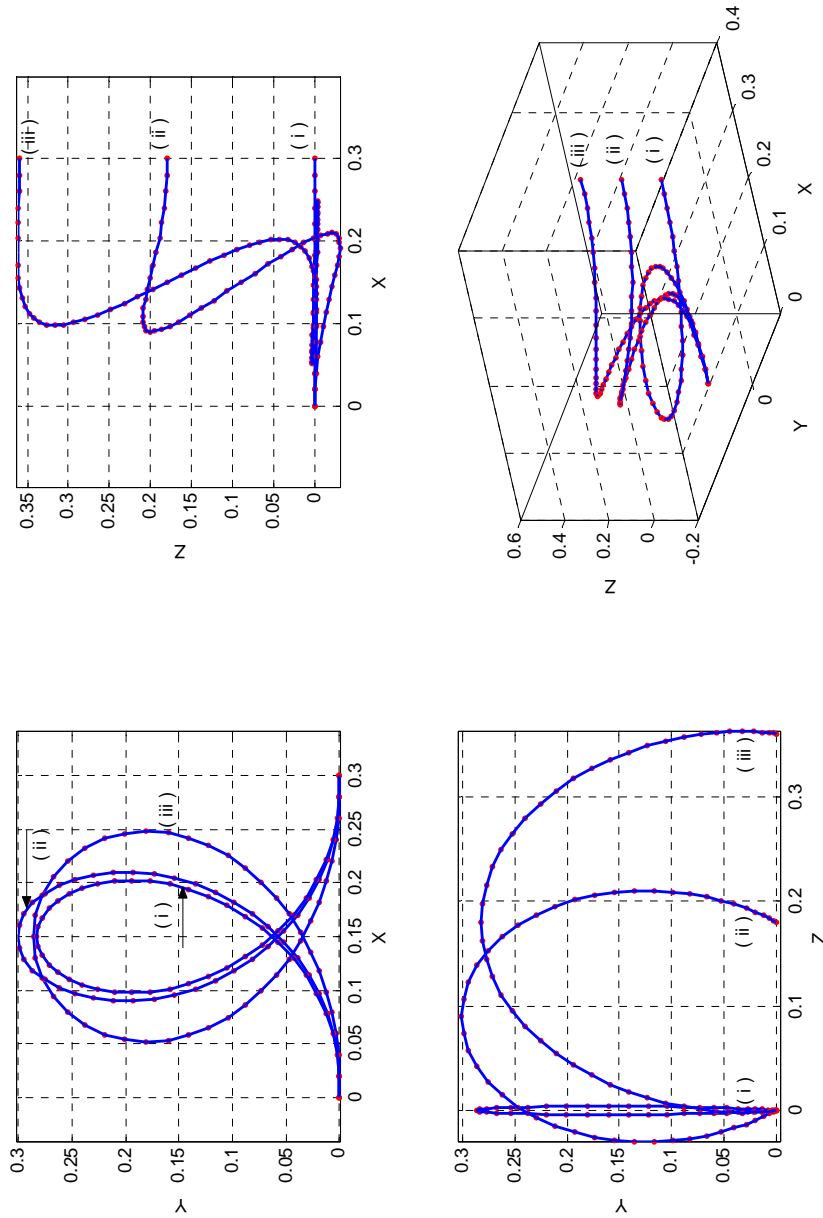


Figure 4.43 Configurations when $D=0.7$ and $c=0$ (i), 0.18 (ii), 0.36 (iii)

As we can see from Figure 4.41, λ_1 will change direction around $c=0.16$. And λ_3 will change its trend during this procedure. Before $c=0.12$, λ_3 increase from 0 to $0.6P_{cr}$. Then it will decrease slowly.

Another more interesting and familiar example is when $D=1$. We fix $D=1$, and change displacement in z -direction c with increment of 0.002. The numerical results and configurations are plotted in Figure 4.44 to Figure 4.46.

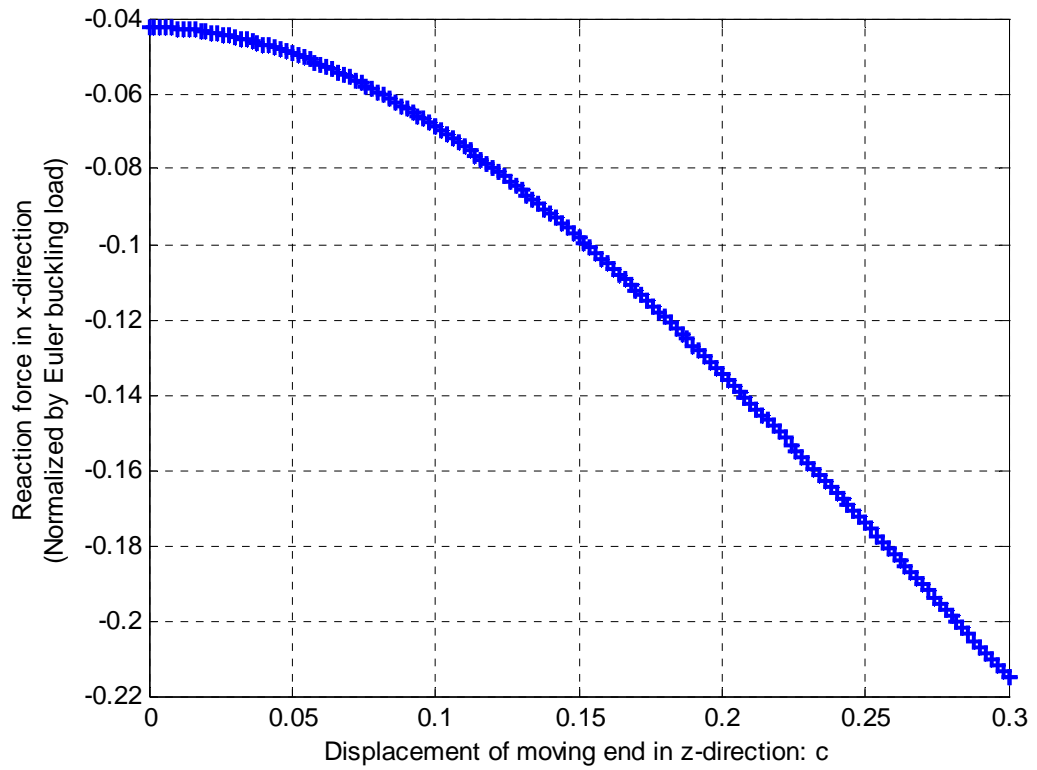


Figure 4.44 Diagram of $c - \lambda_1 / P_{cr}$ (spatial clamp-clamp elastica, $D=1$)

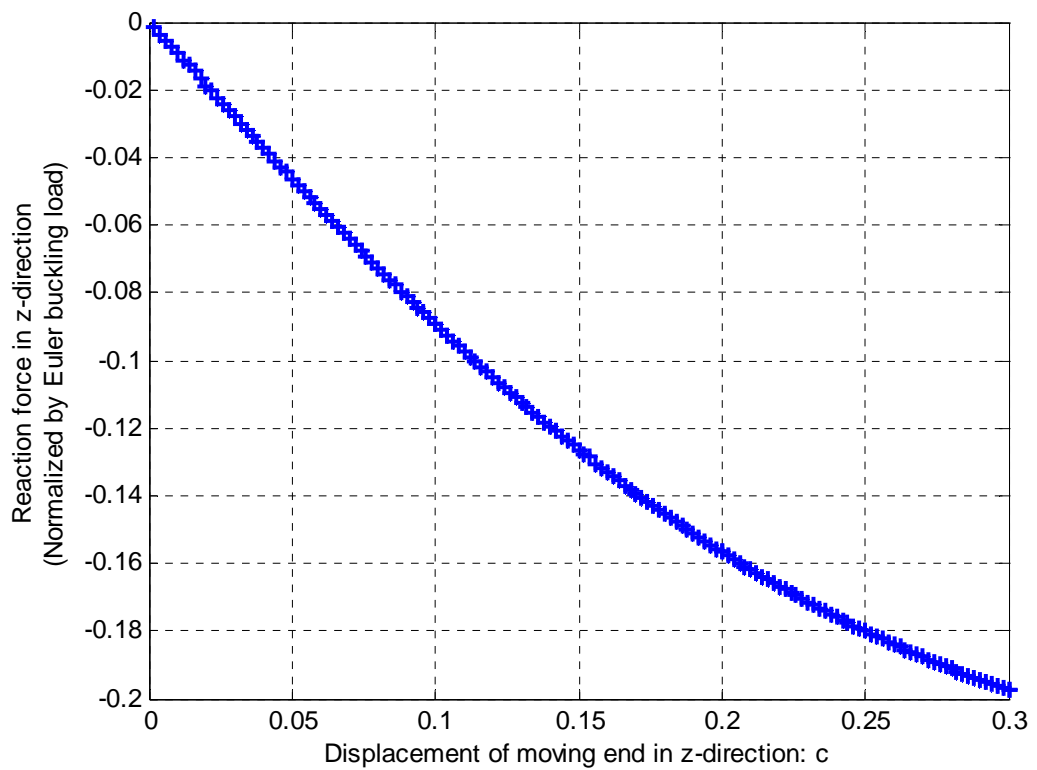


Figure 4.45 Diagram of $c - \lambda_3 / P_{cr}$ (spatial clamp-clamp elastica, $D=1$)

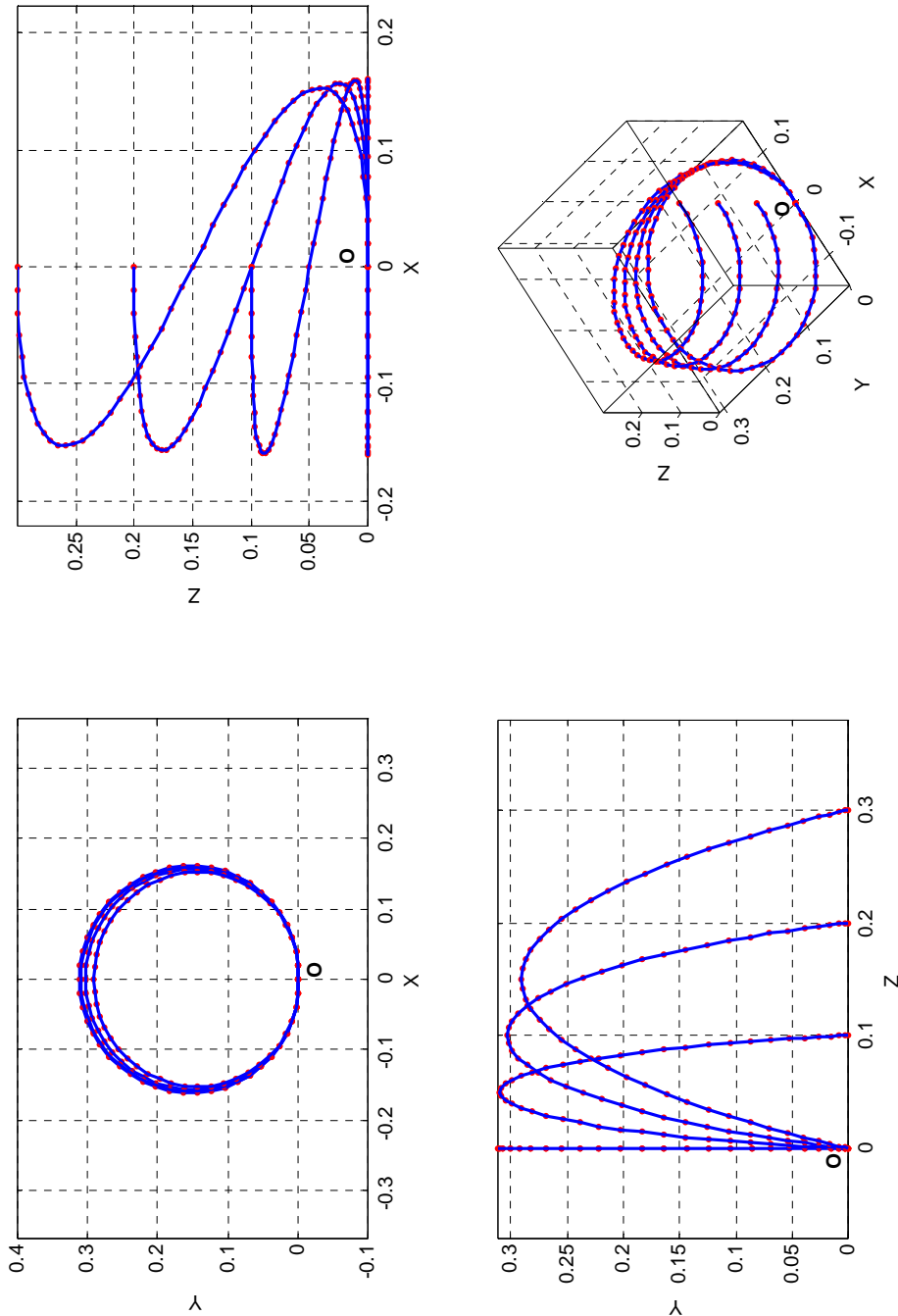


Figure 4.46 Configurations when $D=1$, $c=0, 0.1, 0.2$, and 0.3

The most important result of this example is plotted in Figure 4.45. The reaction force in z -direction is almost linear when c is small. From configurations in Figure 4.46, we can easily connect this problem to an elastic spring. Each configuration can be viewed as a filament of a helix elastic spring. This also explains why the force in z -direction varies linearly with the displacement c . When c is not

small enough, λ_3 will vary nonlinearly. It is also noticed that the paths of $c - \lambda_1 / P_{cr}$ and $c - \lambda_3 / P_{cr}$ have different characteristics when D is different.

4.6 Pin-pin elastica with side-wall constraints

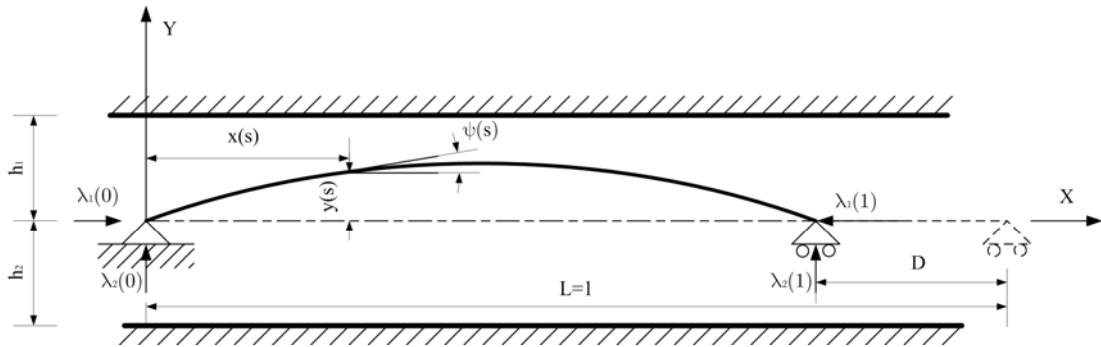


Figure 4.47 Geometry of pin-pin elastica with side-wall constraints

In the previous examples, we have used the numerical method introduced in Chapter 3 to obtain configurations of elastica with different boundary conditions. Since we model the problem as a constraints-satisfying optimization, it is easy to add additional geometric constraints as in the example shown in Figure 4.47. As modeled in section 2.6, a penalty term is added to the original objective function (2.17). By taking this as a constrained optimization problem, Eq. (2.33), subject to constraints, Eq. (2.18), the configuration of a pin-pin elastica with side-wall constraints can be found using the same method developed in Chapter 3. The corresponding reaction force in x -direction and y -direction can also be found. In this section, the sudden change among symmetric, asymmetric and antisymmetric configuration is called a jump.

Firstly, we consider an elastica confined in x - y plane and divided into 50 segments. The two sidewalls are located on the opposite sides of x -axis with a distance $h = 0.25 / L$. And the value b is defined as 0.00001 to describe the characteristic of the “soft” wall. Changing D from 0 to 2 with increment 0.01, the numerical results are plotted in the following figures. In Figure 4.48, the side-walls are plotted as solid lines.

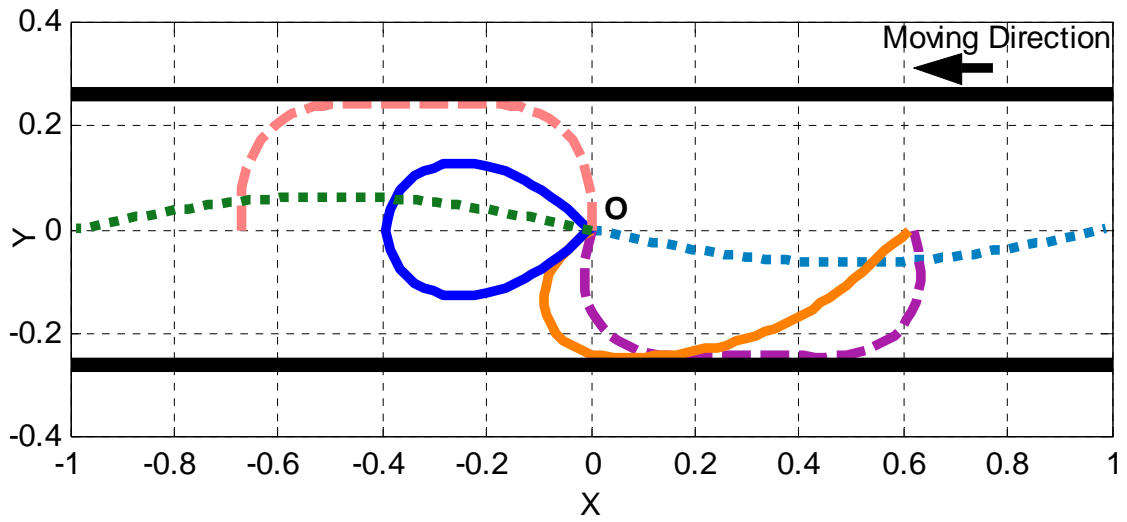


Figure 4.48 Several configurations of pin-pin elastica with side-wall constraints ($h=0.25/L$)

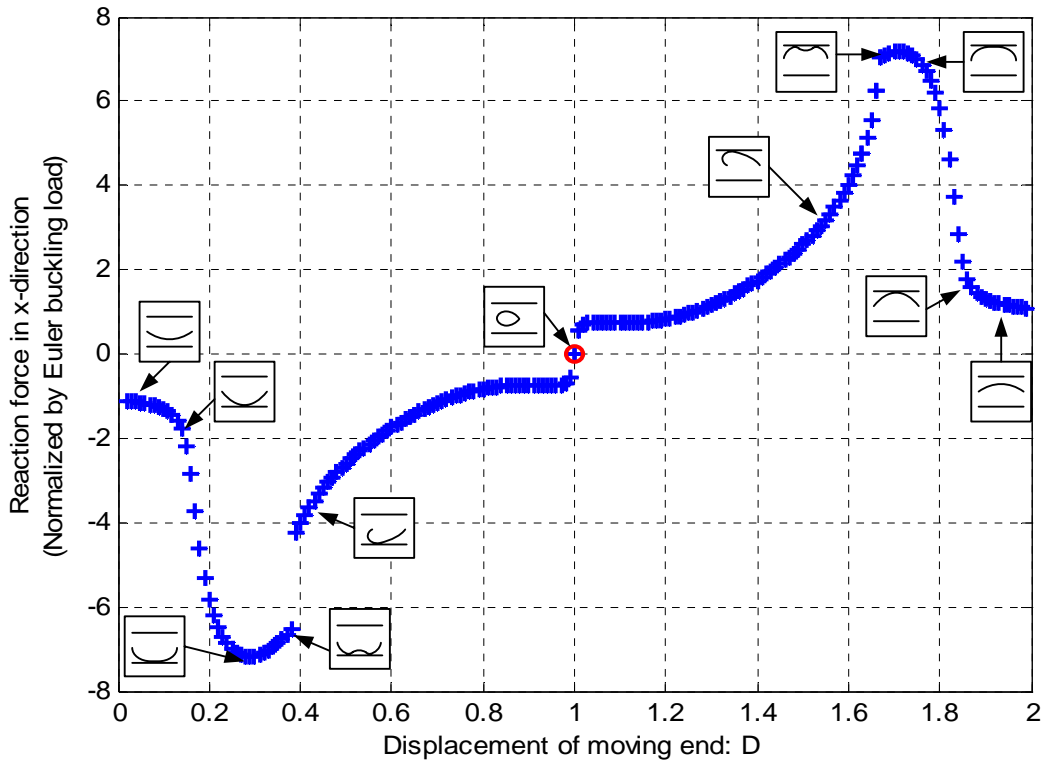


Figure 4.49 Diagram of $D - \lambda_1 / P_{cr}$ (pin-pin elastica, $h=0.25/L$)

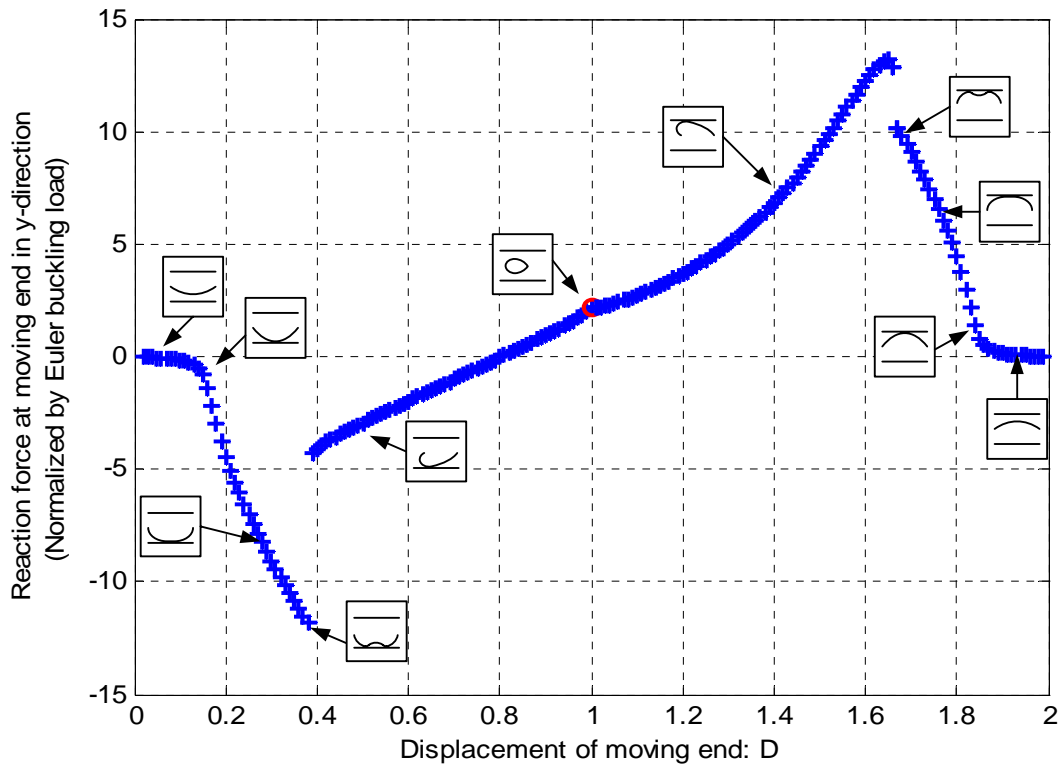


Figure 4.50 Diagram of $D - \lambda_2 / P_{cr}$ (pin-pin elastica, $h=0.25/L$)

From Figure 4.49 and Figure 4.50, we can observe that there is a jump of λ_1 and λ_2 at $D=0.39$. The corresponding configuration changes abruptly from symmetric one to asymmetrical one. As we increase continuously the value of D to 1, the two pin ends coincide. This configuration is identical to one of the configurations shown in Figure 4.9. And at $D=1$, the reaction force in x direction approaches 0, while the reaction force in y direction approaches $2.1867P_{cr}$, as discussed in section 4.1.3.

At the second stage $D \in (1, 2]$, the elastica has contact with the opposite wall. The elastica's behaviour, which is described in terms of reaction forces, demonstrates a similar behaviour as in the first stage. However, because the configuration jumps to an asymmetric configuration, the reaction forces in y direction at two ends are not equal. Here, λ_2 is the reaction force at the moving end. When the elastica sacrifices symmetry to reach lower energy, it can jump to either side. Therefore, the curve of

load-displacement relationship will be different. Figure 4.49 and Figure 4.50 show the load-displacement path when elastica jumps to left. While Figure 4.51 shows the counterpart when elastica jumps to right. The load-displacement curves of reaction force in x direction are identical for two cases (left and right). Due to asymmetry, the two diagrams of $D - \lambda_2 / P_{cr}$ are not same but share some common features. Figure 4.51 can be obtained when we rotate Figure 4.50 about origin for π . Because the left asymmetric configuration and the right one are mirror to each other at a given D , reaction force at the moving end $\lambda_2(1)$ for left asymmetric configuration equals to the reaction force $\lambda_2(0)$ at the fixed end O for the right one under the same geometric constraints. Therefore, the summation of $\lambda_2(0)$ and $\lambda_2(1)$ of these two cases gives the reaction force at the rigid wall. When the two ends coincide, λ_2 for both cases are $2.1867P_{cr}$ and $-2.1867P_{cr}$. The summation gives zero. Physically, it is at this point that there is no contact between the elastica and the side-wall. From the solutions in Section 4.1, it is obvious that unless h of the sidewall is within the range (0.3918, 0.4033), the elastica will have contact with sidewalls after contact happens and when $D \neq 1$. However, when $h \in (0.3918, 0.4033)$, jumping could not be observed.

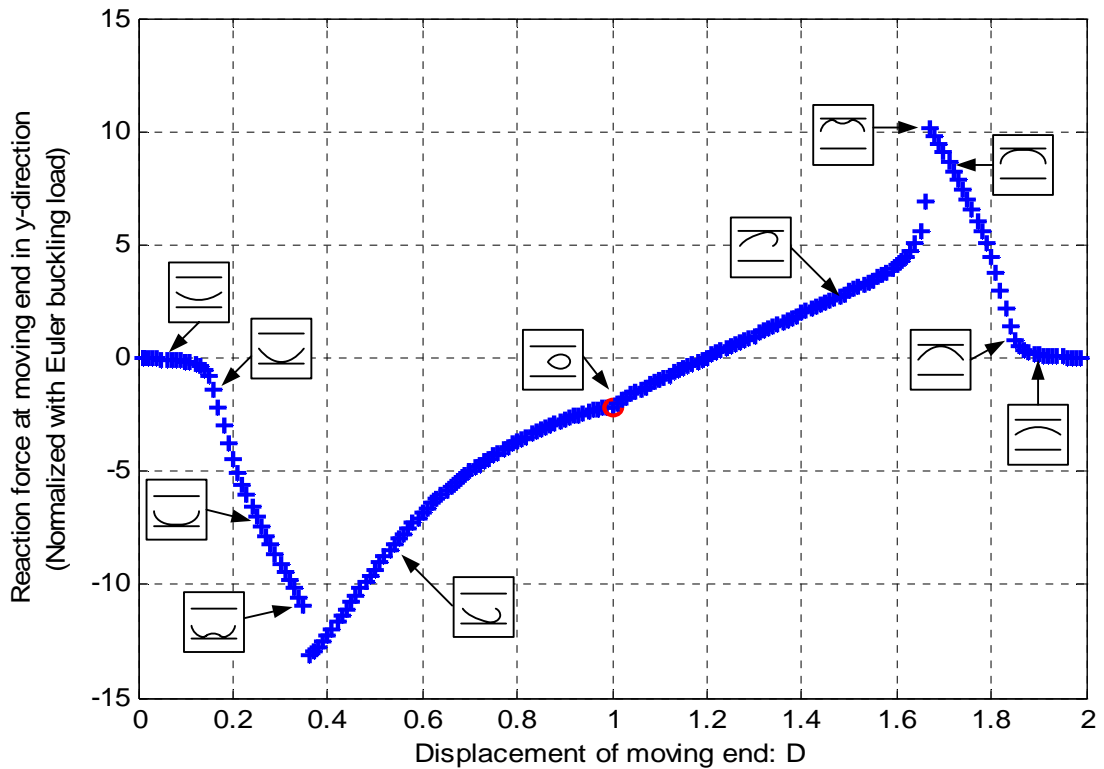


Figure 4.51 Diagram of $D - \lambda_2 / P_{cr}$ (the elastica jumps to asymmetric configuration that is opposite to the one shown in Figure 4.50)

Apart from jumping to asymmetric configuration, the elastica can also jump to an antisymmetric configuration at a critical point. Here, we set $h=0.15/L$. Repeating the numerical procedures, the configurations are obtained and plotted in Figure 4.52. Firstly, we increase D . Point contact, line contact and secondary buckling happens in sequence. After secondary buckling, the elastica gradually goes to the third mode (ii). At a critical point $D=0.47$, the elastica jumps from configuration (ii) to an antisymmetric configuration (iii) in Figure 4.52. In this case, elastica has contact with both side-walls. If D is continuously increased to 1, the configuration plotted in Figure 4.53 is obtained. Next, we decrease D . However, at the previous jumping point $D=0.47$, the load-displacement relationship will not follow the previous path where we

increase D . Rather, it will remain at the second mode. Configurations (iv) and (v) will appear in this procedure. And λ_1 will approach buckling load for second mode $\frac{4\pi^2 EI}{L^2}$.

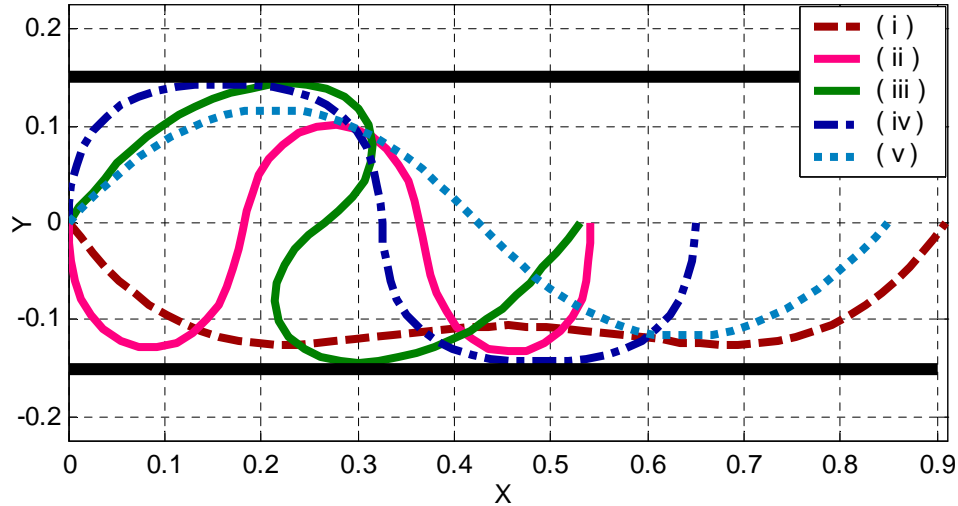


Figure 4.52 Critical configurations of pin-pin elastica with side-wall constraints

($h=0.15/L$)

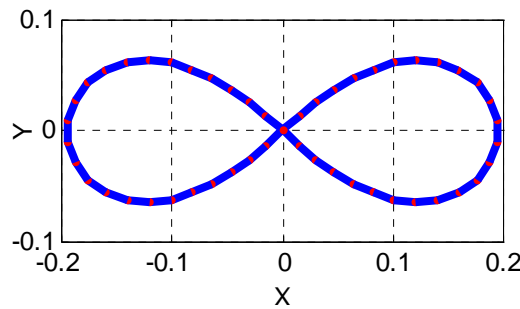


Figure 4.53 Configuration of second mode when two pin ends coincide

Next, the global behaviours are given in Figure 4.54 and Figure 4.55. They combine the load-displacement curves for symmetric configurations, asymmetric configurations and antisymmetric configurations. Figure 4.56 demonstrates the strain energy of the corresponding configurations.

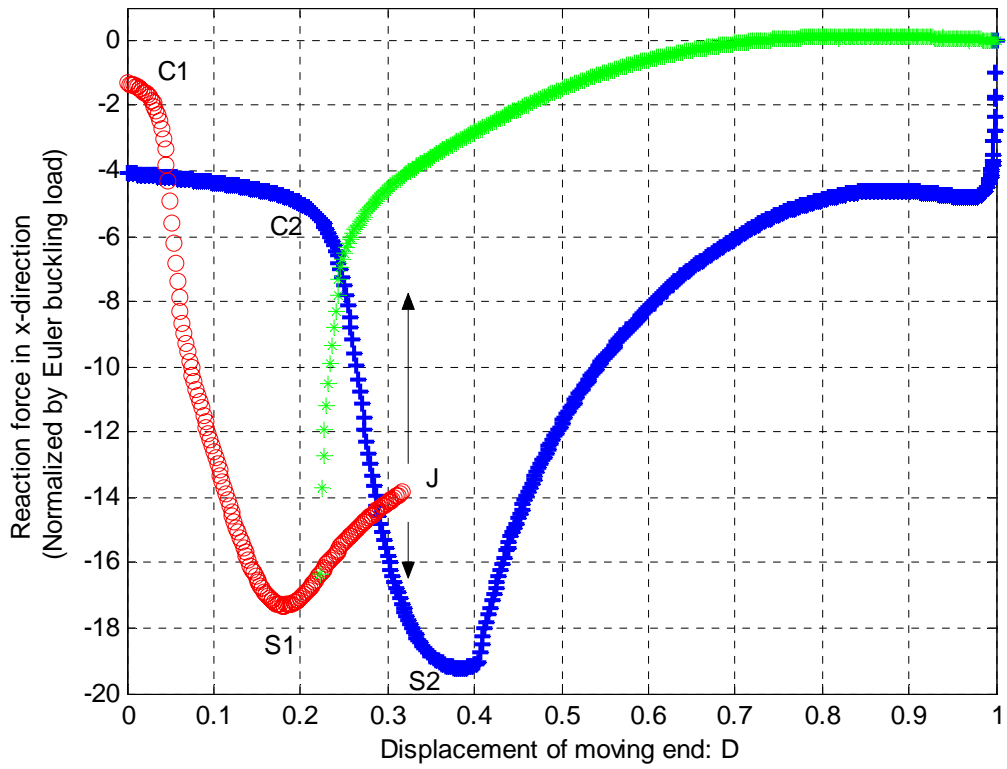


Figure 4.54 Diagram of $D - \lambda_1 / P_{cr}$ (constrained pin-pin elastica, $h=0.15/L$)

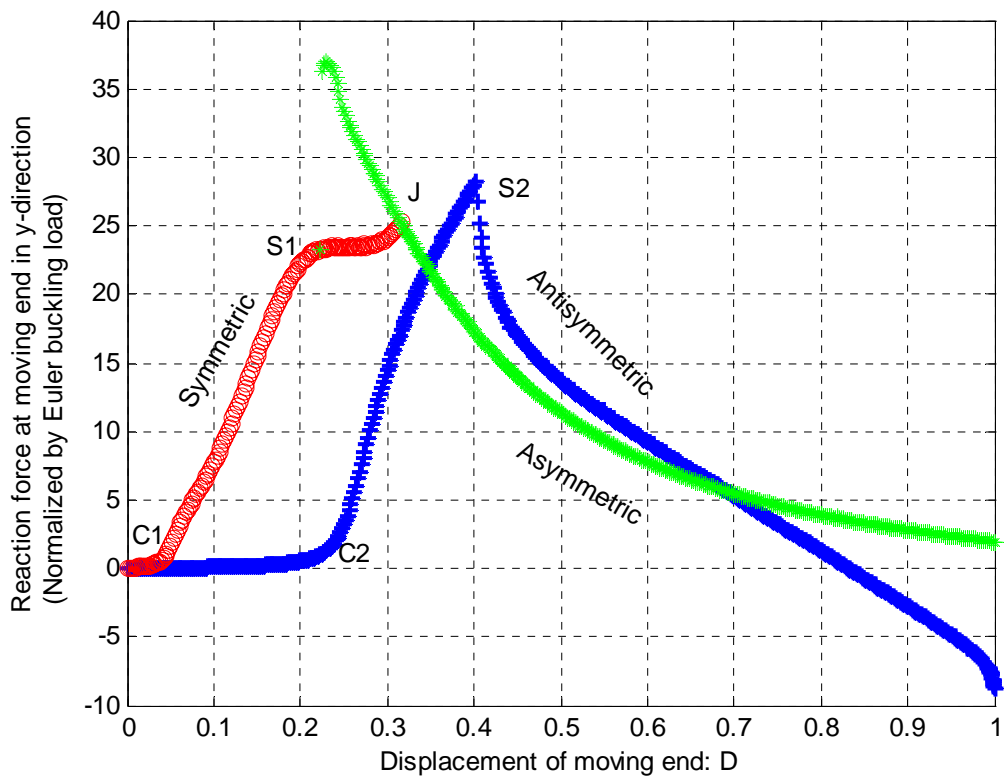


Figure 4.55 Diagram of $D - \lambda_2 / P_{cr}$ (constrained pin-pin elastica, $h=0.15/L$)

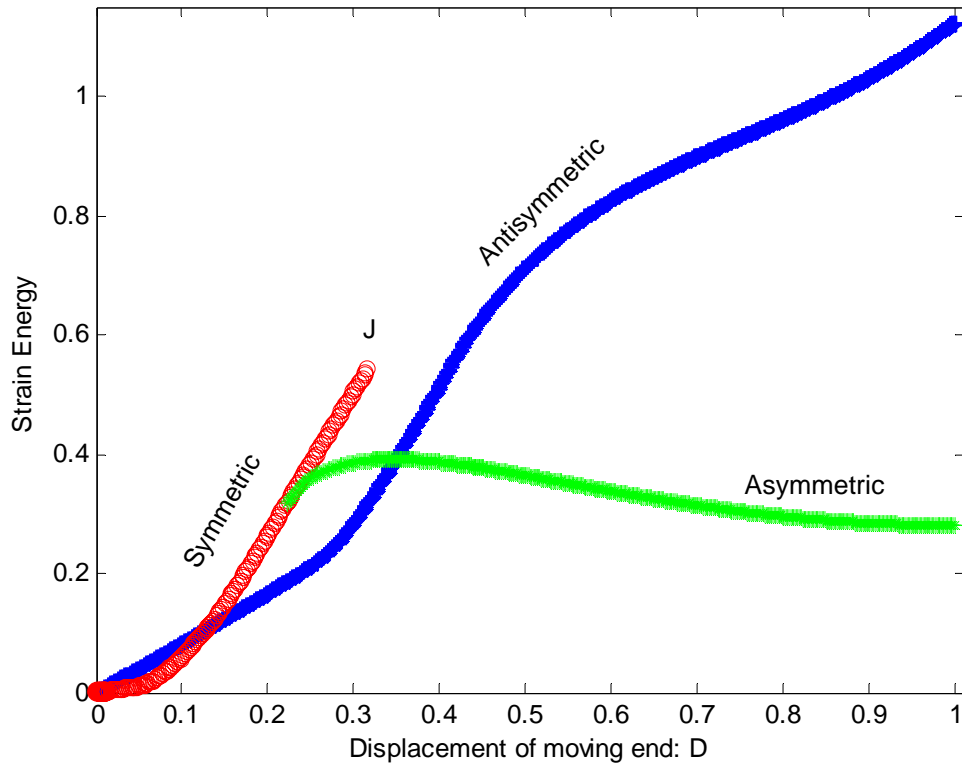
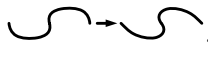


Figure 4.56 Diagram of D – Strain energy, (constrained pin-pin elastica, $h=0.15/L$)

If the control parameter D is increased from 0, λ_1 will start from $\frac{\pi^2 EI}{L^2}$ when buckling happens. As D is gradually increased with step-size 0.002, the elastica's center begins to contact one wall. There should be a sudden change of λ_1 and λ_2 . However, since the model used here is an approximation with penalty term, the change happens continually. Nonetheless, provided b is set small enough, $1e-5$ in this example, the approximation can give reasonable results. In a real structure, some imperfection exists. So the approximation used here can be very close to the real situation. After the point-contact, denoted as CI in above figures, line-contact develops. During this procedure, both λ_1 and λ_2 increase dramatically in magnitudes. The descent of reaction force in x-direction at SI marks the occurrence of secondary buckling. From this point on, the reaction force in y-direction increases slowly. And the instability builds up. Continuing the increment of D , bifurcation happens. The elastica can jump

to either asymmetric configuration or antisymmetric one. A possible point where bifurcation happens is J in the above three figures. Figure 4.56 demonstrates a good explanation for this phenomenon. After $D=0.222$, the strain energy of symmetric configurations will be higher than those of both asymmetric configurations and antisymmetric configurations. Small perturbation may cause the elastica to jump to configurations with lower strain energy. Note that depending on where the jumping happens, the reaction forces will become either higher or lower than those before jumping. The behaviour of this structural system after jumping, either to asymmetric configuration or to antisymmetric one, has been discussed previously. As for the antisymmetric case, one point to pay attention to is $S2$, where the line contact shifts to point contact gradually: .

When we reverse the displacement, the complete load-displacement curve of the second mode will be obtained. It is easy to understand the reverse procedure, and λ_1 will approach the second class of Euler buckling load. If we reverse the path of asymmetric case, the elastica will gradually change back to symmetric secondary buckling configuration. Figure 4.54 and Figure 4.56 show how λ_1 and strain energy of asymmetric configurations converge gradually back. However, the reaction force in y -direction experiences a jump at $D=0.222$. Figure 4.57 shows how the configuration evolves asymmetric single-point-contact configuration to symmetric two-point-contact secondary buckling configuration during this process.

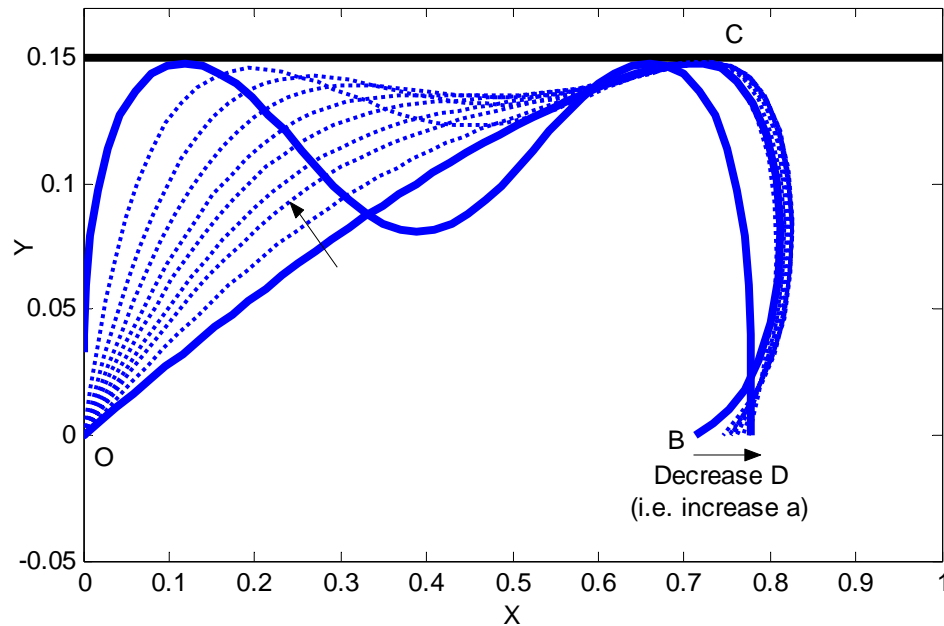


Figure 4.57 Demonstration of how asymmetric configuration evolves to symmetric configuration

4.7 Other applications concerning elastic curve

We have focused our numerical examples and discussion on the well known elastica structure. As discussed in Chapter 1, many applications can be categorized into the study of such elastic curve. The modelling and algorithm developed in this work can easily be implemented to solve such problems. In their paper, Pamplona et.al utilized shooting method to obtain the configurations of liposomes under different point loads [Pamplona 1993]. Due to the axisymmetry of liposome, we can study only half of the structure. And this can be represented with a clamp-clamp elastica as demonstrated in Figure 4.58. However when the point load is not applied, the initial configuration of liposome is a sphere, i.e. the revolution curve is a circle instead of a straight line. Thus it is necessary to generate this initial configuration first, and set it as the reference configuration. Nevertheless, note that EI is a key parameter to determine in order to reduce the study of such spherical structure using planar elastic curve. It will not be discussed here. Rather, we only present only a general family of curves in Figure 4.59.

Both the initial configuration and the one when two clamp ends coincide are highlighted in Figure 4.59.

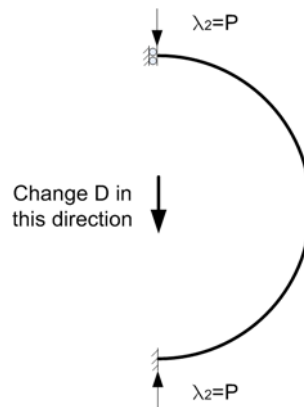


Figure 4.58 Using clamp-clamp elastica to represent half the revolution curve of Lipsome

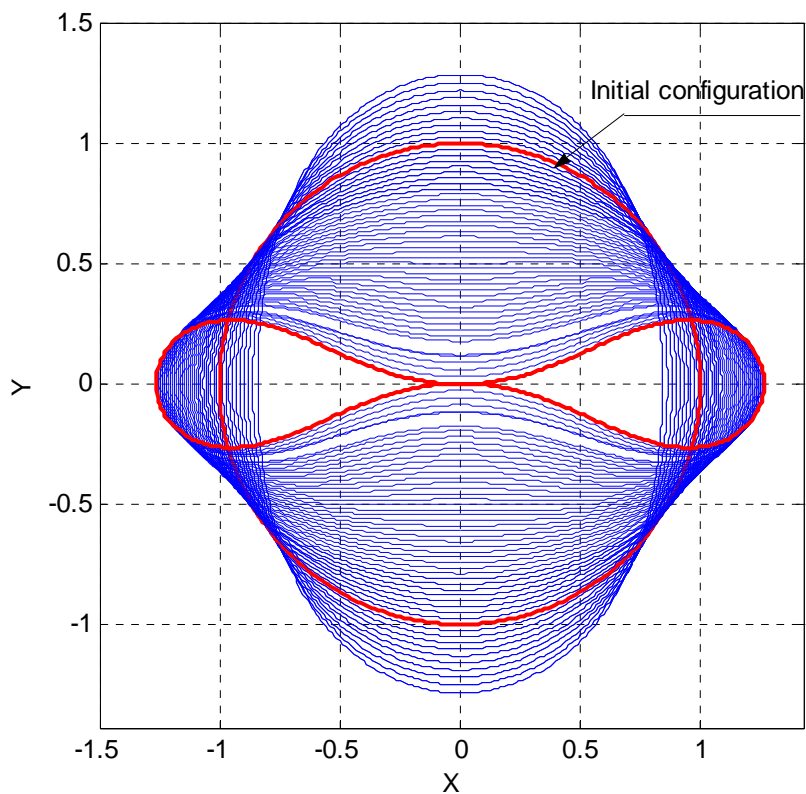


Figure 4.59 Configurations of revolution curve of Lipsome

By changing the distance between the two ends, the structure is under tension or compression in reference of the initial configuration. Interestingly, when the two

points coincide at origin, left/right half of the configuration can be viewed as a well-known intermediate configuration of DNA with racquet shape.

Any other problems that can be represented in terms of elastica can easily adopt the model and algorithm developed in this work. Even though some curves may not be symmetric, they can also be studied using the combination of clamp-pin elastica and clamp-clamp elastica. It is also convenient to define a non-uniform elastica having variable EI along its longitudinal direction without altering the program.

All these examples are studied using “hard loading” D . If the forces applied at two ends are known, we can reduce the number of constraints. For example, if P applied at ends in x -direction, the constraints for a planar elastica will reduce to y_{n+1} equals to the distance between two ends in y -direction. But the objective function will include the work done by P .

CHAPTER 5 Conclusions and Recommendations

5.1 Conclusions

In this work, the post-buckling behavior of elastica under various boundary conditions and constraints is investigated using constrained optimization methods. Two discrete models of elastica are developed. The variables of the first model are the angles with respect to the axis connecting the two ends of the elastica. This model is mainly used in the numerical examples due to its simplicity when expressing the problem in standard optimization form. An alternative model is also developed with the first variable as the angle with respect to the axis at one end, while the other variables are the relative angles of two adjacent segments. It is easy to transform one model to another. But during the searching procedure, the alternative model is more sensitive to numerical perturbation. Therefore, when instability of post-buckling happens, it is easy to observe such phenomenon using the alternative model than the first discrete model. However, the numerical error will be higher when the alternative model is employed. Accordingly, the first model is preferred unless we want to study the instability in post-buckling region.

Based on Bernoulli's principle, the configuration of elastica can be obtained using the constrained optimization techniques. Sequential quadratic programming is the main numerical tool employed. It is efficient when a promising guess is provided. But when the initial guess is not good enough, this gradient-based algorithm cannot guarantee a feasible solution or even convergence. Suppose we have no prior knowledge on the configurations, a robust algorithm is necessary to generate the initial guesses. Genetic Algorithm, which is a stochastic population based numerical tool,

does not depend on the gradient information to determine the next move during the searching procedure. Such advantage makes GA an ideal method to perform search at the initial stage. With a random start, GA will not be stuck at an infeasible solution as SQP does. However, GA cannot provide an exact solution. Hence, it is only used as an auxiliary method to provide initial guesses for SQP to continue. In both optimization tools, a Lagrangian function is constructed. From the *Castigliano's* first theorem, it is shown that the reaction forces at supporting end are the *Lagrange* multipliers of the corresponding equality geometric constraints. To understand the post-buckling behaviour of elastica, path-following strategy is employed to generate the diagram of load-displacement history. The control parameters in this procedure are the respective displacements of one end with respect to another end in x -direction or y -direction. So the geometric constraints are changed step by step.

The comparison study of planar pin-pin elastica with analytical solutions shows that the algorithm proposed in this work can produce accurate results. The discrete model and algorithm developed here can easily be implemented to elastica under other boundary conditions. The critical parameter values of the elastica, such as when maximum deflection happens and when the load change directions, are discussed. The instability of pin-pin elastica when $D=1$ are also observed using the alternative model. The diagram of $D-\lambda_1$ demonstrates a snap-through at $D=1$. The reaction forces in

both x -direction and y -direction are within the range of $[-2.1867 \frac{\pi^2 EI}{L^2}, 2.1867 \frac{\pi^2 EI}{L^2}]$.

As an extension of the planar elastica, the spatial elastica problem can also be solved using the same algorithm. Only the discrete models are different. Here we have only addressed the problem of clamp-clamp spatial elastica with circular section and isotropic material. It is also assumed that the elastica is free to twist. By minimizing the bending energy, the configurations and corresponding reaction forces at supports

can also be calculated. But the out-of-plane buckling will happen after a critical point (around $D=0.4$) is reached. Continuing to increase D , the into-plane jumping will also happen around $D=0.68$. Finally the open rod will form a close rod at $D=1$. Since we formulate the elastica as an optimization problem subject to geometric constraints, the constraints can be easily modified according to our need. Two examples to change the distance in z -direction between two supports are studied. The example with D fixed at 1 gives an approximation to helix. The diagram of $D - \lambda_3$ shows the force of elastic spring varies linearly when c , the deformation in z -direction, is small and nonlinearly when c is large.

Another important application studied is the post-buckling of planar elastica with sidewall constraints. By adding an adaptive penalty term to the objective function, we can study the global behaviour of elastica. Due to the existence of sidewall, the point contact, line contact, secondary buckling and jumping to either asymmetric configuration or antisymmetric configuration will happen in sequence. These are demonstrated in diagrams in section 4.6. The jumping phenomenon can be explained in terms of energy. By breaking symmetry, the structural system can possess lower energy. The path of this kind of problem is not necessarily reversible. If the elastica starts to buckle in the first mode and jumps to the antisymmetric configurations, it will go to the second mode when the loading process is reversed.

The numerical results presented in Chapter 4 are systematic summary of behaviour of elastica. Unlike other numerical tools, this energy-based optimization algorithm requires no re-modelling when boundary conditions and constraints are changed. For example when treating the presence of sidewall constraints, shooting method will require different numerical model in two stages: pre-secondary-buckling

and post-secondary-buckling. In contrast, the model and algorithm presented in this work is straight forward, and can be easily implemented in various applications.

5.2 Recommendations to further study

Throughout this work, the length of elastica is normalized to 1. Bending stiffness K_i is also taken as 1. For a real application, the configuration can be magnified by L . And the corresponding forces are obtained by multiplying P_{cr} , which is calculated using the real parameters.

Elongation of elastica is neglected in this study. It is justified for the usual structural materials [Timoshenko 1961]. However, in some newly emerged fields, the characteristics of materials may be quite different from our assumed structural materials. It would then be wise not to neglect such effects. In such case, the objective function to be minimized should include the strain energy due to change of length at each segment. The geometric equality constraints should also be revised accordingly.

In chapter 4, the spatial elastica is supposed to freely twist. Only bending energy is minimized. In practical applications, torsional resistance should be taken into account. The fixed frame of coordinates may not be suitable to describe the twist angles. Euler angles or Euler parameters are necessary to address such problems. When the effect of torsional resistance is considered, D of the critical point where out-of-plane buckling happens should be larger than the one without torsional resistance. In addition, further study can also be carried out on the extendable elastica.

In the study of constrained Euler buckling, the effect of sidewall is approximated by a penalty term. As discussed in Chapter 2, the parameter b describes how “hard” the side-wall is. To obtain more accurate results, b should be small enough. And the number of discrete segments N should be large enough to prevent

“penetration” from happening. Another way is to construct adaptive constraints. A tentative algorithm is given in Figure 5.1. In this algorithm we first calculate the configuration of elastica, then check if every node along the elastica contact or penetrate the sidewall. If contact or penetration happens, extra constraints will be added to the nodes where penetration happens and re-calculate until the penetration does not happen. After that, it is necessary to check whether the secondary buckling happens. Comparing the penalty method in this work, the tentative algorithm proposed in Figure 5.1 will involve more computation cost. However, the obtained Lagrange multipliers corresponding to the contact points give contact forces.

The sidewall on either side of x -axis can have different distance from the axis. It is also interesting to study the behaviours of elastica when D is fixed and the sidewall distance h changed. On the other hand, when h is very small and we change D from 0, the higher mode will emerge. The jumping to higher mode antisymmetric configuration or symmetric configuration is more likely to happen when h is much smaller than the length of elastica. The sidewalls can also be curved. We need only construct a different penalty function that can describe the geometric features of sidewalls.

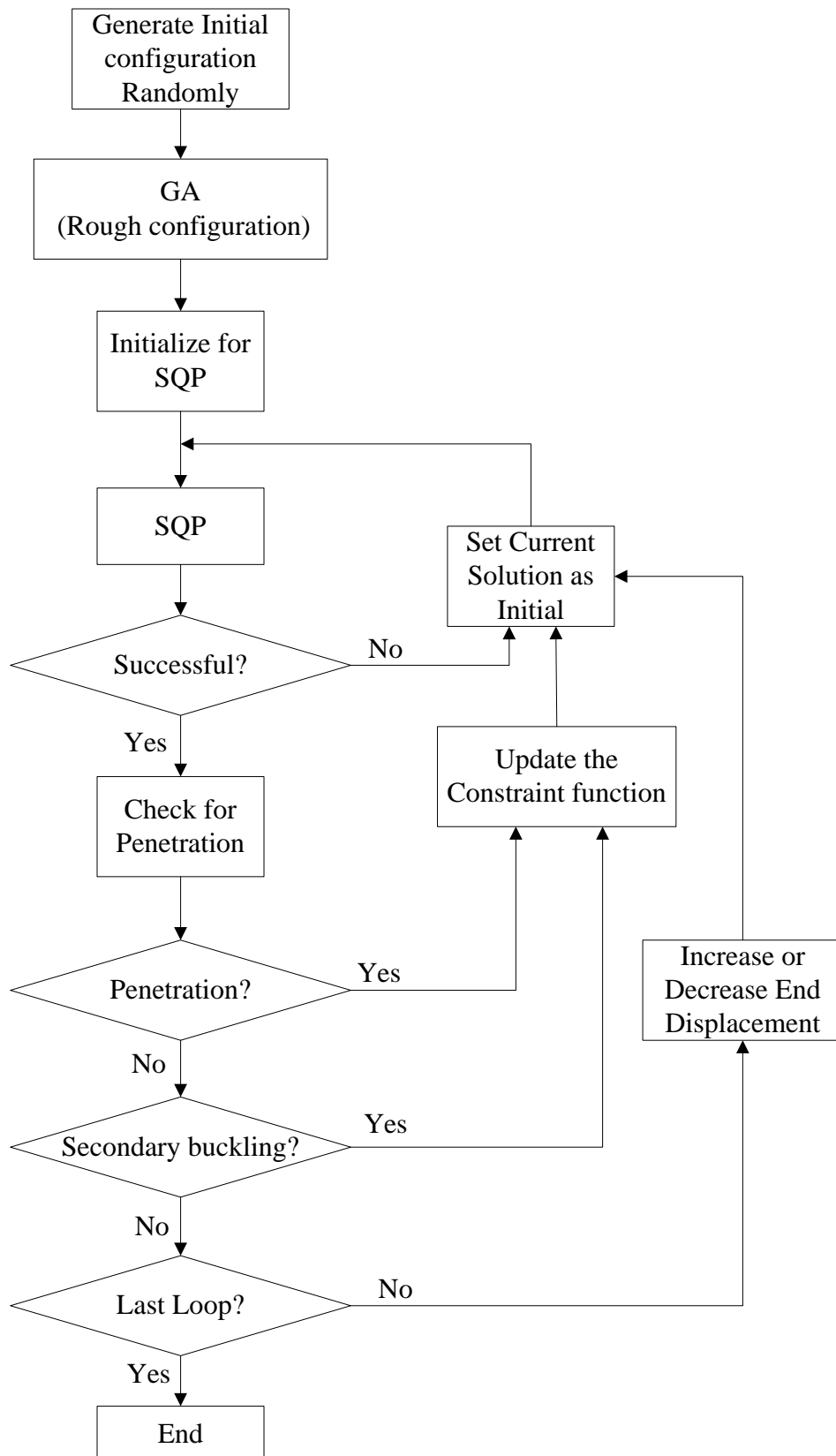


Figure 5.1 A tentative algorithm for constrained Euler buckling

REFERENCES

- [**Antman 1995**] S.S. Antman, “Nonlinear Problems of Elasticity”, Springer-Verlag NY Inc, 1995.
- [**Balaeff 1999**] A. Balaeff, L. Mahadevan, and K. Schulten, “Elastic rod model of a DNA loop in the *Lac* operon”, *Physical review letters*, **83** (1999), pp. 4900-4903.
- [**Bertsekas 1982**] Bertsekas, D. P., “Constrained Optimization and Lagrange Multiplier Methods”, Academic Press Inc, 1982.
- [**Bruckstein 1996**] Alfred M. Bruckstein, Robert J. Holt, and Arun N. Netravali, “Discrete Elastica”, *Discrete Geometry For Computer Imagery, Lyon France*, (2000), pp. 59-72.
- [**Coyne 1990**] J. Coyne, “Analysis of the formation and elimination of loops in twisted cable”, *IEEE J. Ocean Engineerin*, **15** (1990), pp. 72-83.
- [**Domokos 1997**] G. Domokos, P. Holmes, and B. Royce, “Constrained Euler Buckling”, *Journal of Nonlinear Science*, **7** (1997), pp. 281-314.
- [**Euler 1774**] L. Euler, “Methodus inveniendi lineas curvas maximi minimi proprietate gaudentes”, *Opera Omnia I*, **24** (1774), pp. 231-297.
- [**Fain 1999**] B. Fain and J. Rudnick, “Conformations of Closed DNA”, *Physical Review E*, **60** (1999), pp. 7239-7252.
- [**Fletcher 1963**] Fletcher, R. and M.J.D. Powell, "A Rapidly Convergent Descent Method for Minimization," *Computer Journal*, **6**(1963), pp. 163-168.
- [**Godoy 2000**] Godoy, Luis A., “Theory of Elastic Stability: Analysis and Sensitivity”, Taylor & Francis, 2000.
- [**Goldberg 1989**] David E. Goldberg, “Genetic Algorithms in search, optimization & machine learning”, Addison-Wisely Publishing Co. 1989.
- [**Goriely 1997a**] A. Goriely, and M. Tabor, “Nonlinear dynamics of filaments I: Dynamic instabilities”, *Physica D*, **105** (1997), pp. 20-24.
- [**Goriely 1997b**] A. Goriely, and M. Tabor, “Nonlinear dynamics of filaments III: Instabilities of helical rods”, *Proceeding of Royal Society London*, **A 453** (1997), pp. 2583-2601.
- [**Goriely 1998**] A. Goriely, and M. Tabor, “Nonlinear dynamics of filaments IV: Spontaneous looping of elastic rod”, *Proceeding of Royal Society*, **A 454** (1998), pp. 3183-3202.

- [**Haupt 1997**] Randy L. Haupt, and Sue Ellen Haupt, “Practical Genetic Algorithms”, Wiley InterScience – John Wiley & Sons Inc., 1997.
- [**Heijden 2003**] G.H.M. van der Heijden, S. Neukirch, V.G.A. Goss, and J.M.T. Thompson, “Instability and self-contact phenomena in the writhing of clamped rods”, *International Journal of Mechanical Science*, **45** (2003), pp. 161-196.
- [**Holland 1975**] J. Holland, “Adaptation in natural and artificial systems”, The University of Michigan Press, Ann Arbor, 1975.
- [**Holmes 1999**] P. Holmes, G. Domokos, J. Schmitt, and I. Szeberényi, “Constrained Euler buckling: an interplay of computation and analysis”, *Computer methods in applied mechanics and engineering*, **170** (1999), pp. 175-207.
- [**Houck 1995**] Christopher R. Houck, Jeffery A. Joines, and Michael G. Kay, “A genetic algorithm for function optimization: a matlab implementation”, *North Carolina State University Industrial Engineering Technical Report*, 95-09, 1995.
- [**Iseki 1989a**] H. Iseki, R. Sowerby, D. Bhattacharyya, and P. Gatt, “A theoretical and experimental study of a curved strip compressed by a flat plate”, *Journal of Applied Mechanics*, **56** (1989), pp. 96-104.
- [**Iseki 1989b**] H. Iseki, R. Sowerby, N. Chandrasekaran, and P. Gatt, “The elastic-plastic snapping-through of a curved metal strip compressed between two rigid plates (the influence of the supported end condition on the snap-through)”, *International Journal JSME*, **32** (1989), pp. 101-106.
- [**Kratky 1949**] O. Kratky, and G. Porod, “X-ray investigation of dissolved chain molecules”, *Rec. Trav. Chim.*, **68** (1949), pp. 1106-1122.
- [**Kuznetsov 2002**] V.V. Kuznetsov and S.V. Levyakov, “Complete solution of the stability problem for elastica of Euler’s column”, *International Journal of Nonlinear Mechanics*, **37** (2002), pp. 1003-1009.
- [**Love 1927**] A.E.H. Love, “A treatise on the Mathematical Theory of Elasticity”, Cambridge Press, 1927.
- [**Maddocks 1984**] J.H. Maddocks, “Stability of nonlinearly elastic rods”, *Archive of Rational Mechanical Analysis*, **85** (1984), pp. 331-354.
- [**Maddocks 1999**] J.H. Maddocks, and Robert. S. Manning, “Symmetry breaking and the twisted elastic ring”, *Computer Methods in Applied Mechanics and Engineering*, **170** (1999), pp. 313-330.
- [**Maddocks 2000**] J.H. Maddocks, Patrick B. Furrer, and Robert. S. Manning, “DNA rings with multiple Energy Minima”, *Biophysical Journal*, **79** (2000), pp. 116-136.
- [**Manning 1998**] R.S. Manning, K.A. Rogers, and J.H. Maddocks, “Isoparametric conjugate points with application to the stability of DNA minicircles”, *Proceedings of Royal Society*, **A 454** (1998), pp. 3047-3074.

- [**MathWorks 2003**] The MathWorks Inc, “MatLab R13, Optimization Toolbox User’s Guide v2.0”, 2003.
- [**Michalewicz 1992**] Michalewicz. Z, “Genetic Algorithms + Data Structures = Evolution Programs”, Springer-Verlag (Berlin) 1992.
- [**Miyazaki 1997**] Y. Miyazaki, and K. Kondo, “Analytical solution of spatial elastica and its application to kinking problem”, *International Journal of Solids and Structures*, **34** (1997), pp. 3619-3636.
- [**Neukirch 2001**] Sébastien Neukirch, G. van der Heijden, and J.M.T. Thompson, “Finite size effects on twisted rods stability”, *Engineering Math Seminar*, 2001.
- [**Neukirch 2002**] Sébastien Neukirch, G. van der Heijden & J.M.T. Thompson, “Writhing instabilities of twisted rods: from infinite to finite length”, *Journal of Mechanics and Physics of Solids*, **50** (2002), pp. 1175-1191.
- [**Norcedal 1999**] Jorge Nocedal, Stephen J. Wright, “Numerical Optimization”, Springer Verlag, 1999.
- [**Pamplona 1993**] D. C. Pamplona and C. R. Calladine, “The mechanics of axially symmetric liposomes”, *ASME Journal of biomechanical Engineering*, **115** (1993), pp. 149-159.
- [**Plaut 1992**] R.H. Plaut and Z. Mróz, “Uni-directional buckling of a pinned elastica with external pressure”, *International Journal of Solids and Structures*, **29**(1992), pp. 2091-2101.
- [**Plaut 1999**] R.H. Plaut, S. Suherman, D.A. Dillard, B.E. Williams, and L.T. Watson, “Deflections and buckling of a bent elastica in contact with a flat surface”, *International Journal of Solids and Structures*, **36**(1999), pp. 1209-1229.
- [**Powell 1978**] Powell, M.J.D., “A Fast Algorithm for Nonlinearly Constrained Optimization Calculations,” *Numerical Analysis*, G.A.Watson ed., *Lecture Notes in Mathematics*, Springer Verlag, Vol. **630**, 1978.
- [**Rubin 2000**] M. B. Rubin, “Cosserat theories: Shells, rods and points”, Kluwer Academic Publishers, 2000.
- [**Shi 1994**] Y. Shi, J.E. Hearnest, “The Kirchhoff elastic rod, the nonlinear Schrodinger equation, and DNA supercoiling”, *Journal of Chemical Physics*, **101**(6) (1994), 5186-5200.
- [**Stump 1997**] D.M. Stump, W.B. Fraser, and K.E. Gates, “The writhing of circular cross-section rods: undersea cable to DNA supercoils”, *Proceeding of Royal Society London*, **A454** (1997), 2123-2156.
- [**Tan 1992**] Z. Tan, and J.A. Witz, “Loop formation of marine cables and umbilicals during installation”, *BOSS*, **92** (1992), 1270-1285.

- [**Thompson 1969**] J.M.T. Thompson and G.W. Hunt, "Comparative perturbation studies of the elastica", *International Journal of Mechanical Science*, **11**(1969), 999-1014.
- [**Thompson 2000**] J.M.T. Thompson and G.H.M. van der Heijden, "Helical and localised buckling in twisted rods: a unified analysis of the symmetric case", *Nonlinear Dynamics*, **21** (2000), 71-99.
- [**Tony 2002**] Tony F. Chan, Sung Ha Kang, Jianhong Shen, "Euler's Elastica and Curvature-Based Inpainting", *SIAM Journal on Applied Mathematics*, **63** (2002), 564-592.
- [**Timoshenko 1963**] S.P. Timoshenko and J.M. Gere, "Theory of Elastic Stability", McGraw-Hill Inc, 1963.
- [**Villaggio 1997**] Piero Villaggio, "Mathematical models for elastic structures", Cambridge University Press, 1997.
- [**Wagner 1999**] H.D. Wagner, O. Lourie, X.-F. Zhou, "Macrofragmentation and microfragmentation phenomena in composite materials", *Composites Part A: Applied Science and Manufacturing*, **30** (1999), 59-66.
- [**Wang 1981**] C.Y. Wang, "Folding of Elastica-Similarity Solutions", *Journal of Applied Mechanics*, **48** (1981), 199-200.
- [**Wang 1985**] C.Y. Wang, "Post-buckling of a pressurized elastic sheet on a rigid surface", *Journal of Applied Mechanics*, **27** (1985), 703-709.
- [**Wang 1987**] C.Y. Wang, "Crushing of an elastic-perfectly plastic ring or tube between two planes", *Journal of Applied Mechanics*, **54** (1987), 159-164.
- [**Zajac 1962**] E.E. Zajac, "Stability of two loop elasticas", *Trans ASME* (1962), 136-142.
- [**Zhang 2000**] Zhang Yang, Zhou Haijun, and Ou-Yang Zhong-can, "Monte Carlo implementation of supercoiled double-stranded DNA", *Biophysical Journal*, **78** (2000), 1979-1987.